Probabilistic estimation of dune erosion and coastal zone risk

Probabilistic estimation of dune erosion and coastal zone risk

Proefschrift

ter verkrijging van de graad van doctor
aan de Technische Universiteit Delft,
op gezag van de Rector Magnificus prof. ir. K.C.A.M. Luyben,
voorzitter van het College voor Promoties,
in het openbaar te verdedigen op vrijdag 28 februari 2014 om 10.00 uur

door

Fan LI

Master of Science in Hydrology and Water Resources Engineering
Hohai University, China
geboren te Yingkou, China.

Dit proefschrift is goedgekeurd door de promotoren:

Prof.drs.ir. J.K. Vrijling
Prof.dr.ir. P.H.A.J.M. van Gelder

Samenstelling promotiecommissie:

Rector Magnificus,	voorzitter
Prof.drs.ir. J.K. Vrijling	Technische Universiteit Delft, promotor
Prof.dr.ir. P.H.A.J.M. van Gelder	Technische Universiteit Delft, promotor
Prof.dr.ir. S.N. Jonkman	Technische Universiteit Delft
Prof.dr. W. Wang	Hohai University, China
Prof.dr. R. Ranasinghe	Technische Universiteit Delft/UNESCO IHE
Dr. D.P. Callaghan	The University of Queensland, Australia
Prof.dr. D. Solomatine	Technische Universiteit Delft/UNESCO IHE, reservelid

Published by: VSSD, Delft, the Netherlands
ISBN 97890-6562-348-5

Author email: fan.li@tudelft.nl; fan.li.hhu.tud@gmail.com

To my family.

Summary

Coastal erosion has gained global attention and has been studied for many decades. As a soft sea defence structure, coastal sandy dunes protect coastal zones all over the world, which usually are densely populated areas with tremendous economic value. The coastal zone of the Netherlands, one of the most well-known vulnerable areas to coastal hazards, is mainly protected by the dunes. Therefore, the design, maintenance and assessment of the dune safety standard is extremely important for this low-lying country, especially under the circumstance of sea level rise (SLR).

Generally, the safety assessment of the coastal dune includes the prediction of extreme storm events indicated in the form of return periods and the estimation of the dune erosion volume during the extreme storms. Based on the safety levels, a corresponding prudent land-use strategy should be formulated. The aim of this thesis is the prediction and extrapolation of the coastal dune erosion volume and dune retreat distance based on the limited field measurements of wave climate and coastal profile, and in the end, proposing a calculation framework to find the optimal land-use strategy.

The traditional method, proposing a design storm event with a particular probability of exceedance, does not cover all the possible combinations of the wave climate parameters. Hence in practice, this method will lead to inappropriateness in estimation of small dune erosion exceedance probabilities. The Monte-Carlo technique can overcome this drawback by generating a huge number of storm events with different combinations of the wave climate parameters. The difficulty of realizing it is to maintain the statistical characteristics of every involved parameters and simultaneously make sure the dependencies between any

two of them are simulated accurately. In this thesis, four statistical modelling methods are used and tested for the Dutch dataset which includes wave climate and beach profile data. All of these methods can generate synthetic time series of storm events for the purpose of dune erosion estimation The Gaussian copula method is recommended for the Dutch study site.

The connection between the storm events and the consequences of the wave impacts on the dune is the dune erosion model. Considering the principle of the Monte-Carlo method, which relies on repeated random sampling millions of times, a too computationally expensive model is apparently inappropriate. In order to ensure the accuracy on the one hand, and reduce the model running time on the other hand, an empirical dune erosion model (DUNERULE), adjusted by the process based storm erosion model, XBeach model, was used. The dune erosion volumes with different return periods, ranging from 1×100 year-1 to 1×10-6 year-1 under different SLR scenarios are obtained. Three methods of reducing the simulation uncertainty are proposed to remove the physically unreal values. Besides, the exceedance probability curves of the coastal dune retreat distance by the year of 2100 were also predicted.

This method was calibrated and validated in Narrabeen Beach, Australia. This application proves the validity and the applicability of the proposed method in the aspect of wave climate simulation and the dune erosion estimation.

Based on the estimated erosion probabilities, economically optimal land-use strategies were evaluated and compared. To keep far from the unacceptably high erosion risk zone, a buffer zone can be created between the shoreline and the first line of the buildings along the coast. To move the erosion probability contours seaward, the beach nourishment can be carried out. Three different beach nourishment methods were analysed. Due to the many hypotheses and approximations in the computation process, the main point in this PhD research was to propose a generic computational methodology based on the maximum NPV.

This thesis improves the method of probabilistic simulation of sea storms for a dune erosion exceedance probability estimation, simplifies the dune erosion model to make the Monte Carlo approach feasible, estimates the impact of projected SLR to the coastal erosion and recession, and, in the end, proposes a method to optimize land-use planning on the basis of cost benefit analysis.

Fan Li

February 2014 in Delft

Samenvatting

Kusterosie heeft wereldwijde aandacht verkregen en is gedurende vele decennia bestudeerd. Zandduinen, als een zachte zee defensieconstructie, beschermen kustgebieden in meestal dichtbevolkte gebieden met een enorm economische belang over de gehele wereld. Het kustgebied van Nederland, een van de meest bekende kwetsbare en aan risico onderhevige kustgebieden, is voornamelijk beschermd door duinen. Voor dit laaggelegen land, en met name in het geval van zeespiegelstijging (SLR), zijn ontwerp, onderhoud en analyse van de veiligheidsstandaarden van duinen van extreem belang.

Een veiligheidsbeoordeling van het kustduinlandschap omvat in het algemeen de voorspelling van extreme storm gebeurtenissen, aangegeven in de vorm van herhalingstijden en de schatting van het duinerosievolume tijdens deze extreme stormen. Op basis van de veiligheidsniveaus moet een corresponderende en verantwoordelijke strategie voor het landgebruik in de kustzone worden geformuleerd. De doelstelling van deze thesis is, om op basis van beperkte veldmetingen van golfklimaat en kustprofiel, het duinerosievolume en de terugtrekking van het duin te voorspellen en in te schatten, om uiteindelijk een voorstel te doen voor een berekeningskader voor een optimale landgebruiksstrategie.

De traditionele methode, die een ontwerp-storm-gebeurtenis met een bepaalde overschrijdingswaarschijnlijkheid voorstelt, geldt niet voor alle mogelijke combinaties van golfklimaat variabelen. In de praktijk zal deze methode tot onjuiste schattingen van minimale duinerosie overschrijdingswaarschijnlijkheden leiden. De Monte-Carlo techniek kan dit nadeel overwinnen door het genereren van een groot aantal storm gebeurtenissen

met verschillende combinaties van de golfklimaat variabelen. De moeilijkheid bij de realisatie hiervan is het handhaven van de statistische kenmerken van alle betrokken parameters om te garanderen dat de afhankelijkheid tussen elke tweetal variabelen nauwkeurig worden gesimuleerd. In deze thesis zijn vier statistische modelleringsmethoden gebruikt en getest voor de Nederlandse gegevens, inclusief golfklimaat en strandprofiel gegevens. Deze methoden kunt synthetische tijdreeksen van storm gebeurtenissen genereren met duinerosie schattingen als doel. De Gaussiaanse copula methode wordt aanbevolen voor het Nederlandse studie gebied.

De verbinding tussen storm-gebeurtenissen en de gevolgen van golfeffecten op het duin is het duinerosie model. Gelet op het beginsel van de Monte-Carlo methode, gebaseerd op miljoenen willekeurige trekkingen, is een rekenkundig duur model ongepast. Om zeker te zijn van de accuraatheid enerzijds en van een gereduceerde looptijd van het model anderzijds, werd een empirische duinerosie model (DUNERULE), afgestemd op het proces-gebaseerd stormerosie model van XBeach, gebruikt. De duinerosie volumes met verschillende herhalingsperioden, variërend van 1 × 100 jaar-1 tot 1 × 10-6 jaar-1, onder verschillende SLR scenario's, zijn afgeleid. Drie methoden om de onzekerheid van de simulatie te verminderen worden voorgesteld om de physisch niet-realistische waarden te verwijderen. Tevens werden overschrijding waarschijnlijkheid curven van de terugtrekkingsafstand van het kustduin ook voorspeld tot het jaar 2100. Het probabilistische duinerosie model is gekalibreerd en gevalideerd in Narrabeen Beach, Australië. Deze toepassing bewijst de geldigheid en de toepasbaarheid van de voorgestelde methode met betrekking tot de golfklimaat simulatie en de duinerosie inschatting.

Op basis van de geschatte erosie waarschijnlijkheden werden economisch optimale landgebruik strategieën geëvalueerd en vergeleken. Om het onaanvaardbaar hoge erosie risico te vermijden, kan een bufferzone worden aangelegd tussen de kustlijn en de eerste linie van bebouwing langs de kust. Om de erosie waarschijnlijkheidscontouren zeewaarts te verplaatsen, kan strandsuppletie worden uitgevoerd. Drie verschillende suppletiemethoden werden geanalyseerd. Vanwege de vele hypothesen en benaderingen in het rekenproces was het hoofddoel van dit promotie-onderzoek om een generieke berekeningsmethodologie af te leiden gebaseerd op de maximale NPV.

Deze thesis verbetert de methode van probabilistische simulatie van zeestormen voor de inschatting van de duinerosie overschrijdingswaarschijnlijkheid, het vereenvoudigt het duinerosie model om de Monte Carlo aanpak haalbaar te maken, het schat het effect in van de verwachte SLR voor de erosie en recessie van de kust, en tot slot, het stelt voor een methode om de inrichting van het landgebruik op basis van een kosten-batenanalyse te optimaliseren.

Fan Li

Februari 2014 in Delft

Content

Chapter 1 Introduction

Coastal dunes, located at the interface between sea and land, are of great important to the coastal zone safety. They form natural barriers against wind and waves, protecting inland areas from damage due to storms. However, the dunes itself will be eroded under the extreme wave climate situations. A better knowledge of reliable and accurate prediction of the dune erosion probability is fundamental for the coastal zone risk analysis and management, especially in the lower coastal regions facing the threat of Sea Level Rise (SLR). One way of estimating the coastal dune erosion/recession probabilities is to simulate storm event series by analysing the historical observations and employing Monte-Carlo technique.

The main objectives of this thesis are 1) to establish a probabilistic model for coastal dune erosion and retreat distance probability, and 2) propose guidance for land-use planning on the basis of cost-benefit analysis.

1.1 Coastal dune and dune erosion

Coastal dunes play vital role in coastal system. They provide sand reservoir for nourishing, eroding beaches and feeding nearshore sand bars during storms, and provide unique habitats for coastal flora and fauna. In addition, dunes act as soft defence, compared to hard coastal defence (such as dikes and groins) along the coast against storm surge and flooding

by dissipating the wave energy, they are the best and cheapest defence and provide great business value for the local economy.

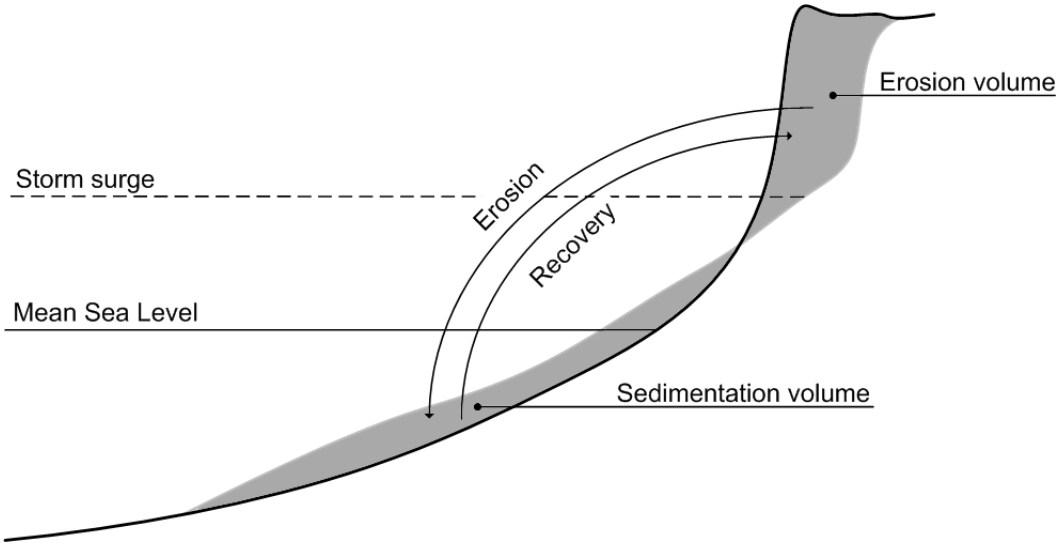

Figure 1.1 Coastal Dune erosion and recovery.

By protecting the inland properties, dunes are eroded during the severe storm events. The cross-shore profile is in a dynamic equilibrium with the sea level and the wave conditions. The storm surge conditions attempt to reshape the profile to a new equilibrium. Higher water level brings the wave farther landward, and the storm waves can reach the dune face and impact it. Under this circumstance, sand starts to be eroded from the dune, and settled at the foreshore. During the storm, the eroded sand will gradually decrease the slope of cross-shore profile and this process will weaken the wave energy and erosion strength and form a new equilibrium with the storm conditions. However, the real equilibrium profile is not expected to be completed every time, the storm duration is always too short for totally forming a new equilibrium profile. Thus, the erosion profile is used to name the new profile shape.

After the storm, the erosion profile does not fit to the normal period conditions, which is the calm period. Therefore, dune recovery will occur. Sediment will be transported shoreward by tide, wave and wind slowly. Sometime later, the cross-shore profile will be restored to pre-storm profile. However, the time scale of recovery is much longer than that of erosion.

A state of equilibrium exists with respect to constant wave and water level, the regular periodic change of the wave and sea level makes the nearshore profile maintain a dynamic equilibrium, without considering the along shore sediment transport. Destructive forces and constructive forces will move the sand seaward and landward alternately. However, SLR or increased storminess will break the equilibrium, and the destructive forces will prevail. Then, the cross shore profile will retreat from a viewpoint of long term morphological changes. Fig. 1.1 shows the erosion and recovery process during and after a storm for a dune coast.

Sea level rising has been observed and projected around the world. Thermal expansion and land-based ice melting are the main contribution factors for SLR, which is expected to continue for centuries. Therefore, attentions should be paid to the coastal defence design to cope with the future coastal hazards, especially the coastal dunes that change with gradually increasing mean sea level (MSL).

A dune breakthrough during storms will bring enormous economic loss and threat the life safety for the residents along the coast. Thus, safe enough dunes are demanded to resist the erosion problem and flooding disasters for low lying areas (e.g., the Netherlands).

A completely safe coastal defence does not exist in practice in the fields of coastal engineering. A probabilistic approach which will propose an appropriate safety standard is usually employed. For example, in The Netherlands, the statutory safety standard are expressed as exceedance probabilities of extreme loading conditions that should be safely withstood, and the safety standards for dunes range from 5×10^{-4} to 1×10^{-4} per year (i.e. 2×10^{3} and 1×10^{4} years, when expressed in terms of return period).

1.2 Monte-Carlo vs. design event method

In the context of coastal engineering, estimating the probabilities of coastal hazards and proposing design standards are vital. For a univariate situation, the probability of the driving force is always the same with the probability of the consequence, that is to say, they have a relationship of one-to-one correspondence. However, in a multivariate environment, the situations become more complicated. For system involving two or more variables, the return period of outcome is not equal to the forcing return period of a particular variate (Hawkes et al., 2002). In this thesis, the coastal dune erosion is caused by storms which involve several wave climate variables, such as wave height, surge level, storm duration and wave period, etc.. Therefore, the multivariate probability of storm variates is not able to represent the dune erosion probability. Two storms, which contain different combination of storm characteristics, may have the same multivariate probabilities, but, they will not always induce dune erosion consequences with the same probability. The main reason is that the effect of each storm parameter on the computed dune erosion is different. For example, two storms with the same return period, one has a longer storm duration, while the other one has a higher significant wave height, the rest of the parameters are the same. Due to the different effect on the dune erosion, this two storm events may cause different dune erosion volumes. Therefore the multivariate exceedance probability of a storm cannot be directly used to represent the exceedance probability of the dune erosion volume caused by the storm.

Several efforts have been spent in solving this ambiguity problem, which may generally fall into two categories: the Monte-Carlo method and the design event method.

A design event, in the case of coastal dune erosion, is a hypothetical design storm event (or the largest historical observed event) that has a particular probability of the erosion. For example, the 1% annual exceedance probability. As mentioned above, one erosion probability does not correspond to unique multivariate probability of the storm events. Approaches, trying to find an appropriate design event which was consistent with the probability of its consequential erosion event, were developed (Corbella and Stretch, 2012; Salvadori et al., 2011).

Monte-Carlo method is a computational algorithm that developed with technology advancement and the invention of the computer. It is usually used for computing the numerical results based on random sampling and the statistical characters of the input variables, especially for the phenomena with significant uncertainties in inputs. In this thesis, the Monte-Carlo method was employed to obtain the erosion probability by simulating the storm variables according to their probability distributions and computing the erosion consequences driven by the simulated storms.

By contrast, the Monte-Carlo method has several advantages: (i) the Monte-Carlo method is conceptually easy to understand, and it is easy to implement in computers; (ii) it is very flexible with regard to the underlying distributions and it can handle multiple sources of uncertainties, while the increasing dimensions will normally add difficulties for the other methods; (iii) the Monte-Carlo method is more preferable when simulating the process with cumulative effect. For instance, for the shoreline retreat distance assessment, the final result does not only rely on the extreme storm events but also the minor storms, which will contribute to the result by accumulation. Whereas, the chief disadvantage of the Monte-Carlo method is slowness compare to the analytical methods, especially, when the structure function is very complicated. This can be overcome by using a supercomputer or using more computers simultaneously.

However, the application of Monte-Carlo method in coastal dune erosion is still limited due to the complicated dependence among storm variables and complex process based coastal dune erosion model.

1.3 Outline of the thesis

1.3.1 Problem definition

Population pressures and economic development have led to an unprecedented growth of value at risk in coastal zones over the last fifty years. To avoid excessive future losses, particularly in the light of projected climate change impacts, and increasing coastal economic value, an accurate quantitative prediction of coastal dune erosion hazards is demanded for sandy coast regions, particularly, the low lying areas, such as The Netherlands, Belgium and

island states. In this thesis, the Noordwijk aan Zee coast (Fig. 1.2), The Netherlands, was selected as a case study to conduct a study, and the Narrabeen Beach, Australia was selected to test the validation of the research methods.

Figure 1.2 Location of Noordwijk in South Holland (from wikipedia).

For any coasts that face the problems of dune erosion hazards, one issue is mostly concerned by the engineers and coastal zone planners:

How can we estimate the coastal dune erosion risk for the end of 21th century with limited historical wave climate observations under the projected SLR?

In order to answer the main research question, some problems below have to be solved:

(1) How can we extrapolate the storm events from the fitted probability distributions of each storm parameters?

(2) How can we convert the storm events into erosion amount?

(3) How can we analyse the erosion and recession probabilities from the simulated erosion amount and what is the influence of SLR on the coastal dune erosion and recession probabilities?

(4) What is the best land-use planning based on the given coastal erosion and recession probabilities?

1.3.2 Study objectives and approach

A Monte-Carlo technique based probabilistic coastal dune erosion estimation framework was developed to answer the questions above. And this method was implemented to a case study in the Netherlands, the Noordwijk aan Zee sandy coast. After that the framework was tested in the Narrabeen Beach, Australia.

First, the coastal management policy in the Netherlands was briefly introduced (Chapter 2).

Second, a multivariate wave climate simulation framework was developed, based on the statistical characters of measurements, extreme distribution theory and dependency structure. Four alternative approaches were used and tested in constructing the multivariate joint distribution and generating the random samples. The random storm series was created by the wave climate samples and the simulated time series (Chapter 3).

Next, a structural function which is able to estimate the values of dune erosion from the simulated storms was proposed. An adjusted simple dune erosion model was validated in the study area with the XBeach (Chapter 4).

The probabilities of dune erosion volume and the retreat distance were analysed based on the Monte-Carlo simulations. And SLR impacts were estimated and compared by computing three scenarios: stable, low projection and high projection in the study area (Chapter 5).

After that, the method was implemented and tested in an Australian case study, and a comparison with the existing research result was made (Chapter 6).

In the end, a probabilistic economic model was proposed to provide guidance for optimal land-use planning. The model includes the cost-benefit analysis and a time dependent probability of coastal dune recession distance (Chapter 7).

The outline of the thesis is shown in Fig. 1.3.

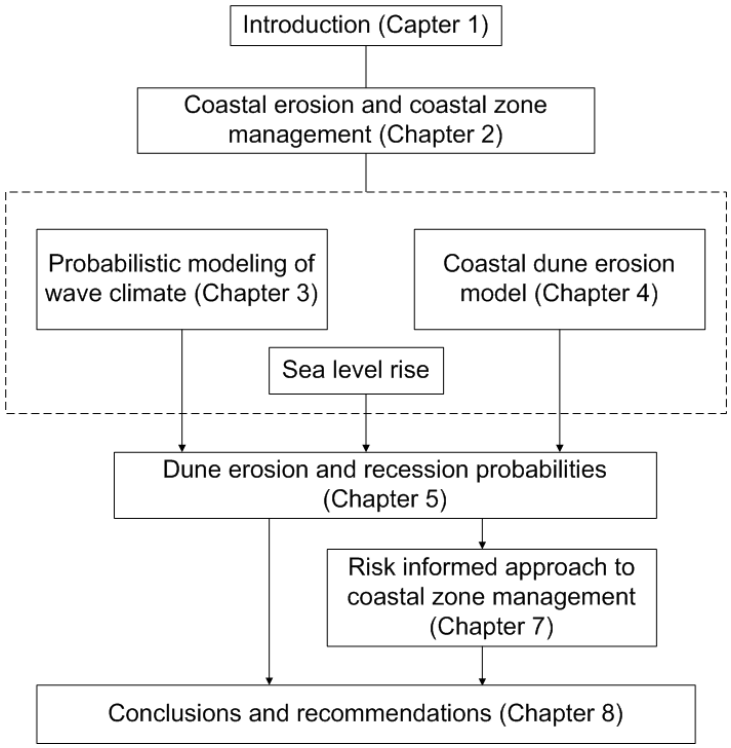

Figure 1.3 Outline of the thesis.

Chapter 2 Coastal erosion and management in The Netherlands

Figure 2.1 Coastal erosion after a heavy storm on 22 February 1990, at Egmond aan Zee (by Ministry of Transport, Public Works and Water Management of the Netherlands).

The Dutch coast along the Southeast part of North Sea may be generally divided into three parts (Fig. 2.2): Delta coast in the south, Holland coast in the centre starts form Hoek van Holland to Den Helder, and the Wadden coast. The length of Dutch coastline is approximately 350 km. About 10% of the coastline is beach flats that are mainly in the Wadden coast, 15% is the man-made sea dikes and sea barriers, and the rest part is the

dunes (Fig. 2.2). Current waves, wind, sediment transport and human activities have result in the present coastline position of the Dutch coast.

Dutch history has many stories and lessons about the threat of the water, both from the sea and the rivers. As existing threatens, a lot of attentions have been paid to the encroaching water. The natural forces govern the landscape of interface between land and water until around Roman times, after that, human activities play an increasing leading role.

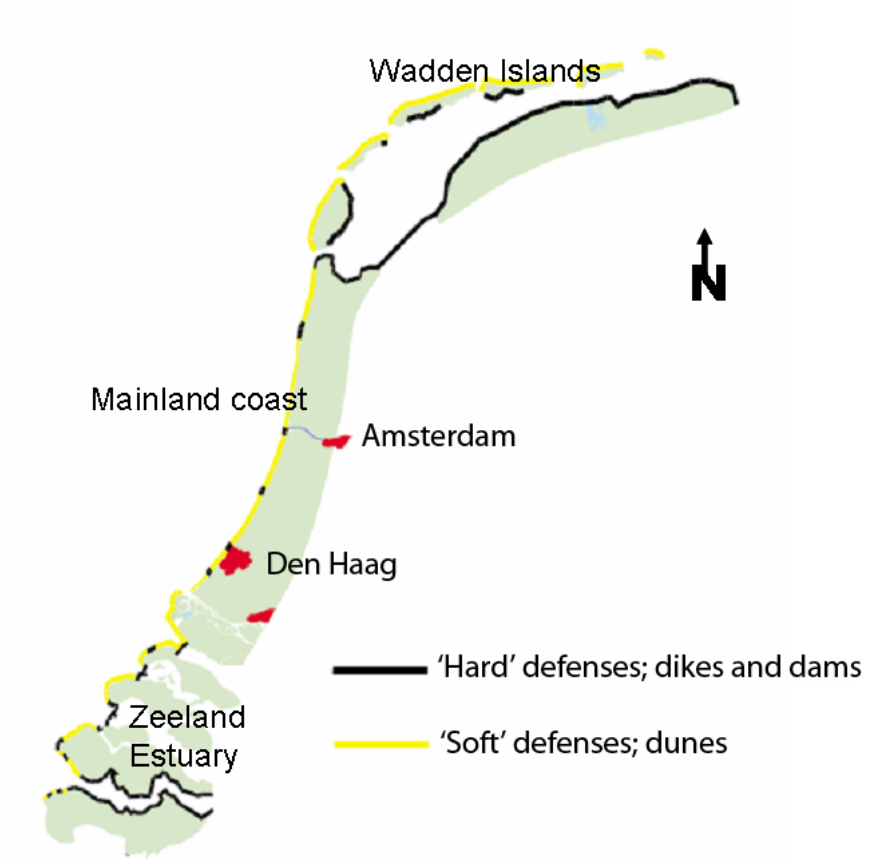

Figure 2.2 Flood defence along the Dutch coast (V&W, 2000).

2.1 Coastal Erosion

Coastal erosion and coastal recession is a phased measurable result of a complex morphological processes occurring in the coastal zone.

In some regions where the dunes are narrow, the hinterland behind the dune with density population and properties is quite vulnerable. In the Netherlands, about 30% areas are below mean sea level. Obviously, the loss will be too enormous in case of failure in resisting the extreme sea storms. Therefore, the safety standard is quite strict. Visiting the beach and the dune area, someone will feel that the dunes are very tall. Considering the specific conditions of The Netherlands, the high safety standard is necessary. The probability of failure of 10^{-5} per year (return period is 100,000 years) was chosen for the most important

parts of the Netherlands. For the less important areas, where is mostly rural areas with small population and less constructions, the acceptable probability of failure is 10^{-4} - 2×10^{-3} per year.

Under natural conditions, the episodic impact of a single storm or storm group will be compensated by dune recovery, however, the long term erosion, that is continuing process of erosion due to adaption of the coastal system to changing conditions (structural erosion), exists. A common natural cause is sea level rise. Human influence often triggers or exacerbates structural erosion.

At present, all the sea defence structures meet the current standard. However, for the coming 200 years, some of the sea defence structures will not meet the norm standard any more when take the global climate change into account. Fig. 2.3a shows the weak links along the Dutch coast. Fig. 2.3b indicates which coastal towns face this risk.

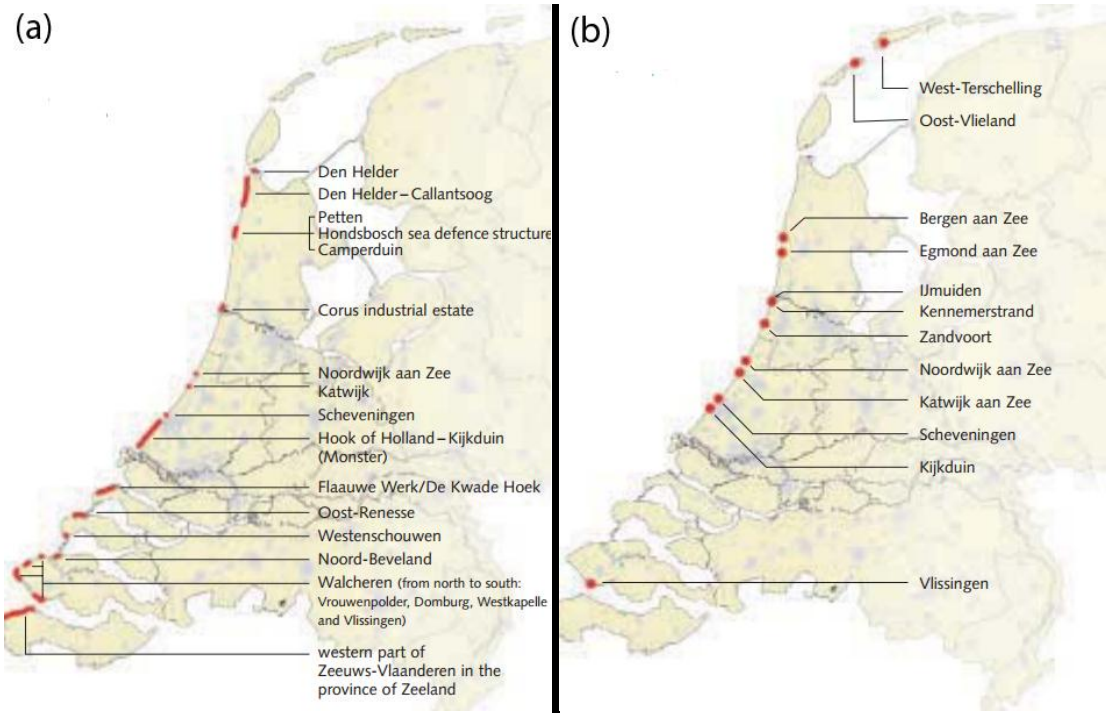

Figure 2.3 Dunes fail to meet the safety standard (on the left) and the towns with buildings in higher erosion risk zone in the Netherlands (V&W et al., 2002).

2.2 Coastal zone policy in the Netherlands

Threatened by the Sea Level Rise and the explosively increasing population and economic value, the coastal erosion management is required from a viewpoint of future development in the low-lying regions.

Traditionally, coastal policy in the Netherlands concerned safety from flooding. Early in the 9th century, collective response against flood hazards was triggered by increasing flood risk

and the complexity of defence construction and maintenance in the Dutch flood prone areas. The structure of water management in the Netherlands reached full growth during the late Middle Ages, and then large land reclamations in the 17th through to the 19th century occurred. A fundamental organizational innovation was the establishment in 1798 of Rijkswaterstaat, a national Bureau for Management and Control of Water-related Issues. The 1953 disaster, claiming 1835 lives and flooding 165,000 hectares of land triggered a huge hydraulic work: the Delta project. And after the storm surge disaster of 1953, coastal policy was dominated by the objective to bring all sea defences to a predefined safety level, the so-called delta strength. During the 80's, the scope of coastal policy gradually extended towards other functions. About half of the Dutch coast is suffered erosion. Therefore erosion management was paid more attention from then on. Moreover, the coastal erosion management will be more necessary due to the more threat to the coastal inhabitants and properties from potential SLR in the future.

The safety policy correspondence to the Dutch conditions has been specified by laws (Delta Act, 1958; Flood Defence Act, 1996; Water Act, 2009): resistance to the flooding and prevention of ecological and social function of the water system. At the level of flooding prevention, the safety policy is to maintain the safety standard that expressed as the probability of exceedance of a certain storm event, or return period. For the three parts of the Dutch coast, i.e. Delta coast, Holland coast and Wadden coast, the safety standard are 1/10000, 1/4000 and 1/2000. In practice, the operability is realized by defining a residual strength of the dunes: the minimum required dune volume to withstand the design storm event (Fig. 2.5). The defined minimum required dune volume and the associate erosion line are the indicator of being safe enough or not. Every 5 years, the position of the erosion line and the residual dune volume behind the erosion line will be tested by using a dune erosion model. In this way, the coastal profile which failed in fulfilling the safety standard will be found and restored (Van Koningsveld and Mulder, 2004).

Delta safety levels focus on the episodic storm erosion hazards along the coast, while structural coastal erosion problems are long-term morphological change of the coastal profile, which is a continuing process of erosion due to adaptation of the coastal system to changing conditions. Human influence often triggers or exacerbates structural erosion. Thus, a new coastal policy to ensure the sustainability of all coastal functions is needed. Discussion on a new policy for coastal defence of dune coasts started in the 1980's (Roeland and Piet, 1995). In 1990 Parliament decided to adopt a 'Dynamic Preservation' policy for the coastline in order to stop further structural erosion of the coast, meaning that the entire coastline will be maintained at its 1990 position.

In order to define the coastline objectively for the dynamic preservation policy, a Momentary Coastline (MCL) had been developed. The calculation of the Momentary Coastline in any given cross-shore profile, is based on the area (or volume per unit length) of sand between two horizontal planes (Hillen, 1991). The upper and lower boundaries are

each located at a distance 'H' from the Mean Low Water Level (MLWL), where 'H' denotes the vertical difference between the dune foot and the mean low water level (Fig. 2.4).

The 'actual' calculation of the Momentary Coastline is based on data from the yearly Dutch coastal bathymetry survey (JARKUS), which has been operational since 1963. JARKUS measures coastal depth profiles from the first dunes up to 1 km in a seaward direction, at alongshore intervals of 250 m (Van Koningsveld and Mulder, 2004).

The 1990 position of Momentary Coastline has been defined as Basal Coastline (BCL, Fig. 2.5), which is a critical value of coastline position according to the management policy. When the Momentary Coastline exceeds the Basal Coastline landward, a measure is needed to restore the coastal dune. Sand nourishment has been a common measure to combat coastal erosion in the Netherlands since the end of the 1970's. When a nourishment project is carried out, sand excavated from the bottom of the North Sea (outside the -20 m depth contour), is added to the near shore zone (De Ronde et al., 2003). Between 1990 and 2000, the average annual nourishment volume has been 6 $\times 10^6$ m^3/year (Roelse, 2002). These nourishments served to maintain the Basal Coastline and thus the amount of sand in front of the dunes.

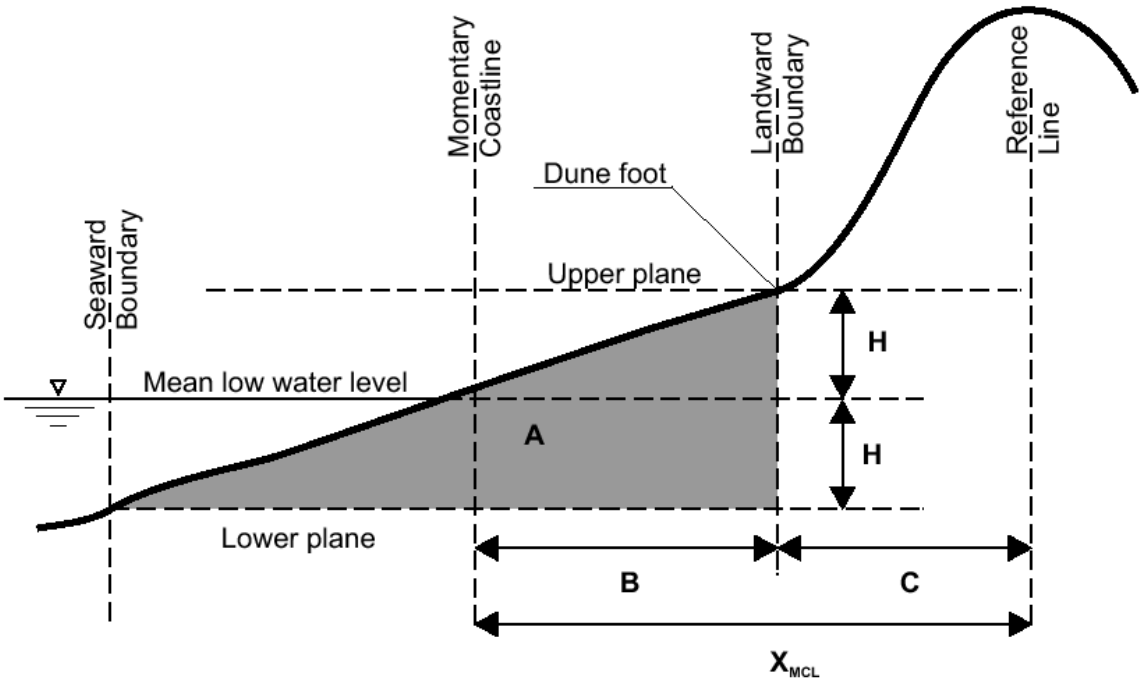

H = Height between dune foot and mean low water [m]
A = Momentary Coastline Zone [m^2]
B = A / 2H = Momentary Coastline position [m]
C = Distance dune foot to reference [m]
X_{MCL} = B + C = Momentary Coastline position + Distance dune foot to reference [m]

Figure 2.4 Calculation of Momentary Coastline, MCL (Hillen, 1991).

Successive evaluations of the policy in 1995 and 2000, pointed out that the Basal Coastline was successfully being maintained (Roeland and Piet, 1995; Roelse, 2002; Roelse and Mulder, 1995). However, problems arise when consider the larger scale morphological developments and SLR in the Basal Coastline policy. For this reason, the Dutch government decided to adopt a more large-scale approach (V&W, 2000). The new policy leads to a new concept, the coastal foundation zone (Fig. 2.5). The Coastal Foundation Zone being defined as the area between the dunes and the -20 m depth contour. In this area, the sediment budget should be maintained. From 2001, the yearly averaged nourishment volume for the entire coastal foundation (so including Basal Coastline nourishments) has been raised from 6 $\times 10^6$ to 12 $\times 10^6$ m^3/year (Fig. 2.6); a volume compensating for the relative loss of sediment due to a sea level rise of 1.8 mm/year (Mulder et al., 2006).

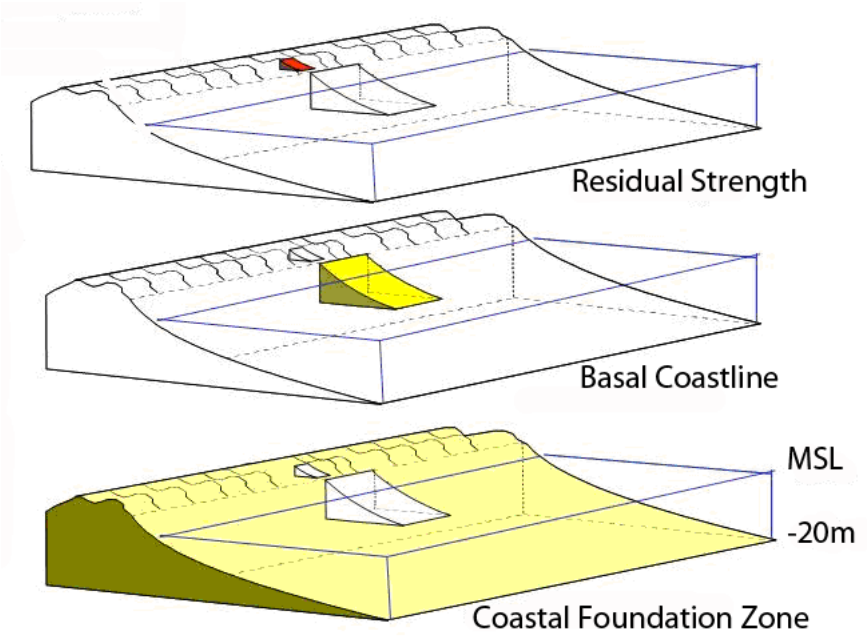

Figure 2.5 Definition of three different scales in coastal management (Mulder et al., 2006).

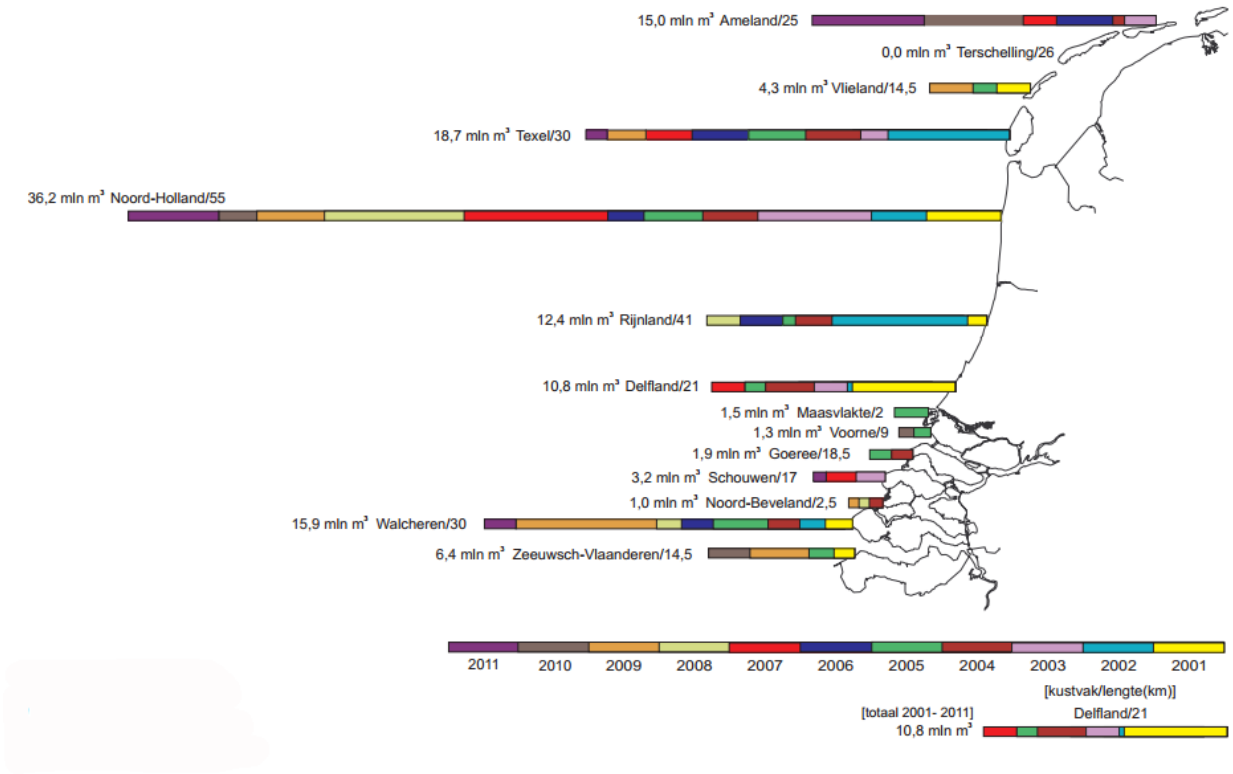

Figure 2.6 Total quality of sand nourishment during 2001~2011(Rijkswaterstaat, 2011).

Chapter 3 Wave climate simulation

In this chapter, approaches of elaborating a full temporal simulation for storm events along the Dutch coast by employing statistical mechanisms are presented.

3.1 Introduction

In the context of coastal engineering, the probabilistic design of marine structures or sea defences is closely related to the statistical prediction of ocean state, such as wave height, period, etc.. These ocean wave climate parameters are the data source for coastal hazards analysis and evaluation of safety level of coastal structures in the concept of the so-called Source-Pathway-Receptor concept (Oumeraci, 2004). One of the challenges for scenario or event based coastal risk assessment is stochastically simulating and describing sea storms which are able to be customarily characterized in term of maximum significant wave height, $H_{s,max}$ (m), peak wave period, T_p (s), peak sea level, h (m), wave direction, θ (degree) and storm duration, D (h). When dealing with the simulation of coastal erosion, time interval between two independent successive storms, that is the everyday wave climate period, is a key variate among others. With the simulated events, the coastal erosion and flooding risk with certain return period will be quantified more accurately compared to the method based on a design event, i.e. large historical event derived from its relative frequency.

Due to the intimate physical connections between these wave climate variates, they are generally partially dependent on each other. Hence, an estimation of the joint probability distribution of wave climate variates is required, especially for the extreme storm events, which are specially concerned by coastal engineers. Univariate marginal distributions received considerable attention in the literatures (Borgman, 1973; Ferreira and Guedes Soares, 2000; Forristall, 1978; Krogstad, 1985; Nerzic and Prevosto, 1998). Furthermore research effort in the past decades has led to a lot of methods to study the bivariate statistical analysis in sea wave state, for instance, the joint probability of waves and sea levels (Hawkes et al., 2002; Li and Song, 2006), joint distribution function of wave height and wave period (Myrhaug and Hansen, 1997; Repko et al., 2005), and correlation between wave height and its duration (Mathiesen, 1994; Soukissian and Theochari, 2001).

Scheffner and Borgman (1992) developed a method for generation of a realistic wave sequence from a small number of stored parameters, including approximately correct distributions of wave height, wave period and wave direction, and dependence and sequencing between them. The method preserves the primary statistical properties of the observed data in the generated storms, however, this method is also known to provide not so accurate estimations of extreme events (Hawkes et al., 2002), which in fact is the focus of the present study (dune erosion is driven largely by extreme storm events). Therefore, in this study the JPM (Joint Probability Method) presented by Callaghan et al. (2008) is used to generate future storm time series. The JPM is specifically designed to provide estimates of extreme storm events while ensuring that the individual properties of each storm (peak wave height, storm duration, wave period, direction, storm surge etc.) will still not depart from their historical statistical distributions. For the purposes of this study, which is to simulate future dune erosion and retreat with an acceptable level of statistical accuracy, the level of physical reality associated with storm time series obtained via the JPM approach should be sufficient.

Recently, copula functions, first mentioned by Sklar (1959), have been increasing popular in applying to various multivariate simulation studies in civil and offshore engineering. De Waal and van Gelder (2005) applied copulas to model extreme wave heights and wave periods; Wahl et al. (2012) applied copulas to statistically analyse storm surges and wind waves; Corbella and Stretch (2012) used copulas to constructed trivariate model of significant wave height, storm duration and wave period; De Michele et al. (2007) used copulas to provide a four-dimension multivariate frequency analysis for significant wave height, storm duration, storm direction, and storm interarrival duration. Copulas are able to correlate two or more variables without changing their marginal distribution. As it will be described in more details, Gaussian copula (also known as normal copula) and Archimedean copula were used to construct the multivariate dependency structure for the significant wave height, storm duration, sea level and peak wave period ($H_{s,max}$, D, h, T_p).

The aim of this chapter is to present an example of a full temporal simulation for storm events along the Dutch coast by means of a statistical mechanism. Based on the existing work, in this chapter, a joint probability distribution model is proposed to derive a multivariate description of the wave climate along the Dutch coast, which may be utilized for coastal risk assessment and integrated coastal management by Monte-Carlo method to avoid the drawback of using a design event. Here four physical variates, i.e. $H_{s,max}$, T_p, h and θ, and two time variates, D and storm frequency F_s, are considered. The storm frequency is the number of the storm events per month.

3.2 Study site and data preparation

In this thesis, the probabilistic erosion model was developed to estimate the coastal erosion hazard at Noordwijk aan Zee coast, the Netherlands (Fig. 3.1b), and the no. 8250 transect (Fig. 3.1a) was chosen as the dune profile for computation.

The wave climate data was collected at Ijmuiden Munitiestortplaats (YM6, period: 1979-1992, location: 52°33'00"N, 4°03'30"E) and Noordwijk Meetpost (MPN, period: 1993-2009, location: 52°16'26"N, 4°17'46"E) in the North Sea over a period of 31 years by the Rijkswaterstaat (www.waterbase.nl), the executive branch of the Dutch ministry of Infrastructure and Environment. The analysis of the wave climate data in 1992 and 1993 of the two gauges indicates that they belong to a homogeneous region in terms of wave climate conditions. Therefore, the observations of the two gauges were merged into one single dataset without adjustment. YM6 station is located 26 km from the coast, where the local depth is 21m. The MPN station is located 9.5km, where the local depth is 18m. The missing data is complemented and corrected by adjacent gauges, to avoid errors and ensure consistency.

The storm events which will cause a morphological change were defined as periods when significant offshore wave height exceeds 3m and simultaneously the tide anomaly, *TA* (m, defined as actual water level minus the astronomical tide level) is simultaneously higher than 0.5m (Quartel et al., 2007). To guarantee the independency of selected storms, the minimum time interval between two storms was set as 24 hours, any two storms with time interval less than 24 hours were considered as one storm event.

The raw observations were selected and processed to obtain a time series of independent storm events characterized by four dimensional variates ($H_{s,max}$, D, T_p, h, θ), while the storminess was represented by F_s. Fig. 3.2 shows the definition for a storm event and the related parameters.

In this thesis, the $H_{s,max}$ is defined as the maximum significant wave height during the defined storm duration, while the storm duration D was defined as the period when the

$H_{s,max}$ and *TA* both satisfy the condition mentioned above. If the time interval between two storms is smaller than 6 hours, *D* will be the period from the start time of the first storm to the end time of the second storm (Fig. 2). The peak wave period T_p is the concomitant wave period of $H_{s,max}$, and the peak sea level *h* is the highest total water level during a storm. And the wave direction is measured at the time when $H_{s,max}$ occurs.

One aspect in the estimation of extreme wave climate that has been routinely ignored is the seasonal effects. During the oceanographic winter period (October to March), the storm events are more frequent and heavier than the storms during the summer period (April to September). In this paper, seasonality was managed by separately simulating the wave climate parameters for winter and summer period.

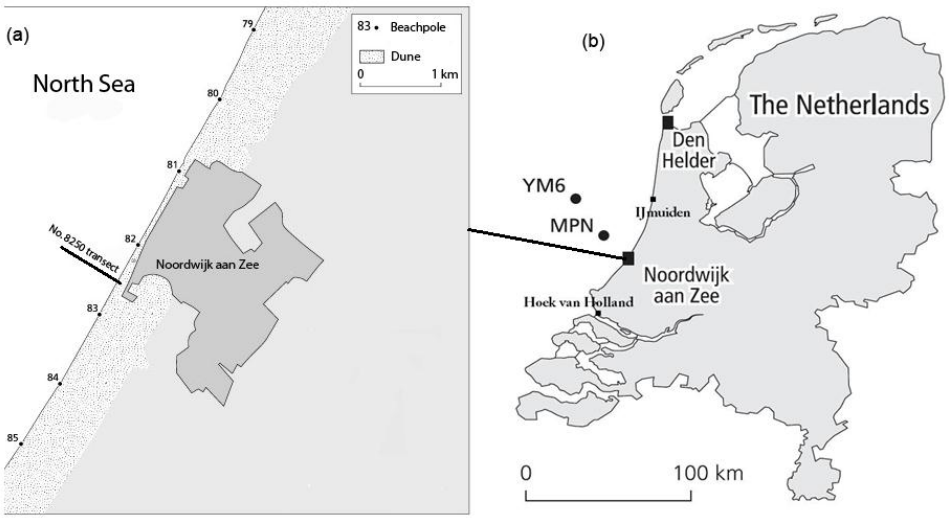

Figure 3.1 Location map of the observation buoys and the 8250 transect, focus on the Noordwijk aan Zee coast.

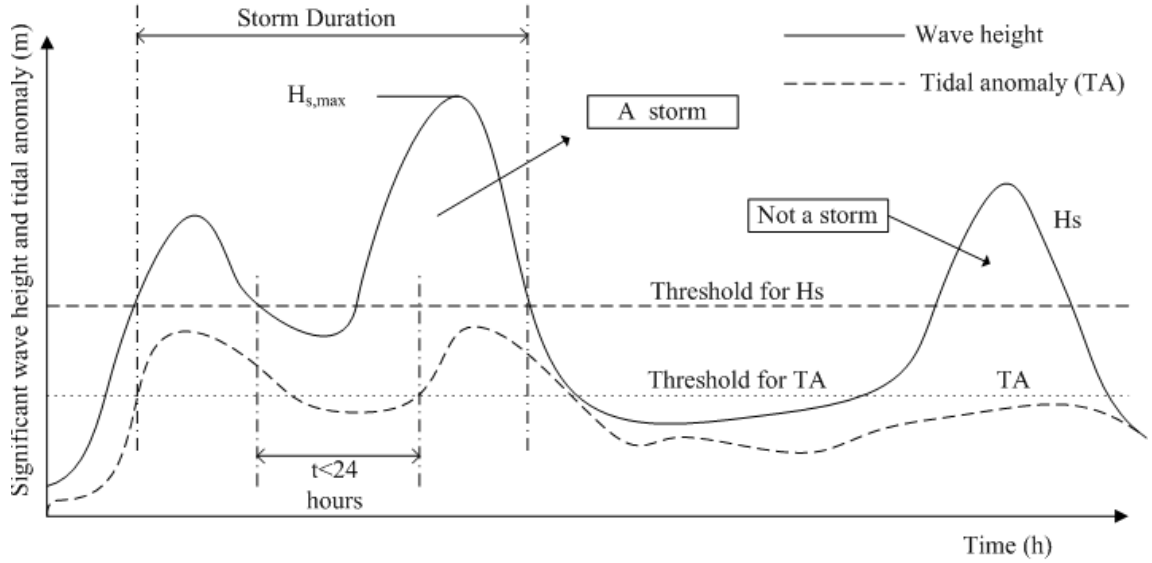

Figure 3.2 Definition for independent storm events (Li et al., 2013).

3.3 Univariate analysis

Based on the statistical characteristics of the measured storms, more simulated storm events are able to be obtained to extend the limit observation data in theory. In order to fit the joint probability distribution to the observations and generate the synthetic storms, three key steps should be followed: fit the probability distributions for each univariate, construct the dependency structure, and simulate the storm sequence from the joint probability distribution and the simulated interarrival of the storms.

3.3.1 Fitting the generalized Pareto (GP) distributions to $H_{s,max}$, D, T_p and h

The extreme value distributions have three types, widely known as the Gumbel, Fréchet and Weibull families respectively. These families give quite different tail behaviour and the selection among them is quite subjective. Once a family is chosen, subsequent inferences do not consider the uncertainty of the distribution type. The Generalize Extreme Value (GEV) has the capability to combine those three families into one single family, however the block maximum algorithm is a waste of data to extreme value analysis if other extremes are available (Coles, 2001). However the weaknesses can be avoided by using GP distribution in the field of coastal engineering (Callaghan et al., 2008; Hawkes et al., 2002).

The GP distribution has three parameters, and its cumulative distribution function (denoted by CDF hereafter) is given by:

$$P(X \le x \mid X > u) = F_{(\xi,u,\sigma)}(x) = \begin{cases} 1-(1+\dfrac{\xi(x-u)}{\sigma})^{-1/\xi} & \text{for } \xi \ne 0 \\ 1-e^{-\frac{x-u}{\sigma}} & \text{for } \xi = 0 \end{cases} \tag{3.1}$$

where, $\sigma > 0$ is the scale parameter; ξ is the shape parameter; u is the threshold. The threshold *u*, should be selected before fitting the distribution function to the data sample. Selecting a proper threshold is sometimes very subjectively, signifying a trade-off between bias and variance. A too low u will lead to a large difference between the distribution of threshold excesses and the GP distribution, result in bias. A too high *u* will lead to a small number of threshold excesses, result in variance. The standard practice is to select the lowest threshold as far as possible. Two methods are available for this purpose: the first one is to determine the threshold by analysing the mean residual life plot, the other one is an assessment of the stability of the parameter estimates.

The first method is based on the mean of GP distribution, $E(Y) = \dfrac{\sigma}{1-\xi}$. Suppose the GP distribution is valid as a model for the excesses of a threshold u_0, thus,

$$E(X-u_0 \,|\, X>u_0)=\frac{\sigma_{u_0}}{1-\xi}. \tag{3.2}$$

If the GP distribution is valid for u_0, then it should be always valid for any threshold that lager than u_0. Hence, for $u>u_0$,

$$E(X-u \,|\, X>u)=\frac{\sigma_u}{1-\xi}=\frac{\sigma_{u_0}+\xi(u-u_0)}{1-\xi}. \tag{3.3}$$

So for $u>u_0$, $E(X-u \,|\, X>u)$ should be a linear function of u. And the locus of points (u, $E(X-u \,|\, X>u)$) is called mean residual life plot (Coles, 2001). An example is shown in Fig. 3.3.

The interpretation of a mean residual life plot is not simple in practice. The selection is quiet subjective and the plot cannot give a definite answer. In Fig. 3.3, the graph appears approximately linear from the start point $u=300$, while this was not an appropriate threshold in line with the analysis result hereafter.

As a complementary technique, another way to select the threshold is based on the theory that for any threshold above u_0, GP shape should be approximately constant and the scale parameter should be linear in *u*, $\sigma_u=\sigma_{u_0}+\xi(u-u_0)$.

The storm $H_{s,max}$ is again used to explain the method, shown in Fig. 3.4. It is still difficult to obtain clear answer from the parameters analysis. Therefore, another method was proposed to overcome the subjective judgement of the threshold selection, the lack-of-fit error analysis.

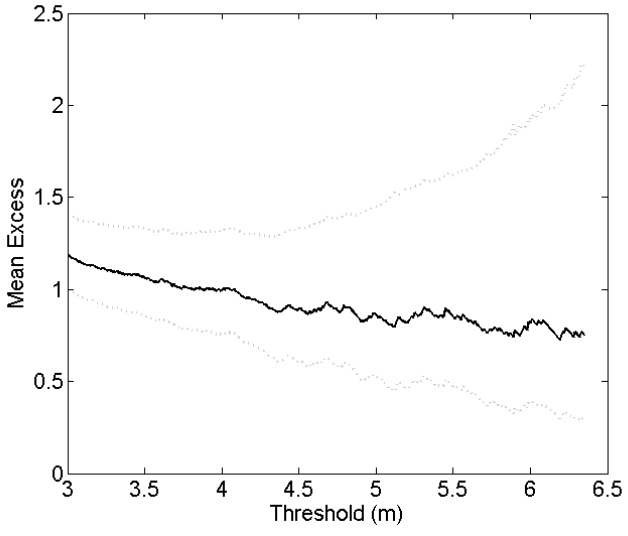

Figure 3.3 Mean residual plot for storm $H_{s,max}$ in winter period from 1979 to 2009 with 95% confidence interval.

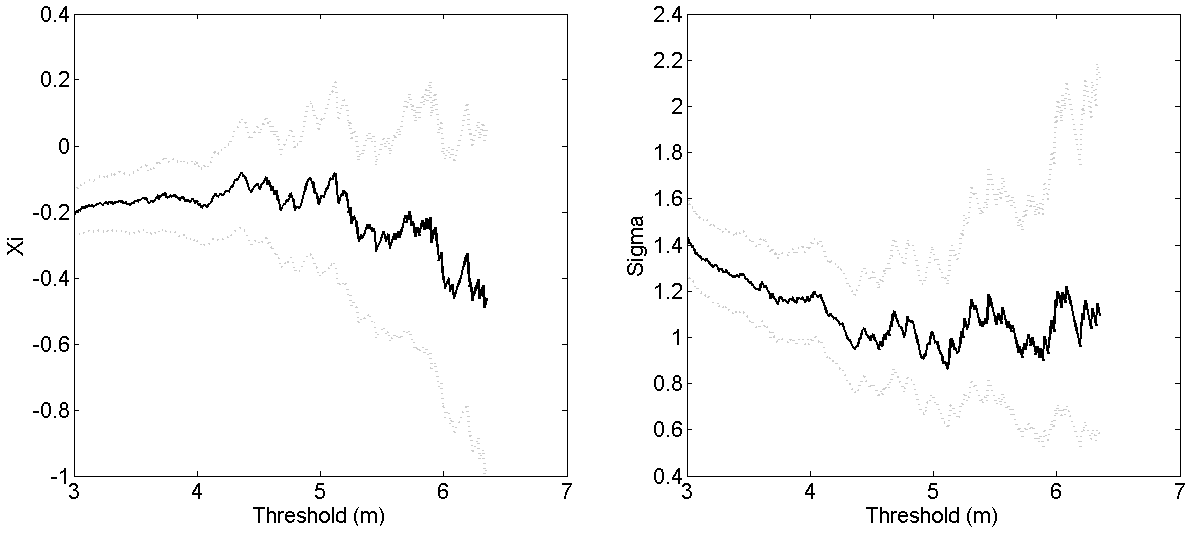

Figure 3.4 Shape and scale parameters against different thresholds with 95% confidence interval.

For coastal hazard assessment, what we most concerned is the unusual conditions. Thus, it is reasonable to choose the *u*, so that the GP distribution fits the extreme data best, rather than a threshold that provides the best fit of the distribution to the whole data sample. Some extreme values of the variates were selected to carry out the root-mean-square-error (RMSE) analysis. The error represents the distance between extreme observations and the modelled curve, Eq. (3.4), and the threshold *u* which can minimize the error was chosen (Table 3.1). For example, $H_{s,max}$ in winter, observations which are higher than 6m (the return period is about one year) are selected to make the error analysis.

$$RMSE = \sqrt{\sum_{1}^{n} \frac{(observed\ value - fitted\ value)^2}{n}} \tag{3.4}$$

where the fitted value is the value extracted from the fitted distribution curve which has the same probability with the observed value, *n* is the number of the values above the selected threshold.

Besides the threshold, the other two distribution parameters were estimated by maximum likelihood estimation (MLE) method, which maximises the probability of the data to derive the distribution parameters. For the maximum significant wave height, storm duration, peak wave period and surge level, the parameters of the fitted probability distributions are listed in Table 3.1, while the comparisons between measurements and fitted distributions are presented in Fig. 3.5. The data below the threshold was represented by the empirical distribution Fig. 3.6.

Table 3.1 GP distribution parameters.

Variate	Winter	Summer
$H_{s,max}$(m)	(u, ξ, σ)=(4.7,-0.18,1.07)	(u, ξ, σ)=(3.0,-0.49,1.48)
D(h)	(u, ξ, σ)=(15,-0.05,13.1)	(u, ξ, σ)=(14,-0.01,13.6)
T_p(s)	(u, ξ, σ)=(6,-0.23,1.12)	(u, ξ, σ)=(5.5,-0.69,1.85)
h(m)	(u, ξ, σ)=(1.9,-0.04,0.24)	(u, ξ, σ)=(1.5,-0.17,0.25)

3.3.2 Determination of the empirical distribution of wave direction and storm frequency

The wave direction θ (with respect to map north) data has a shorter period (1989-2009, from YM6). Fig. 3.7a indicates that storms occur at $\theta \in [200^{\circ}, 383^{\circ}]$ and about 50% of the events concentrate between 200° and 250°. The test for statistically significant dependency between θ and $H_{s,max}$ shows that the correlation is weak (Table 3.2), and the Fig. 3.7b confirms this weak dependency. Consequently, θ was assumed to be independent to $H_{s,max}$. An empirical CDF curve and a bivariate (θ, $H_{s,max}$) plot were shown in Fig. 3.7b.

The storminess can be expressed by either fitting a Poisson distribution to monthly number of storms or fitting a non-homogenous Poisson process to the time interval between consecutive storms (Callaghan et al., 2008). The analysis indicates that the observed data and the fitted Poisson distribution do not have an acceptable agreement, while the non-homogenous Poisson process improves the simulation results but not significantly comparing to the approach used in this chapter, i.e. fitting an empirical distribution to the number of storms within each month, which is simple and effective. The average measured and simulated storm frequency in each month was compared in Fig. 3.8. In order to obtain the time sequence of the storm events within a month, the storm events were assumed to be distributed randomly with the smallest time interval of 6 hours. With the simulated storminess, the discrete storm events became a time series of storm events.

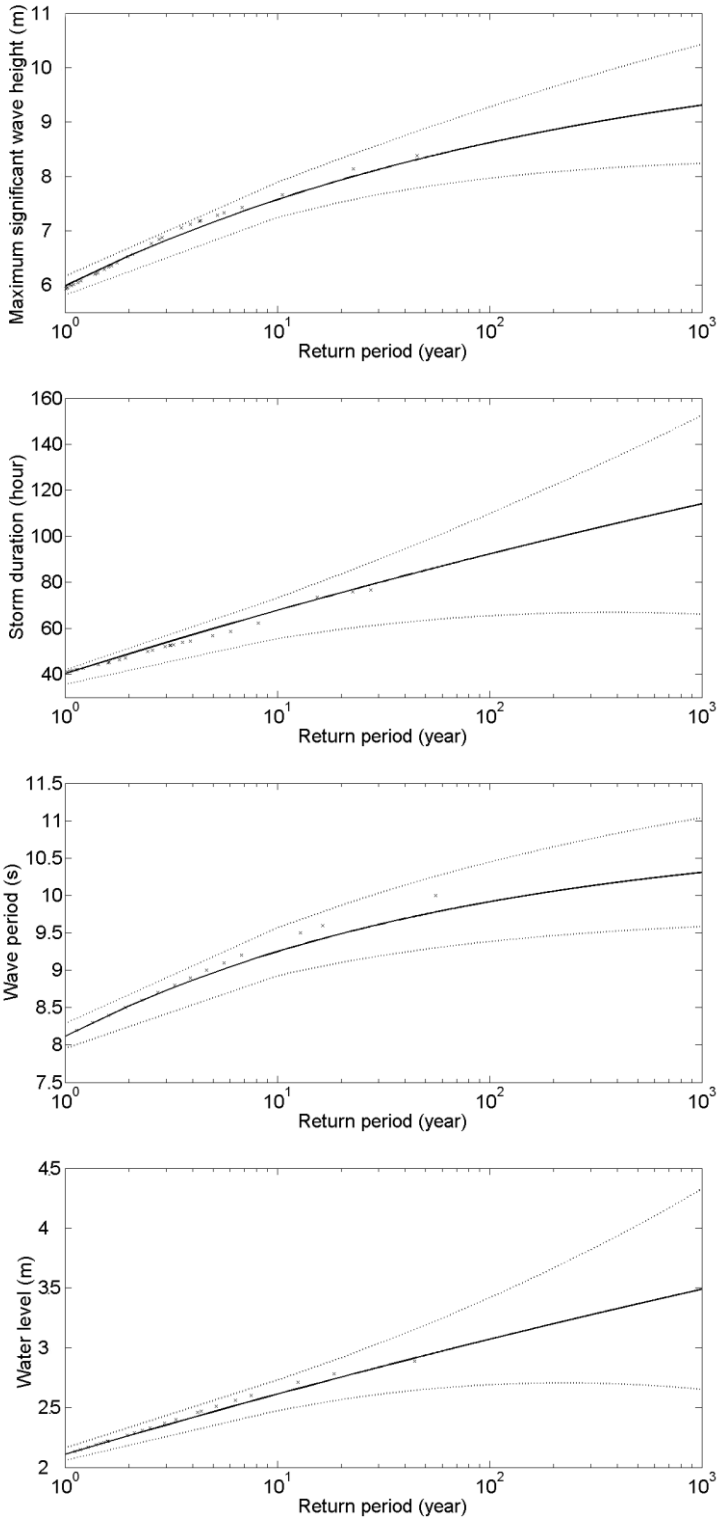

Figure 3.5a The return level plot for $H_{s,max}$ (m), D (h), T_p (s) and h (m) in oceanographic winter season, × are the empirical CDF, and the black solid lines are the fitted model and the dash lines are the 95% confidence limits.

The empirical distribution will give the most precise estimation within the range of observed values. Although problems in using the empirical distribution will arise in estimating exceedance probabilities which are very close to 0 and 1, the accuracy in simulating extreme values of θ and F_s is less important. For the other storm parameters ($H_{s,max}$, D, T_p and h), the extrapolation from observed level to unobserved levels (i.e. the small exceedance probabilities) are vital for coastal protection and engineering design. For the θ, and F_s, they are, on one hand, both limited, and on the other hand, their extreme values have little impacts on the consequences induced by the extreme storm events. Therefore, the empirical distribution is a plausible option for wave direction and storm event frequency simulation.

Table 3.2 Linear correlation coefficients between various variates and $H_{s,max}$.

	D	h	S_p	θ	T_p
Winter	0.544	0.583	0.079	0.246	0.862
Summer	0.611	0.526	0.052	0.281	0.840

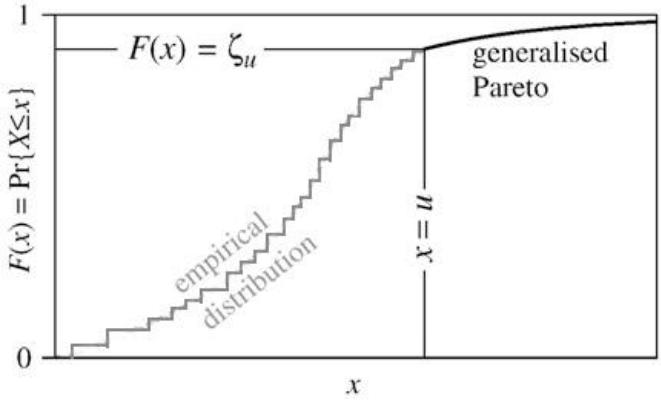

Figure 3.6 Marginal CDFs expressed by GP distributions and empirical distributions, and the transformation form uniform random variable to a quantile value (modified after Callaghan, et al., 2008).

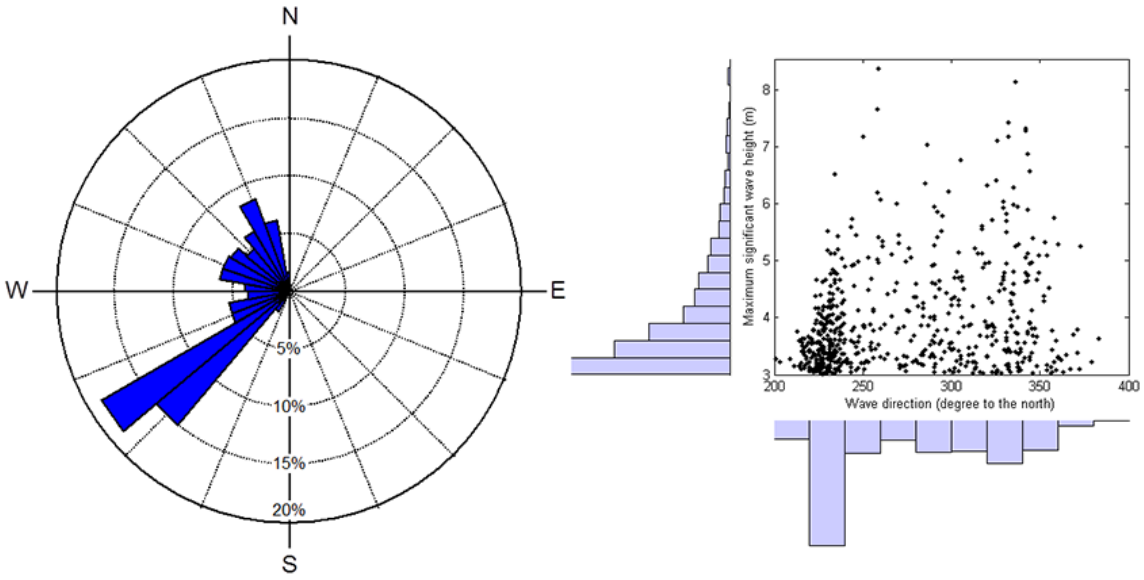

Figure 3.7 (a) Wave direction rose during the storm events, on the left, the length of the directional triangle illustrates the proportion of the determined direction. (b) Observation of θ corresponding to $H_{s,max}$ and the histograms are the empirical PDFs (probability density function).

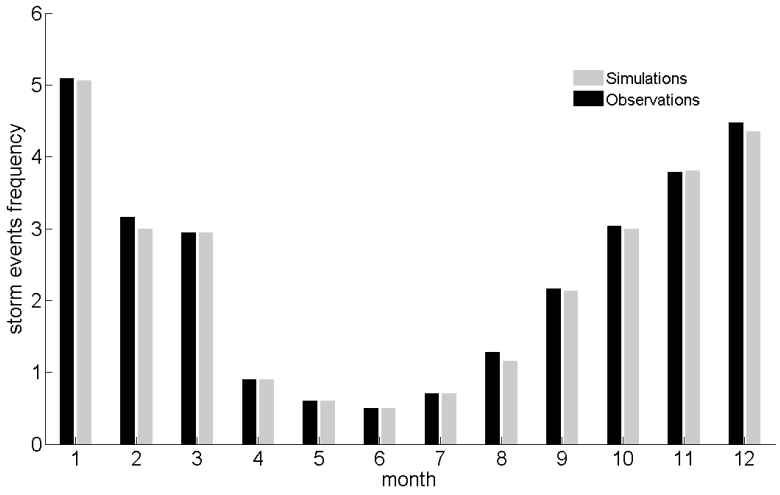

Figure 3.8 Average monthly storm frequencies of simulations and observations.

3.4 Construction of the dependency structure

The four-dimension multivariate ($H_{s,max}$, D, T_p, h) are often treated using univariate frequency analysis, even they are actually dependent. A thorough statistical description of storm characters requires the joint use of marginal distribution laws to simulate the storm events. In this thesis, three alternative methods were used and test for this purpose. They are the Gaussian copula method, physics-combined Gaussian copula method and the logistics method (Coles, 2001; Tawn, 1988). The difference between the first two methods is the way of simulating the peak wave period, T_p. The T_p can be simulated directly by copula or by the independent wave steepness and their intimate physical connection introduced later.

As wave height is typically the dominant variate for coastal erosion, it was chosen as the conditional variate when construct the dependency structure and make the two dimensional comparison to the observations (Li et al., 2014).

3.4.1 Copula method

Copulas are mathematical tool for dealing with multivariate extremes, and become increasing popular in the field of civil engineering.

Provided *d*-dimensional random vector ($X_1, X_2, ..., X_d$) with marginal CDFs $F_{X_1}, ..., F_{X_d}$ with domain ***R***, Sklar's theorem (Sklar, 1959)then says that joint distribution function F_X can be written as a function of its marginal distribution functions:

$$F_X(x) = C(F_{X_1}(x_1), ..., F_{X_d}(x_d)) \tag{3.5}$$

where $C:[0;1]^d \to [0;1]$. The function *C* is a copula function which is used to model the dependency between variables. Eq. 3.5 indicates that the copula function can be used to construct joint probability function based on the marginal distributions. If *C* is a d-copula and $F_{X_1}(x_1), ..., F_{X_d}(x_d)$ are distribution functions, then the function F_X is a d-dimensional joint distribution with marginal functions $F_{X_1}(x_1), ..., F_{X_d}(x_d)$. Moreover, when the marginal distributions are continuous, the copula function *C* is unique (Nelsen, 2006). The copula function is equal to one for independent random variables, while for the dependent variables, constructing the copula function becomes complex.

The copula functions can be grouped into several families according to their parametric forms. Only two important families were introduced in this section, they are Archimedean copulas and Elliptical copulas, more information about the copula families can be found in Nelsen (2006).

3.4.1.1 Archimedean copulas

The Archimedean copula:

$$C(x_1, ..., x_2) = \begin{cases} \varphi^{-1}(\sum_{i=1}^{d} \varphi(F_i(x_i))) & \text{if} \quad \sum_{i=1}^{d} \varphi(F_i(x_i)) \le \varphi(0) \\ 0 & \text{otherwise} \end{cases} \tag{3.6}$$

where $\varphi(x)$ is the generator function and $\varphi(x)^{-1}$ is the inverse function. Three classical generator functions are frequently used:

$\varphi(x) = x^{-\kappa} - 1$ (Clayton copula), $\varphi(x) = -\log(\frac{e^{-\kappa x} - 1}{e^{-\kappa} - 1})$ (Frank copula) and $\varphi(x) = (-\log x)^{\kappa}$ (Gumbel copula), the κ parameter summarizes the dependency between marginal components. For the bivariate copula based on Eq. 3.6, the Archimedean copulas are:

$$C(u,v) = (u^{-\kappa} + v^{-\kappa} - 1)^{-1/\theta} \quad \text{(Clayton copula)} \tag{3.7}$$

$$C(u,v) = -\frac{1}{\kappa}\ln[1 + \frac{(e^{-\kappa u} - 1)(e^{-\kappa v} - 1)}{e^{-\kappa} - 1}] \quad \text{(Frank copula)} \tag{3.8}$$

$$C(u,v) = e^{\{-[(-\ln u)^{\kappa} + (-\ln v)^{\kappa}]^{1/\kappa}\}} \text{(Gumbel copula)} \tag{3.9}$$

Fig. 3.9 shows the different tail dependence for the Archimedean family. The Clayton copula has lower tail dependence, and the Frank copula has no tail dependence, while the Gumbel copula has upper tail dependence.

The Archimedean copulas are usually used for bivariate cases, while they become problematic with higher dimensions. On the one hand, a single parameter is not sufficient for describing the dependency structure of more than two dimensions. On the other hand, the number of parameters quickly grows with dimension, which will increase the complexity of computation (Renard and Lang, 2007).

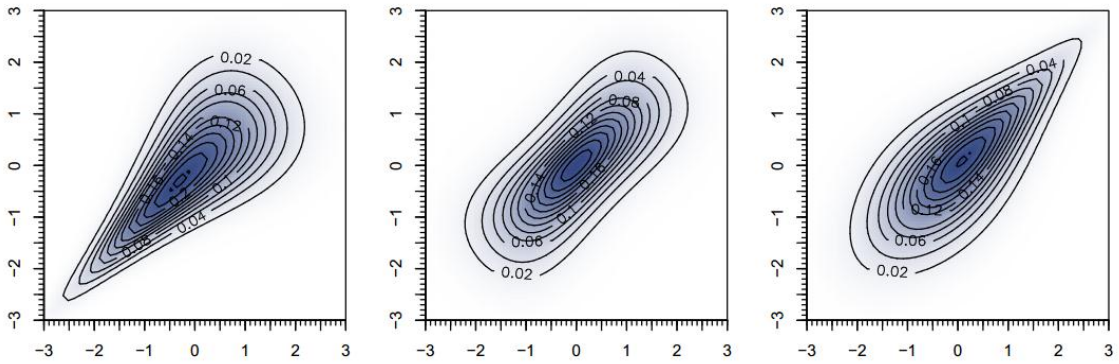

Figure 3.9 The probability density functions of Clayton, Frank and Gumbel copula (From left to the right) (after Schölzel and Friederichs (2008)).

An important property of Archimedean copulas, which concerns the conditional probability, makes the application practical for higher dimensional variables. Let (*U,V*) be uniform random variables on [0,1], joined via a copula function *C*. The conditional distribution functions can be obtained by partial differentiation (Nelsen, 2006):

$$P(U \le u \,|\, V = v) = \frac{\partial C(u,v)}{\partial v}. \tag{3.10}$$

Thanks to this property, a Gibbs sampling approach (Geman and Geman, 1984) is possible to apply with Archimedean copulas to generate four-dimension storm state parameters.

Based on a visual inspection of the historical measurements (Fig. 3.10) and the tail behaviour of each copula, the Clayton copula, Gumbel copula and Frank copula were fitted to ($H_{s,max}$, D), ($H_{s,max}$, T_p) and ($H_{s,max}$, h) respectively. Fig. 3.11 shows the plausible selection for each pair. For better comparison, the marginal distributions were converted to standard normal distribution.

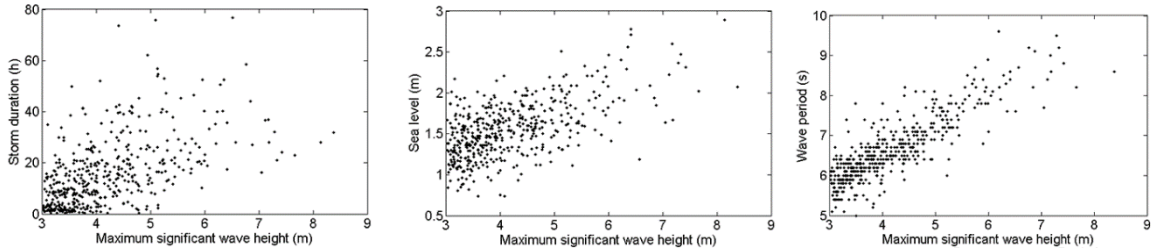

Figure 3.10 Historical measurements of storm parameters.

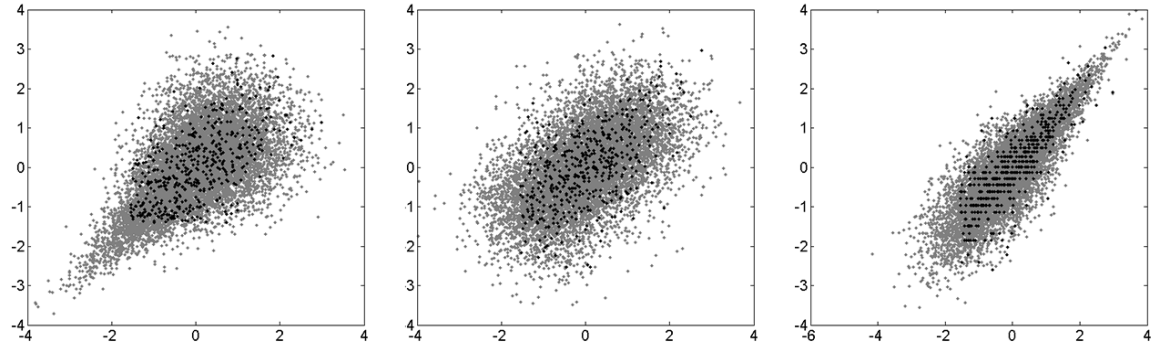

Figure 3.11 Archimedean copula fit for ($H_{s,max}$, D), ($H_{s,max}$, T_p) and ($H_{s,max}$, h) (from left to right). The black dots are the observations and the grey dots are the simulations.

This approach was put into practice with the following steps, using x for the CDF of $H_{s,\max}$, y for the CDF of D, z for the CDF of T_p and s for the CDF of h:

1. Calculate the empirical CDF of each storm parameter via kernel density estimation (KDE), $F_X(X \le x)$, $F_Y(Y \le y)$, $F_Z(Z \le z)$ and $F_H(S \le s)$;

2. Fit the dependency parameters via Canonical Maximum Likelihood (CML) method for each copula, the maximum likelihood function is:

$$L(u,v\,|\,\kappa)=\prod_{i=1}^{N}\frac{\partial C(u,v)}{\partial u\partial v}\,|\,u_i v_i,\ \ (u_i,v_i)\in(0,1);\tag{3.11}$$

3. Generate a uniform random number $A\sim(0,1)$ and $B\sim(0,1)$, and let $y_0=F_Y^{-1}(A)$;

4. Solve the conditional distribution function of x_1 given y_0, $B=P(X\le x_1\,|\,Y=y_0)=\dfrac{\partial C_{XY}(x_1,y_0)}{\partial(y_0)}$, and find the solution of x_1;

5. Generate uniform random numbers $(C,D,E)=U(0,1)$, and solve the conditional distribution functions

$$C=P(Y\le y_1\,|\,X=x_1)=\frac{\partial C_{XY}(x_1,y_1)}{\partial(x_1)},$$

$$D=P(Z\le z_1\,|\,X=x_1)=\frac{\partial C_{XZ}(x_1,z_1)}{\partial(x_1)},$$

$$E=P(S\le s_1\,|\,X=x_1)=\frac{\partial C_{XH}(x_1,s_1)}{\partial(x_1)}$$

for (y_1,z_1,h_1).

6. Repeat step 4 and 5 for n times (*n* depends on the monthly storminess and the number of the simulation years) by iterations to get the simulated wave climate,{(x_1, y_1, z_1, s_1),...,(x_n, y_n, z_n, s_n)};

7. Transform the CDFs to the physical scale by their inverse marginal CDFs (Fig. 3.6).

Hereinto,

$$\frac{\partial C_{XY}(u,v)}{\partial(u)}=[1+u^{\kappa_{XY}}(v^{-\kappa_{XY}}-1)]^{-\frac{1+\kappa_{XY}}{\kappa_{XY}}},\tag{3.12}$$

$$\frac{\partial C_{XZ}(u,v)}{\partial(u)}=\frac{e^{-u\kappa_{XZ}}(e^{-v\kappa_{XZ}}-1)}{(e^{-v\kappa_{XZ}}-1)(e^{-u\kappa_{XZ}}-1)+e^{-\kappa_{XZ}}-1},\tag{3.13}$$

$$\frac{\partial C_{XH}(u,v)}{\partial(u)}=\frac{(-\ln u)^{\kappa_{XH}-1}[(-\ln u)^{\kappa_{XH}}+(-\ln v)^{\kappa_{XH}}]^{\frac{1-\kappa_{XH}}{\kappa_{XH}}}}{ue^{[(-\ln u)^{\kappa_{XH}}+(-\ln v)^{\kappa_{XH}}]^{1/\kappa_{XH}}}}.\tag{3.14}$$

The simulated wave climate was shown in Fig. 3.12.

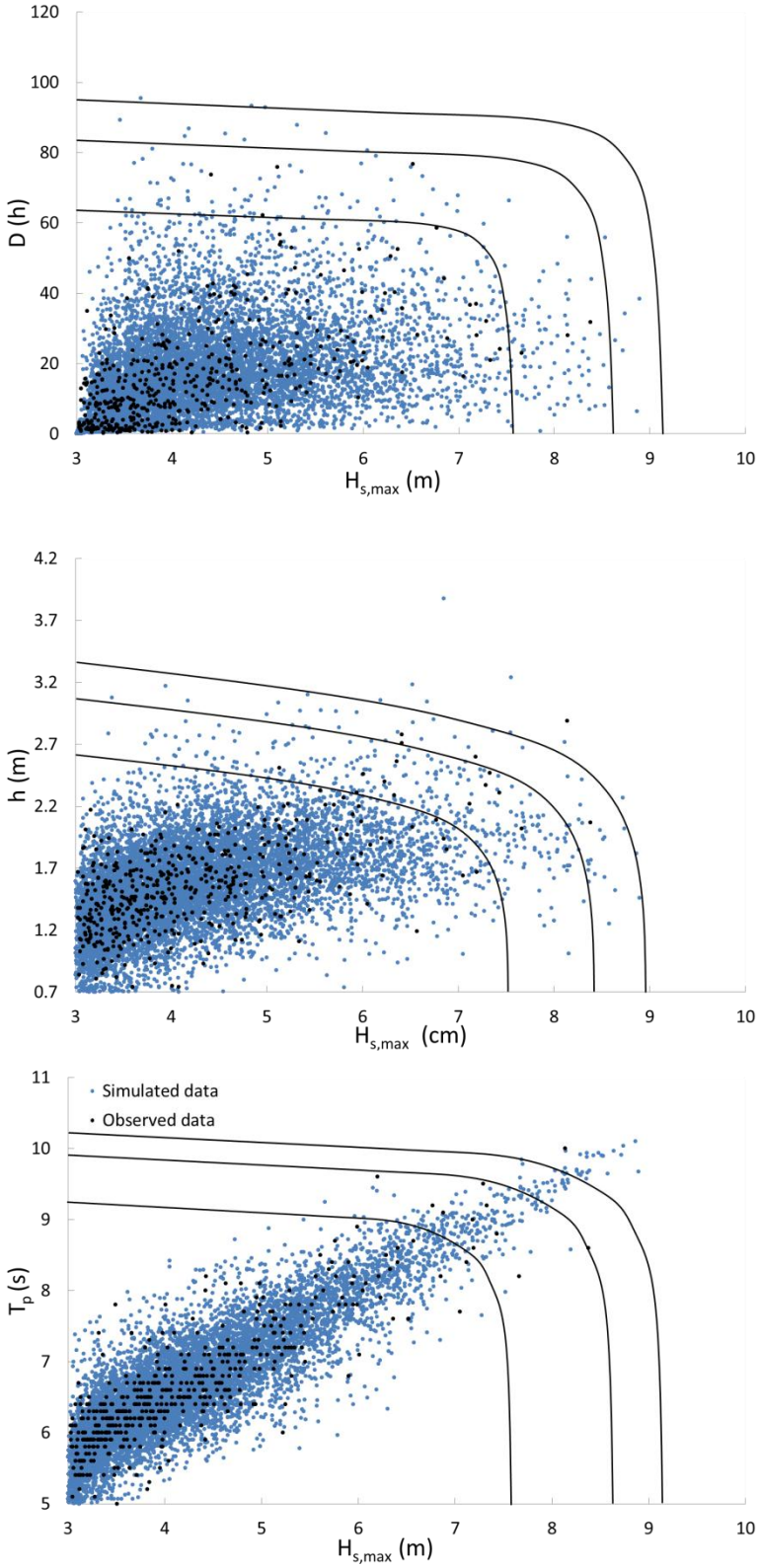

Figure 3.12 Archimedean copulas method simulated 10^4 storms (blue dots) and observed wave climate (black dots), ($H_{s,max}$, D), ($H_{s,max}$, h) and ($H_{s,max}$, T_p) from top to bottom in winter season. The solid curves are the return period contours (10, 100 and 500 years respectively).

A progressive gravity wave has the physical limit, and the wave period is also limited by physical mechanisms. Michell (1893) found that in deep water the theoretical limit for wave steepness is about 1/7. Havelock (1918) confirmed his finding. Hence, the simulated wave period, which is beyond the limit, was discarded. This rule is also followed by the other simulation approaches.

3.4.1.2 Gaussian copula

The Elliptical copula is an alternative copula family to simulate the joint distribution, and it is more easily to extend to higher dimension. The most well-known Elliptical copula is Gaussian copula (also known as normal copula). This copula, which is a distribution over the unit cube $[0, 1]^d$, can be easily generalized to a higher number of dimensions. It is constructed from a multivariate normal distribution over R^d using the probability integral transform. For a given correlation matrix $\Sigma \in R^{d\times d}$, the Gaussian copula can be expressed as follows:

$$C_R(u) = \Phi_\Sigma(\Phi^{-1}(u_1),...,\Phi^{-1}(u_n)) \tag{3.15}$$

where Φ_Σ is the joint distribution function of the *n*-variate standard normal distribution function, and Φ^{-1} denotes the inverse of the univariate standard normal distribution. Hence the multivariate CDF can be written as:

$$F(x_1,...,x_d) = C(F_1(x_1),...,F_d(x_d)) = \Phi_\Sigma(\Phi^{-1}(F_1(x_1)),...,\Phi^{-1}(F_d(x_d))) \tag{3.16}$$

Fig. 3.13 illustrates the principle of Gaussian copula.

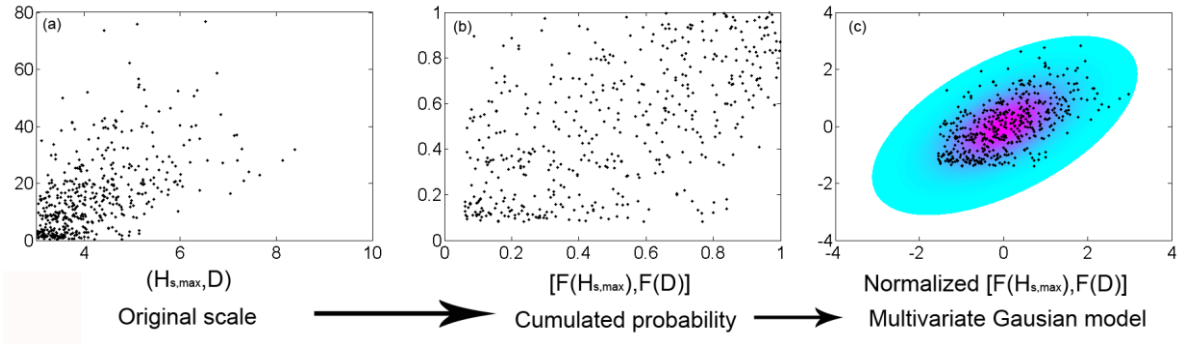

Figure 3.13 Principle of the Gaussian copula, using ($H_{s,max}$, D) as an example.

In practice, the Gaussian copula method is implemented as follows:

1. Transform the observed data to the scale of Gaussian copula using the KDE method and inverse normal distribution function;

2. Fit a Gaussian copula to the computed CDF and derive a [$n \times n$] matrix of linear correlation coefficients for the Gaussian copula, i.e. Σ mentioned above;

3. Generate random samples from the fitted Gaussian copula;

4. Transform the generated samples back to the original scale by using inverse CDFs.

An advantage of the Gaussian copula is that it can be easily extended to higher dimension compared to the other alternative copulas. Fig. 3.14 and 3.17 (upper panel) show the dependency between various variates and $H_{s,max}$ for 10^4 simulations, and the two-dimensional comparison between the observations and the simulations.

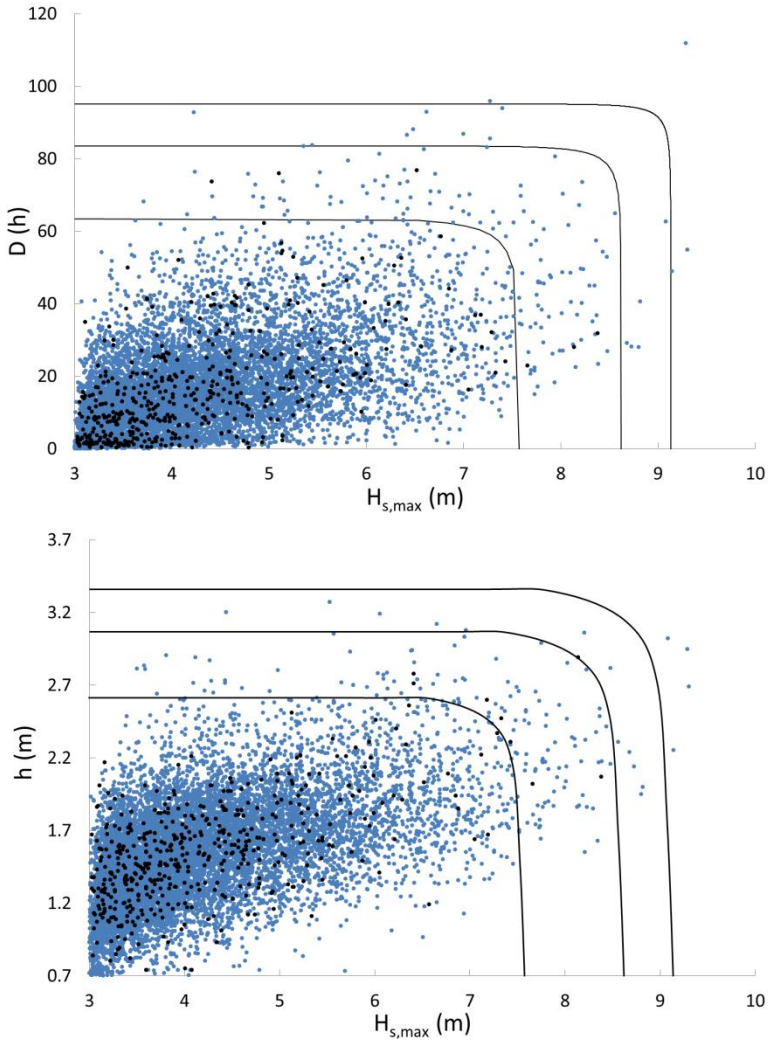

Figure 3.14 Simulated 10^4 storms (blue dots) and observed wave climate (black dots) using Gaussian copula, ($H_{s,max}$, D) in the upper panel and ($H_{s,max}$, h) in winter season (bottom panel), and the return level contours (10, 100 and 500 years).

3.4.2 Physics-combined Gaussian copula method

A method based on a function describing wave steepness (S_p) as a function of $H_{s,max}$ and T_p was used for dependency modelling for $H_{s,max}$, and T_p (Vrijling and Bruinsma, 1980), meanwhile the dependence structure for the rest variables were constructed in the same way as mentioned in Sect. 3.4.1.2. A basic assumption for this method is that the S_p is independent on $H_{s,max}$, which is plausible for the Dutch offshore wave climate (Table 3.2 and Fig. 3.15).

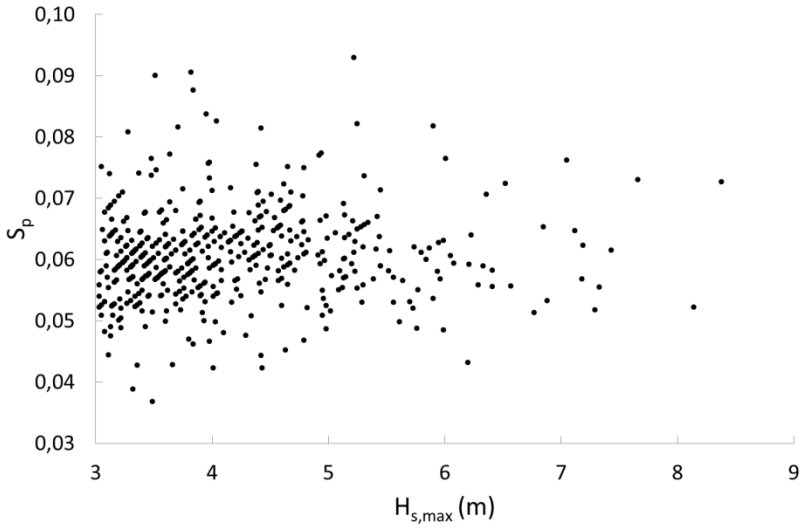

Figure 3.15 Historical measurement of wave steepness

According to the linear wave theory, wave steepness S_p is defined as:

$$S_p = H_{s,\max} / L_0 = H_{s,\max} \Big/ \frac{gT_p^2}{2\pi} \tag{3.17}$$

where L_0 is the deep water wave length and g is the gravity acceleration. Therefore, T_p can be expressed by rearranging Eq.(3.17):

$$T_p = \sqrt{\frac{2\pi H_{s,\max}}{gS_p}}. \tag{3.18}$$

S_p can be randomly generated from its fitted probability distribution. And $H_{s,max}$ was generated through the Gaussian copula. For the study site, a log-logistic distribution is fitted to wave steepness according to its statistical character (Fig. 3.16),

$$F(\ln(x)|\mu,\sigma) = \frac{1}{1+e^{-[\ln(x)-\mu]/\sigma}} \tag{3.19}$$

where μ and σ are the location and scale parameters. Fig. 3.17 (lower panel) shows the comparison between the simulated and measured ($H_{s,max}$, T_p) obtained by the physics-based method.

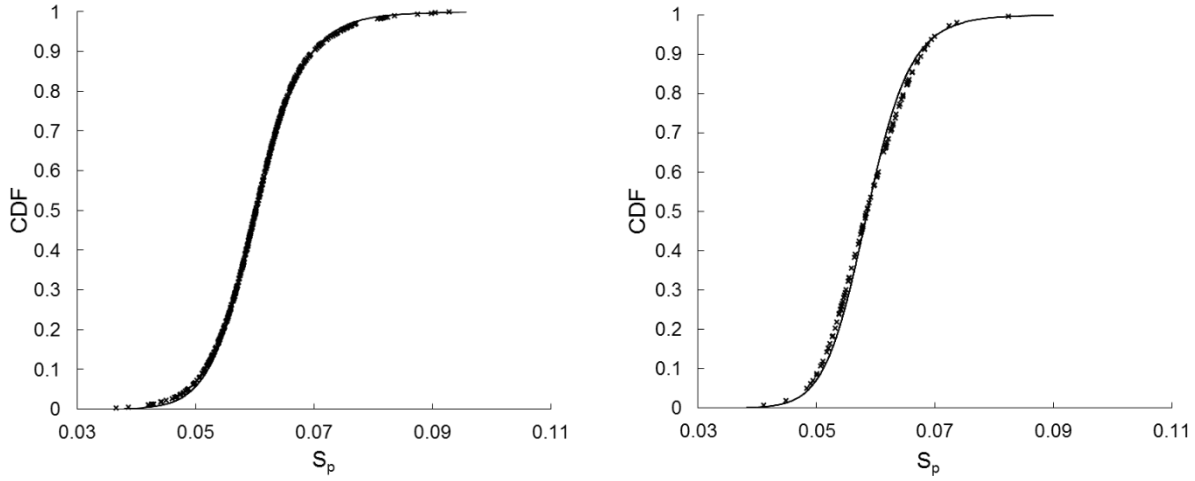

Figure 3.16 Empirical (×) and fitted (solid curves) CDF for S_p in oceanographic winter (left) and summer season.

3.4.3 Logistics model

The logistics model is usually used to construct the joint probability distribution for the bivariate case.

$$F(\tilde{x},\tilde{y}) = \Pr(\tilde{X} \le \tilde{x}, Y \le \tilde{y}) = \exp[-(\tilde{x}^{-1/\alpha} + \tilde{y}^{-1/\alpha})^{\alpha}] \tag{3.20}$$

where $\tilde{x} > 0$ and $\tilde{y} > 0$ are rescaled Fréchet variates (converted from physical scale, *x* and *y*) and $\alpha \in (0,1)$ is the dependence parameter. When $\alpha \to 1$ in Eq. (9), $F(\tilde{x},\tilde{y}) = \exp[-(\tilde{x}^{-1} + \tilde{y}^{-1})]$, corresponding to independent variables; When $\alpha \to 0$, $F(\tilde{x},\tilde{y}) = \exp[-\max(\tilde{x}^{-1}, \tilde{y}^{-1})]$, corresponding to perfectly dependent variables. Hence, the bivariate extreme value distributions generated by the Eq. (3.20) cover all the different types of dependence structure, form independence to perfect dependence.

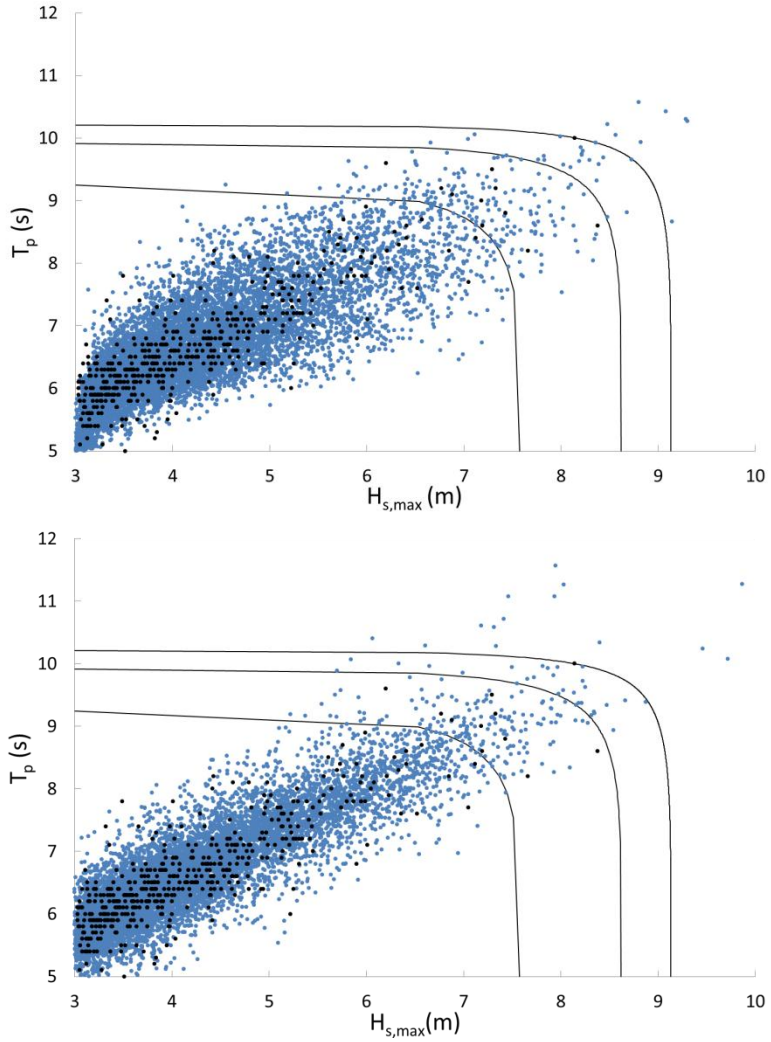

Figure 3.17 Simulated 10^4 storms (blue dots) and observed wave climate (black dots), ($H_{s,max}$, T_p) in winter with Gaussian copula method (upper) and physics-combined Gaussian copula (bottom), and the return level contours (10, 100 and 500 years).

In order to obtain the dependency parameter α, the likelihood function can be written as:

$$L(\alpha;(\tilde{x}_1,\tilde{y}_1),\ldots,(\tilde{x}_n,\tilde{y}_n)) = \prod_{i=1}^{n} \psi(\alpha;(\tilde{x}_i,\tilde{y}_i)) \tag{3.21}$$

where,

$$\psi(\alpha;(\tilde{x}_i,\tilde{y}_i)) = \begin{cases} \dfrac{\partial^2 F}{\partial\tilde{x}\partial\tilde{y}}\Big|_{\tilde{x}_i,\tilde{y}_i} & if\ \ (x,y)\in R_{1,1}, \\ \dfrac{\partial F}{\partial\tilde{x}}\Big|_{\tilde{x}_i,\tilde{u}_y} & if\ \ (x,y)\in R_{1,0}, \\ \dfrac{\partial F}{\partial\tilde{y}}\Big|_{\tilde{u}_x,\tilde{y}_i} & if\ \ (x,y)\in R_{0,1}, \\ F(\tilde{u}_x,\tilde{u}_y) & if\ \ (x,y)\in R_{0,0}, \end{cases} \tag{3.22}$$

$\tilde{u}_x$ and $\tilde{u}_y$ are the threshold parameters of the marginal distributions and converted to the Fréchet scale and

$$R_{0,0}=(-\infty,u_x)\times(-\infty,u_y),\ R_{1,0}=[u_x,\infty)\times(-\infty,u_y],$$
$$R_{0,1}=(-\infty,u_x]\times[u_y,\infty),\ R_{1,1}=[u_x,\infty)\times[u_y,\infty).$$

The transformations

$$\tilde{X}=-[\ln\{1-\varsigma_u[1+\xi(\frac{X-u}{\sigma})]^{-1/\xi}\}]^{-1} \tag{3.23}$$

induces the variable with Fréchet margins for $X>u$. X is one of the wave climate parameters, $\varsigma_u=\Pr\{X>u\}$.

After maximizing $\sum_1^n \ln[\psi(\alpha;(\tilde{x}_i,\tilde{y}_i))]$, the dependency parameters for ($H_{s,max}$, D),($H_{s,max}$, T_p),and ($H_{s,max}$, h) were found and listed in table 3.3.

Table 3.3 Dependency parameter (α) between variates and $H_{s,max}$, 95% confidence intervals are in the brackets.

	D	T_p	h
Winter	0.70 (0.64, 0.77)	0.42 (0.32, 0.51)	0.62 (0.54, 0.70)
Summer	0.67 (0.55, 0.80)	0.41 (0.21, 0.62)	0.72 (0.61, 0.84)

To simulate the four-dimensional joint distribution of wave climate, we estimated the D, T_p and h by using their conditional probabilities given $H_{s,max}$ (Coles and Tawn, 1991) and Gibbs sampling method (Geman and Geman, 1984). Thus, the logistics model can be put into practice in the following way (Callaghan et al., 2008), using $\tilde{x}$ for Fréchet $H_{s,max}$, $\tilde{y}$ for Fréchet D, $\tilde{z}$ for Fréchet T_p, $\tilde{h}$ for Fréchet h:

1. Generate a random number *A~U(0,1)*, and let $\tilde{y}_0=-(\ln A)^{-1}$;

2. Solve the conditional distribution function of $\tilde{x}_1$ given $\tilde{y}_0$

$$A=\Pr\{\tilde{X}\le\tilde{x}_1\,|\,\tilde{Y}=\tilde{y}_0\}=(\tilde{x}_1^{-1/\alpha}+\tilde{y}_0^{-1/\alpha})^{\alpha-1}\tilde{y}_0^{(1-1/\alpha)}e^{-(\tilde{x}_1^{-1/\alpha}+\tilde{y}_0^{-1/\alpha})^{\alpha}+\tilde{y}_0^{-1}} \tag{3.24}$$

with the dependence parameter of ($H_{s,max}$, D), and find the solution of $\tilde{x}_1$;

3. Generate a random numbers *(B,C,D)~U(0,1)*, solve the conditional distribution functions

$$B = \Pr\{\tilde{Y} \le \tilde{y}_1 \,|\, \tilde{X} = \tilde{x}_1\} = (\tilde{x}_1^{-1/\alpha} + \tilde{y}_1^{-1/\alpha})^{\alpha-1} \tilde{x}_1^{(1-1/\alpha)} e^{-(\tilde{x}_1^{-1/\alpha} + \tilde{y}_1^{-1/\alpha})^{\alpha} + \tilde{x}_1^{-1}} \quad (3.25)$$

$$C = \Pr\{\tilde{Z} \le \tilde{z}_1 \,|\, \tilde{X} = \tilde{x}_1\} = (\tilde{x}_1^{-1/\alpha} + \tilde{z}_1^{-1/\alpha})^{\alpha-1} \tilde{x}_1^{(1-1/\alpha)} e^{-(\tilde{x}_1^{-1/\alpha} + \tilde{z}_1^{-1/\alpha})^{\alpha} + \tilde{x}_1^{-1}} \quad (3.26)$$

$$D = \Pr\{\tilde{H} \le \tilde{h}_1 \,|\, \tilde{X} = \tilde{x}_1\} = (\tilde{x}_1^{-1/\alpha} + \tilde{h}_1^{-1/\alpha})^{\alpha-1} \tilde{x}_1^{(1-1/\alpha)} e^{-(\tilde{x}_1^{-1/\alpha} + \tilde{h}_1^{-1/\alpha})^{\alpha} + \tilde{x}_1^{-1}} \quad (3.27)$$

with the dependence parameters of ($H_{s,max}$, D),($H_{s,max}$, T_p),and ($H_{s,max}$, h) for $\tilde{y}_1$ (initial value for the next iteration), $\tilde{z}_1$ and $\tilde{h}_1$;

4. Repeat step 2 and 3 for n times by iterations and get the simulated Fréchet wave climate, {($\tilde{x}_1$, $\tilde{y}_1$, $\tilde{z}_1$, $\tilde{h}_1$),...,($\tilde{x}_n$, $\tilde{y}_n$, $\tilde{z}_n$, $\tilde{h}_n$)};

5. Transform the Fréchet wave climate to the physical scale by using

$$x = u + \frac{\sigma}{\xi}[(\frac{1-e^{-1/\tilde{x}}}{\varsigma_u})^{-\xi} - 1] \text{ when } e^{-1/\tilde{x}} \ge 1-\varsigma_u \quad (3.28)$$

where x is the physical scale, $\tilde{x}$ is the Fréchet scale. When $e^{-1/\tilde{x}} < 1-\varsigma_u$, .

when $x < u$, x was computed from its empirical distribution. Fig. 3.18 shows the dependency between various variates and $H_{s,max}$ for 10^4 simulated storm events during the winter period.

3.4.4 Goodness-of-fit test

The simulation quality is studied and analysed in this section.

For the univariate marginal distribution, the Kolmogorov-Smirnov test (Kolmogorov, 1941) and the Chi-square test (Pearson, 1900) are mostly used to assess whether the fitted distribution is a suitable model for the observational date in the field of engineering. The K–S test is a non-parametric test and can be used to decide if a sample comes from a population with a specific distribution by comparing the empirical cumulative frequency with the assumed distribution function,

$$D_n = \max_x \left| F(x) - F_e(x) \right| \quad (3.29)$$

where D_n is a random variable whose distribution depends on sample size n, $F(x)$ and $F_e(x)$ are the fitted CDF and empirical CDF respectively. For a special significance level $\tilde{\alpha}$, if the discrepancy is small with respect to what is expected from a given sample size, the fitted distribution is accepted. With the simulation result mentioned above (Fig. 3.5 and 3.16), the K-S tests indicated that the simulation of each wave climate was credible at the significance level of 0.05 both in winter and summer except the variable of T_p for the winter period in

physics-combined copula method, which was rejected at the significance level 0.05 but accepted at the significance level 0.01 (p-value is 0.03, highlighted in Table 3.4).

The Chi-square test is performed by grouping the data into cells, calculating the observed and expected counts for those cells, and computing the Chi-square test statistic χ^2:

$$\chi^2 = \sum_{i=1}^{N} (O_i - E_i)^2 / E_i \tag{3.30}$$

where O_i is the observed number of data points in the ith cell, E_i is the expected number of data points in the ith cell and N is the number of non-empty cells. The statistic has an approximate Chi-square distribution when the counts are sufficiently large. If $\chi^2 < C_{1-\tilde{\alpha},f}$, the fitted distribution is statistically significant, where $C_{1-\tilde{\alpha},f}$ is the Chi-square distribution at the cumulative probability $(1-\tilde{\alpha})$, f is the degree of freedom, and $f = N-1-m$, m is the number of parameters for the assumed distribution. The results of Chi-square test for the univariate distributions indicate that all the marginal fitting are statistically significant at the significance level of 0.05.

To quantify the four-dimensional simulation quality, the multivariate goodness-of-fit was carried out.

Besides the univariate distribution, the Chi-square test is also able to be applied for testing the goodness-of-fit of multivariate distributions. The four-dimensional space ($H_{s,max}$, D, T_p, h) was divided into 750 cells, and the Chi-square statistics are 526 (Ⅰ, Archimedean copula), 287 (Ⅱ, Gaussian copula), 347 (Ⅲ, physics-combined Gaussian copula) and 329 (IV, Logistics model) using Eq. (3.30) for the methods in Sect. 3.4. The test results (Table 3.5) show that only the method Ⅱ and IV are acceptable both at a significant level of 1% and 5% (the rejected values are highlighted in the Table 3.5). The simulation quality for these two methods is almost the same. However, the copula simulation appears to be more favoured due to lower values of the Chi-square statistic, thus the simulation quality can be ranked as Gaussian copula > Logistics model > physics-combined Gaussian copula > Archimedean copula according to the Chi-square test result. Moreover, the Gaussian copula is the easiest way compared to the other methods. Therefore, the Gaussian copula is used in the following parts of this thesis.

3.5 Storm sequence simulation

Science the joint statistical distribution of the four-dimensional wave climate has been studied and the simulations have been generated in the above-mentioned section, the storm time series can be simulated by adding the independent wave direction parameter, θ, and the storminess parameter F_s. The empirical distribution of storm frequency was used to obtain the number of storms for every month. For any one month, based on the simulated

number of storms, the storm events of corresponding number can be simulated, after that, these storm events were distributed randomly in this month. By repeating this process for *n* times, storm sequence of *n*/12 years will be generated.

Within time scale of one month, it is plausible to assume the $H_{s,max}$ occurs randomly. But, the time interval between adjacent storms should be noticed, it should be longer than 6 hours according to the definition of independent storms in Fig. 3.2. The as many as required simulated storm sequence on the basis of limit observations can be by far generated.

Table 3.4 K-S test result for univariate simulation, where W for winter season and S for summer season, the Roman numerals indicate the method used in Section 3.4.1.1, 3.4.1.2, 3.4.2 and 3.4.3.

		P-value			
		Ⅰ	Ⅱ	Ⅲ	Ⅳ
$H_{s,max}$	W	0.96	0.77	0.96	0.94
	S	0.83	0.20	0.21	0.46
D	W	0.94	0.88	0.74	0.97
	S	0.09	0.09	0.10	0.13
h	W	0.72	0.8	0.59	0.90
	S	0.75	0.9	0.78	0.73
T_p	W	0.20	0.10	**0.03**	0.07
	S	0.15	0.21	0.48	0.17
S_p	W			0.53	
	S			0.75	

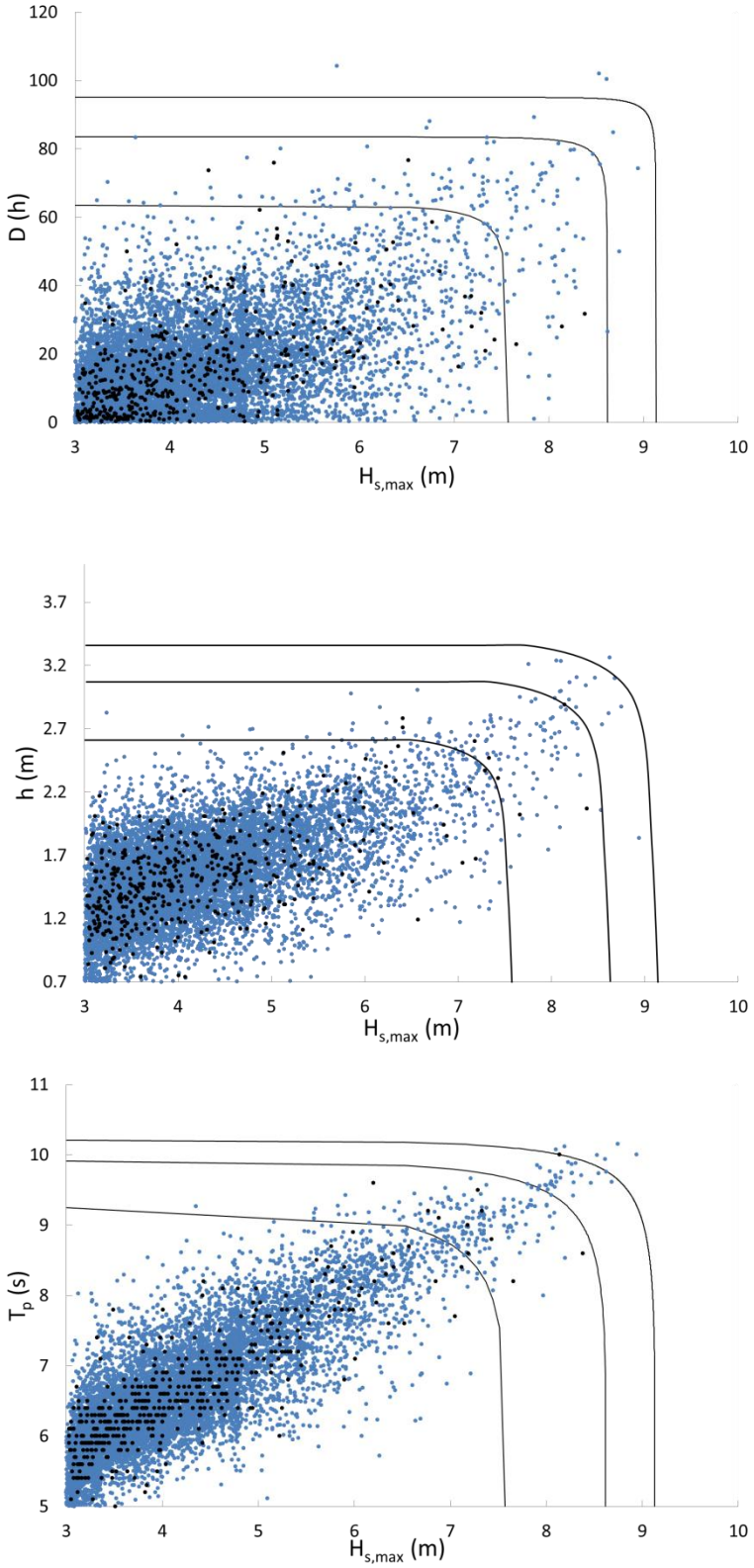

Figure 3.18 Simulated 10^4 storms (blue dots) and observed wave climate (black dots) using Logistic model, ($H_{s,max}$, D), ($H_{s,max}$, h) , and ($H_{s,max}$, T_p) (from top to bottom), in winter by using logistics model, and the return level contours (10, 100 and 500 years).

Table 3.5 Chi-square test for univariate and joint simulation

		Ⅰ		Ⅱ		Ⅲ		Ⅳ	
		$C_{0.95,f}$ ($C_{0.99,f}$)	χ^2	$C_{0.95,f}$ ($C_{0.99,f}$)	χ^2	$C_{0.95,f}$ ($C_{0.99,f}$)	χ^2	$C_{0.95,f}$ ($C_{0.99,f}$)	χ^2
$H_{s,max}$	W	19.68	8.20	18.31	10.11	16.92	6.38	15.51	4.85
	S	19.68	19.02	19.68	13.10	19.68	12.39	5.99	2.31
D	W	15.51	6.82	15.51	5.94	14.07	4.56	12.59	5.46
	S	16.92	1.77	21.03	1.47	19.68	1.88	12.59	1.65
h	W	35.17	15.85	19.68	3.65	18.31	2.42	18.31	2.61
	S	21.02	19.43	11.07	6.01	14.67	6.68	12.59	5.24
T_p	W	16.92	14.26	14.07	9.35	21.03	11.05	16.92	11.22
	S	19.43	**21.03**	25.00	22.15	18.31	5.90	16.92	11.32
S_p	W					25.00	21.31		
	S					19.68	8.69		
Multivariate	W	349(368)	**526**	354(373)	287	342(361)	**347**	353(372)	329
($H_{s,max}$, D, h, T_p)	S	322(340)	**384**	304(321)	277	306(323)	223	342(361)	340

3.6 Discussion

In this chapter, we developed a model to simulate and extrapolate storm sequences from limited observations of wave climate. In this model, four multivariate dependency structures were constructed and compared. With this simulation model, as many simulated storm events as required can be generated for the purpose of coastal hazard analysis and coastal zone management planning.

In summary, the storm simulation includes four steps: fit each observed storm parameter with marginal distributions; construct the dependency structure; simulate the wave climate from the obtained joint probability; give the discrete storm events a time sequence by using the simulated storm frequency.

Several studies tried to construct a multivariable dependency structure by using Archimedean copulas (Corbella and Stretch, 2013; De Michele et al., 2007; Nelsen, 2006). The Gibbs sampling technique coupling with the Archimedean copulas in this paper provides the simplest way for simulating a four dimensional sea storm. Although it is not the recommended approach for the study site data set, it can be noted that the complications of the method are avoided when applying the Archimedean copulas to high-dimensional variables. Moreover, different combinations of the copulas can be applied, which makes the method very flexible. The Gaussian copula was firstly applied to the four dimensional

oceanographic data in the Northern Sea, and it shows its simplicity and effectiveness in storm simulation.

In this chapter, we used $H_{s,max}$ as the connection with the other variables and fitted the bivariate copulas for ($H_{s,max}$, D), ($H_{s,max}$, h) and ($H_{s,max}$, T_p). Other parameters can also be used as the connection variable due to their mutual strong dependency. When applying the Gaussian copula, the asymptotic dependence properties of the data should be noted, as the Gaussian copula is asymptotically independent, which means that the largest values in all components of the multivariate variables cannot occur simultaneously. For high-dimensional multivariate cases, the Gaussian copula was supported when applied to hydrological (Renard and Lang, 2007) and coastal data (Bortot et al., 2000).

The major limitation of the purely statistical model is the lack of physical constraints. Theoretically, the storm parameters of very low probabilities can become limitlessly high, thus the model will generate impractical samples. The method in Section 3.4.2 described the physical relations between $H_{s,max}$ and T_p, which were not able to constrain the parameters to their physical bounds. The physical limitation of wave steepness was also considered in this study. Michell (1893) found that in deep water the theoretical limit for wave steepness is about 1/7. Havelock (1918) confirmed his finding. All the simulated ($H_{s,max}$, T_p) were proven to be within this theoretical limit. In order to include more physical limits, one possible solution for this is to investigate the storm driving forces and the local climatic system for determining the upper limit of the possible wave climate parameters.

Four optional methods for constructing the dependency structure were used and the simulation results were compared, the Archimedean copula method (Ⅰ), Gaussian copula method (Ⅱ), physics-combined Gaussian copula (Ⅲ) and the logistics model (IV). The study and analysis indicated that method Ⅱ and method IV can provide credible storm events predictions at the statistical significance level of 5% for winter and summer season, while the method Ⅱ is able to provide credible simulations at 5% significant level in summer, but failed in winter. The method Ⅰ failed at 1% significant level for both winter and summer season. For 1979 to 2009 Dutch offshore wave climate dataset, the simulation results obtained from method Ⅱ and method IV are very close, and the method Ⅱ simulation result looks a little better according to the Chi-square test. In brief, all these dependency simulation methods can be employed to generate massive synthetic storm events for probabilistic computation, while the selection of the methods should be very data specific and based on the goodness-of-fit test mentioned in this paper. In addition on the goodness-of-fit test, engineering judgment and specific considerations should be taken into account for specific purpose when apply the probability simulation model. Moreover, the marginal distributions and copula function can be replaced by other distribution patterns and copula functions based on the statistical characters of the local wave climate data.

Chapter 4 Dune erosion model

In this chapter, a coastal dune erosion model will be validated for the study site to transform the storm sequence to the dune response.

4.1 Introduction

Once the storms occur, the coast protected by hard structures, such as dikes, will not be eroded. Storm induced hazards will happen in the form of overtopping and dike breaching. While for the coast protected by sand dunes, the coastal profile will reacts to the storms by coastal erosion and accretion. Numerous cross-shore erosion models have been proposed and applied to simulate the coastal changes due to the storms around the world.

Schoonees and Theron (1995) evaluated ten of the most well-known mathematical cross-shore transport models with regard to different model requirements. Vellinga (1982) introduced an analytical model for estimation of the erosion induced by the impact of a storm on a beach profile (DUROS). van Gent et al. (2008) developed dune erosion prediction methods that take effects of wave periods on dune erosion into account (DUROS+). Kriebel and Dean (1993) proposed a convolution method to estimate the coastal profile after a storm based on an equilibrium profile concept. Larson et al. (1990) proposed a semi-process based model, SBEACH. Larson et al. (2004) proposed a simply model based on an assumption

that there is a linear relationship between the wave impact and the weight of sand eroded from the dune.

Roelvink et al. (2009) developed a process-based and time dependent 2DH model of the nearshore and coast called XBeach. It has been validated for a wide range of storms, of varying intensity, across Europe (Van Dongeren et al., 2009). Unfortunately, the XBeach cannot be used directly in a Monte Carlo framework due to its computationally expensive character. For a normal computer, a 10-hour storm will cost about 5 minutes to compute the erosion, and a one-time 100-year storm erosion simulation will cost more than 100 hours. Therefore the DUNERULE (van Rijn, 2009) was selected, which was developed by studying the effects of various key parameters on the computed dune erosion for a reference. The simplicity of the DUNERULE makes it possible to carry out the Monte Carlo simulation within an acceptable time frame. Ideally, the DUNERULE should be calibrated by historical measurements of coastal profile before and after a storm, however, these measurements are not available at the study site, which is very common in the other coastal areas. Therefore, the DUNERULE was calibrated by XBeach.

In the following sections, the dune erosion model will be calibrated and validated for the study site. The alongshore sediment transport was neglected because of simplicity, which is acceptable for the study site based on the observations.

4.2 General description of dune erosion model

In this thesis, the selected erosion model should have the characters which are compatible with the Monte-Carlo simulation technique. The erosion model should give a credible simulation result for one storm event within an acceptable time.

4.2.1 DUROS and DUROS+

The DUROS is one of the most common analytical models for the estimation of coastal dune profile changes impacted by sea storm. The model was developed from a series large-scale physical model tests. The model estimates the post-storm profile and dune erosion volume according to the profile changes compared to the initial profile. The DUROS+ developed the DUROS by taking into account the influence of wave periods. The post-storm profile described by DUROS is given by the equation:

$$\frac{7.6}{H_s}\cdot y = 0.4714[(\frac{7.6}{H_s})^{1.28}\cdot(\frac{w_s}{0.0268})^{0.56}\cdot x+18]^{0.5}-2.0\,, \qquad (4.1)$$

where H_s is the significant wave height (m), w_s is the sediment fall velocity of sand with a diameter $d = d_{50}$(m/s), *y* is the depth beneath surge level (m) and *x* is the horizontal cross-

shore distance from point Q, which is positive seaward. Equation 4.1 describes the curve QR in Fig. 4.1. The slope of PQ is fixed at 1:1 and the slope of RS is fixed at 1:12.5. By horizontally shifting the constructed erosion profile (PQRS) until the erosion and accretion volume are equal, the dune erosion volume will then be obtained. The location of transition point R (x_R , y_R) is given by :

$$\begin{aligned} x_R &= 250 \cdot (\frac{H_s}{7.6})^{1.28} \cdot (\frac{0.0268}{w_s})^{0.56} \\ y_R &= 5.717 \cdot (\frac{H_s}{7.6}) \end{aligned} \tag{4.2}$$

The sediment fall velocity can be obtained by the equation proposed by Hydraulics (1983):

$$^{10}\log(\frac{1}{w_s}) = 0.476(^{10}\log d_{50})^2 + 2.18\,^{10}\log d_{50} + 3.226. \tag{4.3}$$

Considering the effect of the wave period, the Eq. 4.1 is modified by van Gent et al. (2008):

$$\frac{7.6}{H_s} \cdot y = 0.4714[(\frac{7.6}{H_s})^{1.28} \cdot (\frac{T_p}{12})^{0.45} \cdot (\frac{w_s}{0.0268})^{0.56} \cdot x + 18]^{0.5} - 2.0 \tag{4.4}$$

And the location of R (x_R , y_R) is given by:

$$\begin{aligned} x_R &= 250 \cdot (\frac{H_s}{7.6})^{1.28} \cdot (\frac{0.0268}{w_s})^{0.56} \\ y_R &= 5.717 \cdot (\frac{H_s}{7.6}) \end{aligned} \tag{4.5}$$

This 1D erosion model ignores the alongshore sediment transport and assumes the coastline is straight. It is not able to give the profile change process, but only the final post-storm profile with stationary extreme wave climate variables. While in reality, the wave climate variables are time dependent. Moreover, the model does not take into account the influence of the wave direction and the storm duration. Although, the model has been widely used for the Dutch coast, it was mainly applied to compute the safety standard based on the design event method. Therefore, in this thesis, we did not use this model.

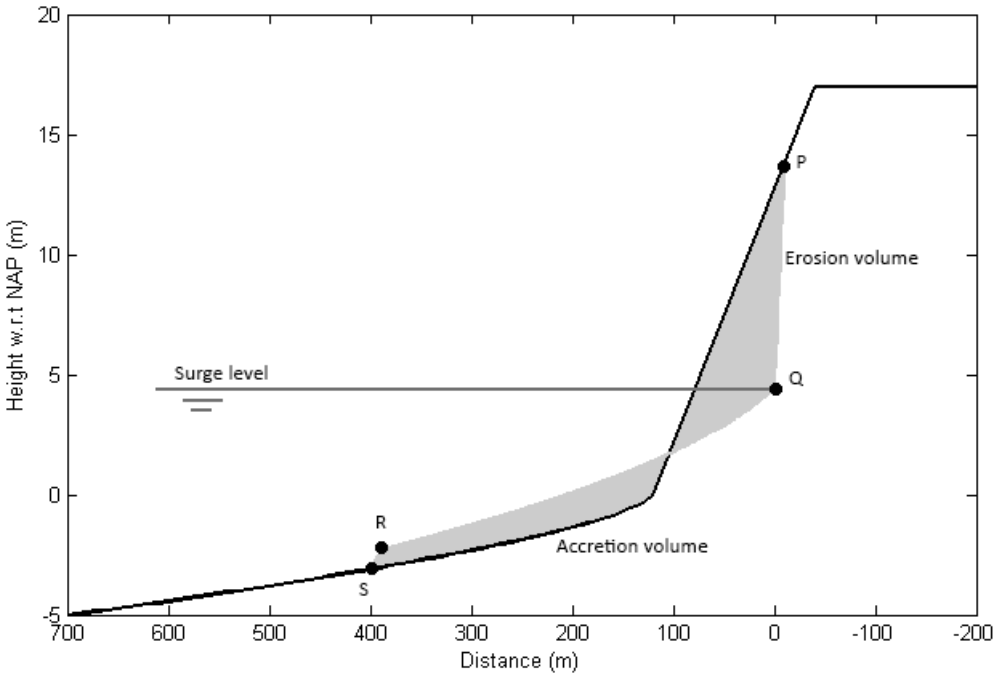

Figure 4.1 Dune erosion profile.

4.2.2 XBeach

The XBeach is a two-dimensional model for wave propagation, long wave, mean flow, sediment transport and morphological changes of the near shore area, beaches, dunes and back barrier during the time-varying storm conditions. The main input of the XBeach includes coastal profile, wave climate, and bed materials.

The model solves the depth-averaged nonlinear shallow water equations using a wave action balance formulation:

$$\frac{\partial A}{\partial t}+\frac{\partial c_x A}{\partial x}+\frac{\partial c_y A}{\partial y}+\frac{\partial c_{\theta_0} A}{\partial \theta_0}=-\frac{D_w}{\sigma} \tag{4.6}$$

in which, where *t, x, y,* θ_0 represent the time (h), distance (m) and angle of incidence (degree) with respect to the *x*-axis, *c* is the wave celerity (m/s), D_w is the wave energy dissipation (w/kg) and the wave action, A, is given by:

$$A(x,y,t,\theta_0)=\frac{S_w(x,y,t,\theta_0)}{\sigma_f(x,y,t)} \tag{4.7}$$

where, S_w (J) represents the wave energy density in each directional bin and σ_f is the intrinsic wave frequency.

The total wave energy dissipation, i.e. directionally integrated, due to wave breaking is modelled according to Roelvink (1993):

$$\bar{D}_w = 2\alpha f_{ref} E_w Q_b$$
$$Q_b = 1 - e^{[-(\frac{H_{rms}}{H_{\max}})^n]}, H = \sqrt{\frac{8E_w}{\rho_w g}}, H_{\max} = \frac{\gamma \tanh kh}{k} \quad (4.8)$$

where, $\bar{D}_w$ is the total wave energy dissipation (w/kg), $\alpha = O(1)$, f_{ref} is the representative intrinsic frequency, E_w is the total wave energy (w) summed over all directional bins, H_{rms} is root mean square wave height (m), ρ_w is the water density (kg/m^3), n and γ are the free parameters, h is the water level (m), k is the wave number and the E_w is given by:

$$E_w(x,y,t) = \int_0^{2\pi} S_w(x,y,t,\theta) d\theta \quad (4.9)$$

The model uses the Generalized Lagrangian Mean (GLM) formulation (Andrews and McIntyre, 1978; Walstra et al., 2000) to represent the depth-averaged undertow and its effect on bed shear stresses and sediment transport. Sediment transport is modelled by using a depth average advection diffusion equation (Galappatti, 1983), *x*-axis only:

$$\frac{\partial hC_d}{\partial t} + \frac{\partial hC_d u^E}{\partial x} + \frac{\partial}{\partial x}(D_h h \frac{\partial C_d}{\partial x}) = \frac{hC_{eq} - hC_d}{T_s} \quad (4.10)$$

where C_d (kg/m^3) is the depth averaged sediment concentration varying on the infragravity time scale, u^E is the cross shore velocity (m/s) including the effects of short wave skewness and asymmetry, D_h is the horizontal diffusion factor, C_{eq} (kg/m^3) is the equilibrium suspended sediment transport concentration, and the adaption time T_s (h) is defined by:

$$T_s = \max(f_{T_s} \frac{h}{w_s}, 0.2)s \quad (4.11)$$

in which, f_{T_s} is the sediment transport depth factor, w_s is the sediment fall velocity (m/s), and s is specific weight $\rho_{sediment} / \rho_{water}$.

Bed up-dating at each time step is based on the continuity equation:

$$\frac{\partial z_b}{\partial t} + \frac{f_{mor}}{(1-p)} \frac{\partial q_x}{\partial x} = 0 \quad (4.12)$$

where p is the porosity, f_{mor} is a morphological acceleration factor and q_x represents the sediment transport rates in *x*-axis. More detailed information about the XBeach can be

found in Roelvink et al. (2009) and all code and document are available at XBeach open source community (www.xbeach.org).

This open source numerical model can give robust estimation of the dune erosion induced by time-varying storm conditions. It is regarded as a state-of-the-art coastal dune erosion model, while the disadvantage is its computationally expensive property.

4.2.3 DUNERULE

The simplified dune erosion rule (DUNERULE) was proposed by van Rijn (2009) from the cross-shore profile model (CROSMOR model), which is based on a 'wave by wave' modelling approach solving the wave energy equation for each individual wave. The CROSMOR model was used to study the effects of various key parameters on the computed dune erosion volume for a reference case that is defined by (Vellinga, 1982) in table 4.1. The computed dune erosion volume for the reference case is 170m^3/m.

Table 4.1 Parameters of Dutch coastal profile; Reference Case.

Parameters	Prototype conditions used by Vellinga(1986)
Offshore significant wave height (m)	7.6 (Pierson and Moskowitz spectrum)
Offshore peak wave period (s)	12
Offshore water depth (m)	21
Storm surge level (m)	5 (w.r.t NAP*)
Storm duration (h)	5
Median sediment diameter (μm)	225
Coastal slope (-)	1:45
Incidence angle (degree)	0

*NAP (Normaal Amsterdams Peil in Dutch) is a vertical datum and the zero level of NAP is approximately Mean Sea level.

A simple equation that indicates the sensitivity of each parameter to the erosion volume was given by van Rijn (2009):

$$R = 170\left(\frac{h}{5}\right)^{\alpha_1}\left(\frac{H_{s,\max}}{7.6}\right)^{\alpha_2}\left(\frac{D}{5}\right)^{\alpha_3}\left(\frac{T_p}{12}\right)^{\alpha_4}\left(\frac{m}{0.0222}\right)^{\alpha_5}\left(\frac{0.225}{d_{50}}\right)^{\alpha_6}\left(1+\frac{\theta_0}{100}\right)^{\alpha_7} \tag{4.13}$$

where, R is the dune erosion volume per unit length (m^3/m), α_1=1.3 for $h<5$ and α_1=0.5 for $h>5$, $\alpha_2=\alpha_4=\alpha_7$=0.5; α_3=0.5 for $D<5$ and α_3=0.2 for $D>5$, α_5=0.3, α_6=1.3, θ_0 is the incidence angle and $\theta_0 \le 30^\circ$.

Equation 4.13 was tested for various storm erosion field databases, and the results indicate that the DUNERULE is most valid for dune erosion under major storms, but also yields realistic result for minor storm events. For more information, please refer to van Rijn (2009).

The DUNERULE is much simpler than XBeach and easier to apply than DUROS. And the model is quite flexible because of its adjustable coefficients. Therefore, in this thesis, the advantage of simplicity of DUNERULE and the robustness of XBeach was coupled by adjusting the coefficients of DUNERULE mode based on the XBeach.

4.3 XBeach model setup

The time dependent XBeach inputs are wave height (H_s), wave period (T) and sea level (h). The H_s and T were assumed to be cosine functions and reach the peak value at the middle time of storm duration. They start to rise at the beginning of the storm with the minimum value of 3m and $0.7\times T_p$, which is chosen pragmatically according to the observations, and fall down to the minimum value again at the end of storm duration (Fig. 4.2).

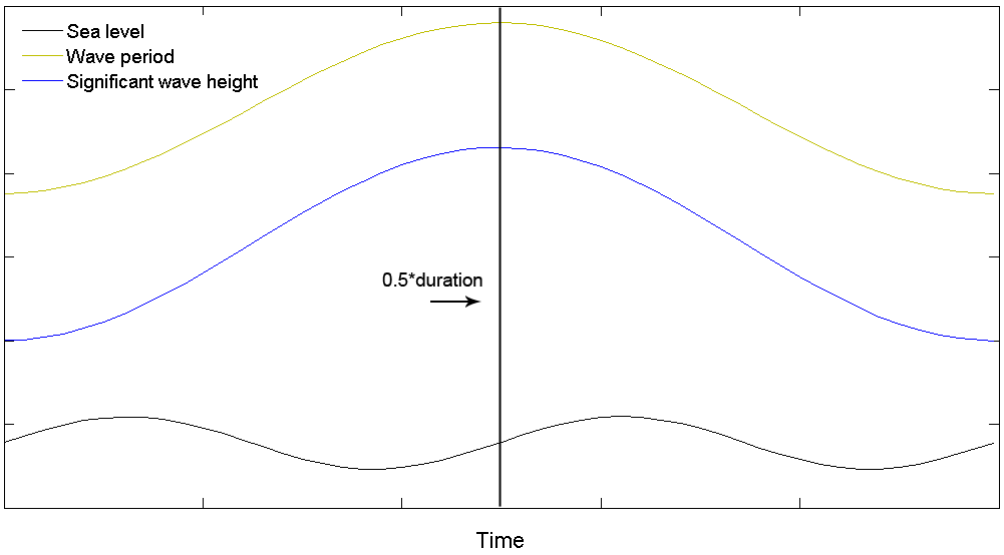

Figure 4.2 Time dependent wave climate parameters.

The selection of time dependent function for sea level is a little more complicated, as the tidal phase will influence the final erosion volume significantly. Fig. 4.3 shows the impact of tidal phase on the final erosion result. The erosion volume behaves as a trigonometric curve. To mitigate this influence in the Monte-Carlo framework method, the mean value was employed in the following computations, that is, tidal phase of $\frac{1}{2}\pi$ in Fig. 4.2 and 4.3.

The No.8250 transect in 2006 was selected as the computation coastal profile (Fig 3.1 and 4.4), and the median sand grain size (d_{50}) is 200μm.

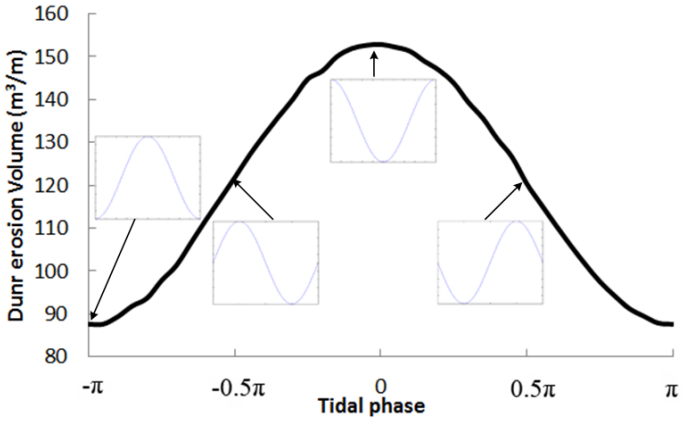

Figure 4.3 Computed dune erosion volumes (m^3/m) by using XBeach and different tidal phases, the smaller curves are the time dependent sea level.

4.4 Adjusted DUNERULE for study site

The DUNERULE was validated based on the XBeach estimates due to the lack of morphological changes record of the beach profile in the study site. The JARKUS only consists of annually coastal profile surveys, which is not sufficient for short term erosion model validation. Therefore, the previously validated process based XBeach was assumed to represent reality, i.e. no model uncertainty. With that assumption, the DUNERULE, that calibrated by XBeach simulations, was therefore also supposed to give reasonable and robust estimates of the numerically predicted erosion volumes. 298 storm events with different combinations of wave climate variables were used to estimate the DUNERULE coefficients.

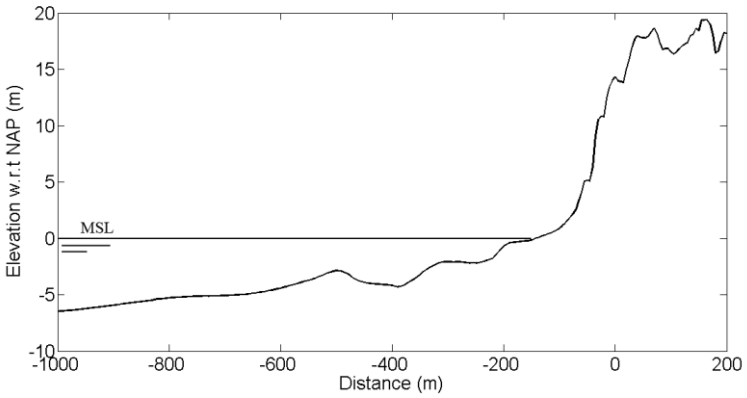

Figure 4.4 Cross-section of No. 8250 transect, NAP (Normaal Amsterdam Peil in Dutch) is the Amsterdam ordnance datum.

At first, the DUNERULE parameters were adjusted with constant wave direction, and the incidence angle was fixed as 0 (i.e. 298° to the map north at the study site). The dune erosion volume will increase when the incidence angle increases from 0 and the erosion volume will decrease when the incidence angle continues to rise. Thus, the influence of wave direction was not able to be described by one monotonic function. A piecewise function will be proposed after determining the rest model parameters.

By applying the trial and error method, the model parameters which make the computed results of DUNERULE closest to the XBeach estimates (Fig. 4.5) were determined without considering the changing wave direction.

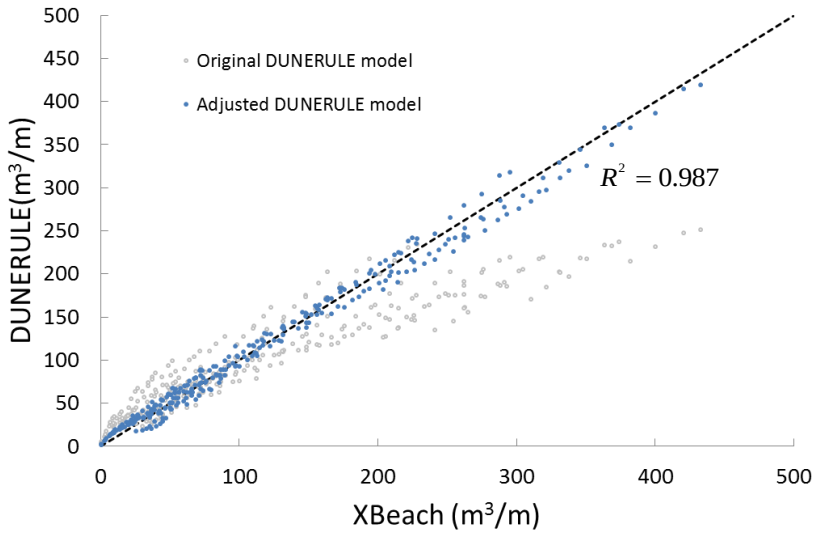

Figure 4.5 Comparison between the DUNERULE and XBeach model, the blue dots are the results produced by the adjusted DUNERULE model, the grey circles are produced by the original DUNERULE model, R^2 is the coefficient of determination.

When the incidence angle of coming wave increases, two adversary effects occur. 1) Oblique incident waves produce a longshore current in the shallow surf zone resulting in an increase of the transport capacity in the shallow surf zone and a larger erosion capacity and 2) oblique incident waves are refracted in the nearshore zone resulting in a decrease of the wave height and hence transport capacity in the surf zone. The first effect will stronger than the second one at first in the range of $0 \sim 18^{\circ}$, and that results an increase trend. Based on the XBeach, an empirical piecewise function for wave direction was obtained, and the adjusted DUNERULE was given as follow:

$$R = 153 A_d \left(\frac{h}{5}\right)^{\alpha_1} \left(\frac{H_{s,\max}}{7.6}\right)^{\alpha_2} \left(\frac{D}{5}\right)^{\alpha_3} \left(\frac{T_p}{12}\right)^{\alpha_4} \tag{4.14}$$

where, α_1 =1.5 for $h < 5$ and α_1 =0.2 for $h > 5$, α_2 =0.3 for $H_{s,\max} < 7.6$ and α_2 =0.9 for $H_{s,\max} > 7.6$, α_3 =0.4, α_4 =1.3 for $T_p < 12$ and α_4 =0.9 for $T_p > 12$, and A_d is given by:

$$A_d = \begin{cases} 1-0.01(270-\theta) \text{ for } \theta \le 270; \\ 1-0.01(\theta-326) \text{ for } \theta \ge 326; \\ 1-0.0107(26-\left|\theta-298\right|) \text{ for } 270<\theta<326. \end{cases} \quad (4.15)$$

In Eq. (4.14), the coastal slope (0.02) and median bed material diameter (200μm) were merged in the equation as constant.

4.5 Dune recovery

For an erosion simulation model with storm time series, the dune recovery rate is vital for both estimating the probabilities of episodic erosion and the long term erosion consequences. The coastal profile will try to reach an equilibrium state according to the sea wave state. Therefore, after an erosion event, the coastal dune will be recovered by sediment transport of wave and aeolian transport of wind to cope with the new wave climate, that is, dune recovery.

The erosion-recovery processes (Fig. 4.6) were simulated on the basis of equilibrium profile concept, i.e. the dune volume will not increase when it reaches the equilibrium volume under the normal wave climate situations, and will not be eroded more if the volume difference from the equilibrium volume is more than the potential erosive capability of the coming storm. For example, a dune has an equilibrium sand volume of 500m^3/m (V_{eq}) with respect to MSL=0, the local dune recovery rate is 0.5 m^3/m/day, a storm with 20m^3/m erosive potential capability (V_p) will diminish the net dune volume to 480m^3/m. After 20 days, the dune will be recovered to 490m^3/m (500-20+20×0.5=490m^3/m), then a storm with 5m^3/m erosive potential capability comes, due to the low erosive capability, the net dune volume will still be 490m^3/m, rather than 485m^3/m. After another 20 days, the dune sand volume becomes 500m^3/m and maintains it until the next storm occurs.

A trial and error method was again employed to estimate the dune recovery rate (C_r). The dune profile at the Noordwijk coast is stable during the observation period, which is plausible according to the field bathymetry measurement. Various C_r values have been tested for 100 years with the simulated storm events in Chapter 3 for 1000 times based on JARKUS data at the Noordwijk coast. The C_r which will maintain the stable dune sand volume is determined via trial and error application of the calibrated DUNERULE and Monte-Carlo technique to Noordwijk coast without SLR. That is, we computed the probabilities of net dune erosion volume with various dune recovery rates and then selected the value which can make the distribution mode be 0 (Fig. 4.7). The 0.3m^3/m/day dune recovery rate thus was determined and adopted in the dune erosion volume and net dune erosion probabilities estimation.

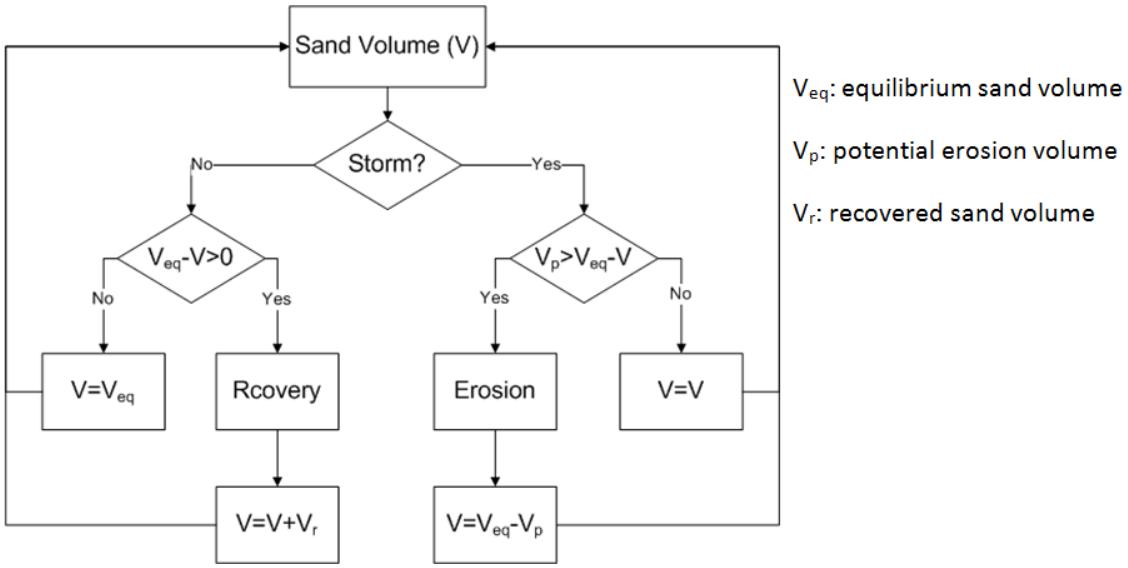

Figure 4.6 Flow chart of erosion-recovery process.

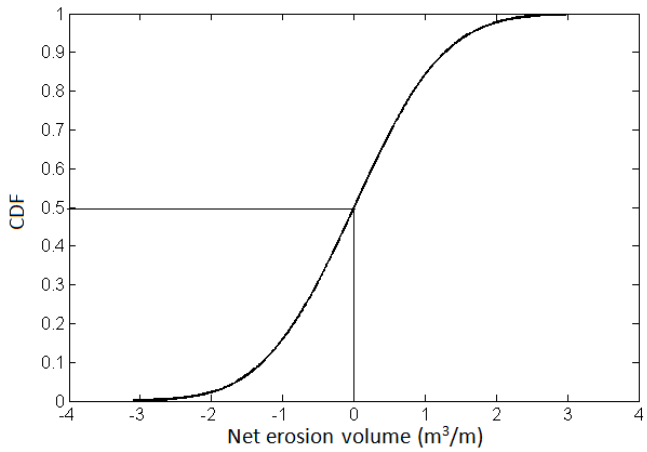

Figure 4.7 CDF of net erosion volume after 100-year simulation when the recovery rate (C_r) is 0.3m^3/m/day.

To compute the equilibrium dune sand volume under SLR, we assumed that the equilibrium dune volume has a linearity correspondence with the mean sea level when the other hydrodynamic loads are average. The time-dependent equilibrium dune volume under SLR scenarios during the simulation period was computed by XBeach with average wave climate parameters ($H_{s,max}$=1.4m, T_p=4s) and the rising sea level over time.

4.6 Model uncertainty

Only the uncertainty induced by the differences between the XBeach model and the DUNERULE model is considered in this section. While the estimation uncertainty come from the computation of XBeach is ignored due to the lack of field observation data.

The model uncertainty was analysed by using Root-Mean-Square Error (RMSE) which was used to measure the differences between values predicted by DUNERULE and values computed by XBeach. The value differences that assumed to have a normal distribution were used to represent the model uncertainty induced by substituting XBeach for adjusted DUNERULE (Eq. 4.14). Thus, the predicted values equal to the sum of XBeach results and the additional uncertainty, ∇,

$$DUNERULE = XBeach \cdot (1+\nabla) \tag{4.16}$$

where $\nabla \sim N(bias, RMSE)$ and

$$bias = \frac{\sum_{i=1}^{N}(x_i/y_i - 1)}{N}$$
$$RMSE = \sqrt{\frac{[\sum_{i=1}^{N}(x_i/y_i - 1)]^2}{N-1}} \tag{4.17}$$

where x_i and y_i are the DUNERULE and XBeach simulations. Fig. 4.8 shows the 95% confidence interval of the model uncertainty.

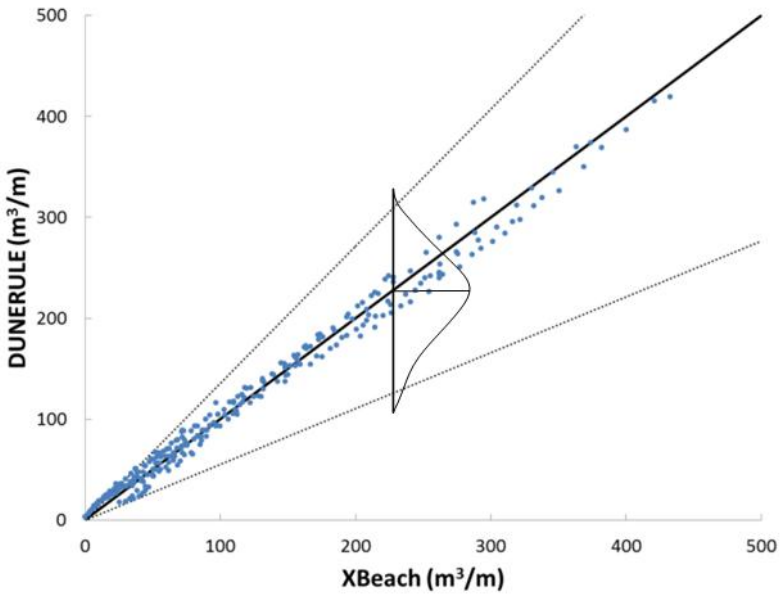

Figure 4.8 The 95% confidence interval of the model approximation (dot lines).

4.7 Discussion

The aim of this chapter is to find an effective and quick dune erosion model which can be used in the following chapters. In this chapter the XBeach was generally introduced and used

for dune erosion simulation and the DUNERULE was calibrated and validated based on the XBeach simulations because of its simplicity and timesaving character, thus it is possible to be employed as the structure function in the Monte Carlo simulation framework. The strong relationship (Fig. 4.7 and 4.8) indicated that it is credible to compute the dune erosion volume by employing DUNERULE instead of XBeach when considering the model uncertainty caused by model simplification. This model uncertainty will contribute to the final simulation results in the next chapters.

The dune recovery process during the interarrival time was illustrated by a flow chat and the recovery rate in the study site was obtained by a trial-and-error method. Due to overwhelming erosion capability during the storms, in the meantime the dune recovery was ignored.

The XBeach simulation results were assumed to represent the actual erosion volume in the case study, this is a compromise due to the lack of morphological change measurements before and after storms. The ideal situation is that the DUNERULE can be adjusted based on the measurements data if it exits, however this cannot be satisfied in many cases.

Chapter 5 Dune erosion probabilities with rising sea level

In this chapter, the coastal morphological response to the storms will be represented by computing the erosion volume probability and dune retreat distance probability under SLR scenarios for the year of 2100. The statistical prediction was obtained by importing the simulated storms (Chapter 3) into the structural function for dune erosion response (Chapter 4) and processing the output using a probabilistic method.

5.1 Introduction

The previous works are the preparations for the coastal erosion probability estimations. Due to the lack of dune erosion field measurements for most coast zone around the world, it is impossible and impractical to fit the quantitative dune response with a probability distribution directly. Thus, we extended the existing hazard source data and transformed it into the required coastal response.

The coastal morphological response was quantified by defining two parameters, coastal dune erosion volume, R (m^3/m), and dune retreat distance, RD (m). The R indicates the short term dune erosion (induced by individual or several consecutive storms) while the RD indicates the long term dune erosion trend. The dune erosion volume was defined as the eroded area above the crossing point of coastal dune profile curves of pre- and post-storm, i.e. the shaded area in Fig. 5.1. The retreat distance was defined as the horizontal distance

between dune foot (3 m w.r.t. NAP was adopted in this thesis) and the furthest distance an eroded extent can reach. And the blue curve in the Fig. 5.1 is the empirical relationship between the erosion volume and the retreat distance. The nonpositive *RD* indicates that the storm is too small to erode the sand above the dune foot, only the sand below the dune foot is eroded.

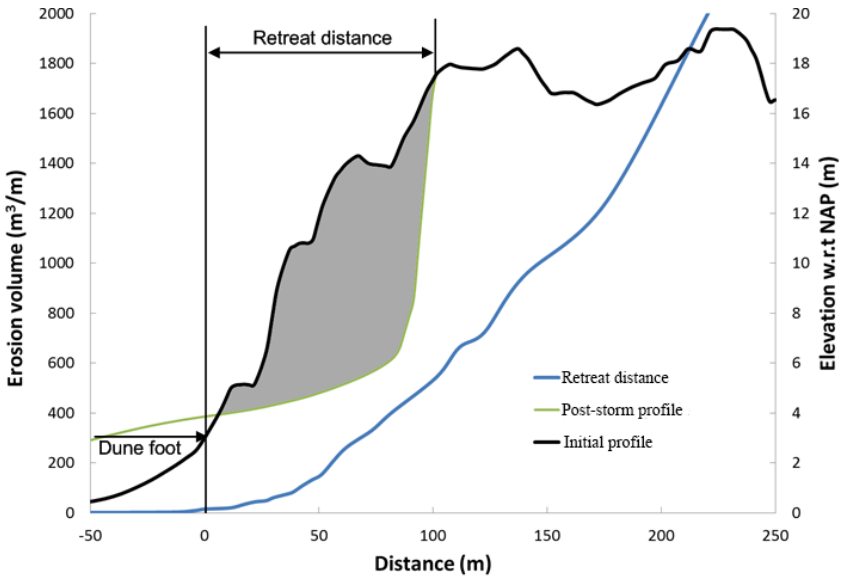

Figure 5.1 Definition of erosion volume *R* and retreat distance *RD* and the relativity between them.

The goal of this chapter is to quantify the dune erosion probability, estimate the impact of SLR on it and the in the end make a comparison with the well-known Bruun Rule. The statistical uncertainty of the erosion volume distributions was estimated in the form of a distribution. Besides, three methods of reducing the estimation uncertainty was proposed. According to the analysis result of Chapter 3, the Gaussian copula was selected to simulate wave climate for erosion probability estimation.

5.2 Sea level rise

For a low-lying country or region like the Netherlands, the possible impacts of sea level rise induced by climate change are a major concern. Three major factors directly lead to SLR. They are sea water thermal expansion due to the global warm, melting of glaciers and ice caps and loss of ice mass from Greenland and Antarctica.

Since the middle 19th century, sea level has been rising, and it is expected to continue for centuries. In 2007, the Intergovernmental Panel on Climate Change (IPCC) projected that during the 21st century, sea level will rise another 0.18 to 0.59m with respect to 1990 (Solomon, 2007), in response to various scenarios for greenhouse gas emissions (Parry et al., 2007). The IPCC Fourth Assessment Report uses several emission scenarios to predict the global climate change in the end of 21th century, however the emission situation for the future is almost impossible to predict, thus, the projection of SLR by the year of 2100 includes a large uncertainty. However, in view of the tremendous impact of SLR on the

human's living environment, it is still advisable to take SLR into account when estimating the natural hazards which are induced or aggravated by SLR.

In this thesis, a SLR projection of 0.4m to 1.05m (moderate scenario and the worst case scenario respectively) was considered on the coast of the Netherlands from 1990 to 2100 according to the recent research of Katsman et al. (2011).

On the basis of equilibrium profile concept, it is assumed that the equilibrium dune volume has a positive correlation with the mean sea level when the other hydrodynamic loads are stable over time. The time-dependent equilibrium dune volume under SLR scenarios during the simulation period was computed by XBeach with average wave climate parameters (that is the wave climate during the inter arrival time) and the rising sea level over time. The *R* and *RD* with SLR is able to be simply estimated by increasing the sea level, *h*, in Eq. 4.14. And SLR trend curve is approximated using a fourth order polynomial function (Ranasinghe et al., 2012).

5.3 Probability of dune erosion volume R

As mentioned before, the probability of dune failure of 10^{-5} per year (return period is 100,000 years) was chosen for the most important parts of the Netherlands. We computed the return period of *R* up to 10^6 years for the study site.

First of all, a 100-year storm sequence (2001~2100) was generated by Gaussian copula, empirical distributions of wave direction θ and the storm frequency F_s discussed in Chapter 3. Then estimate the potential erosion volume for each storm with DUNERULE. After that, according to the dune recovery process (Fig. 4.5), the differences between the post-storm dune volume and initial dune volume after every storm, i.e. *R*, will be calculated and recorded. The GP distribution was fitted to the *R* and the quantiles for the return periods ranging from 1 year to 10^6 years was obtained. For each GP distribution fitting, the lack-of-error analysis (Eq. 3.4) was again carried out for selecting the threshold. One example of the computed *R* and the fitted GP distribution was shown in Fig. 5.2. For estimating the uncertainty, the whole computation procedure above was repeated for 10^4 times and thus 10^4 distribution curves were obtained. And for each return period, there exists 10^4 quantiles which contain the uncertainty information. One example of 10^5 years return period was shown in Fig. 5.3. In this figure, not all the curves were presented in order to avoid a chaotic picture.

For estimating the confidence interval at the 95% confidence level and the distribution mode, a continuous distribution was required to fit the quantiles. The lognormal distribution was chosen based on the statistical analysis of the quantiles for every return period (Fig. 5.3 on the right). The distribution mode is the value that occurs most frequently in a probability distribution

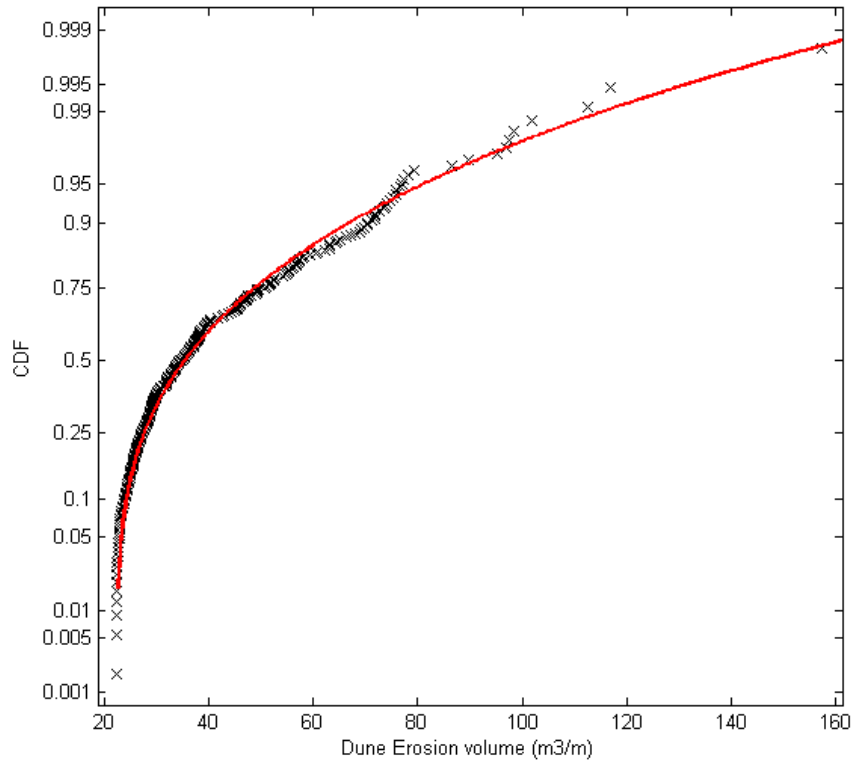

Figure 5.2 Example of an empirical and fitted CDF of *R,* SLR=1.05m.

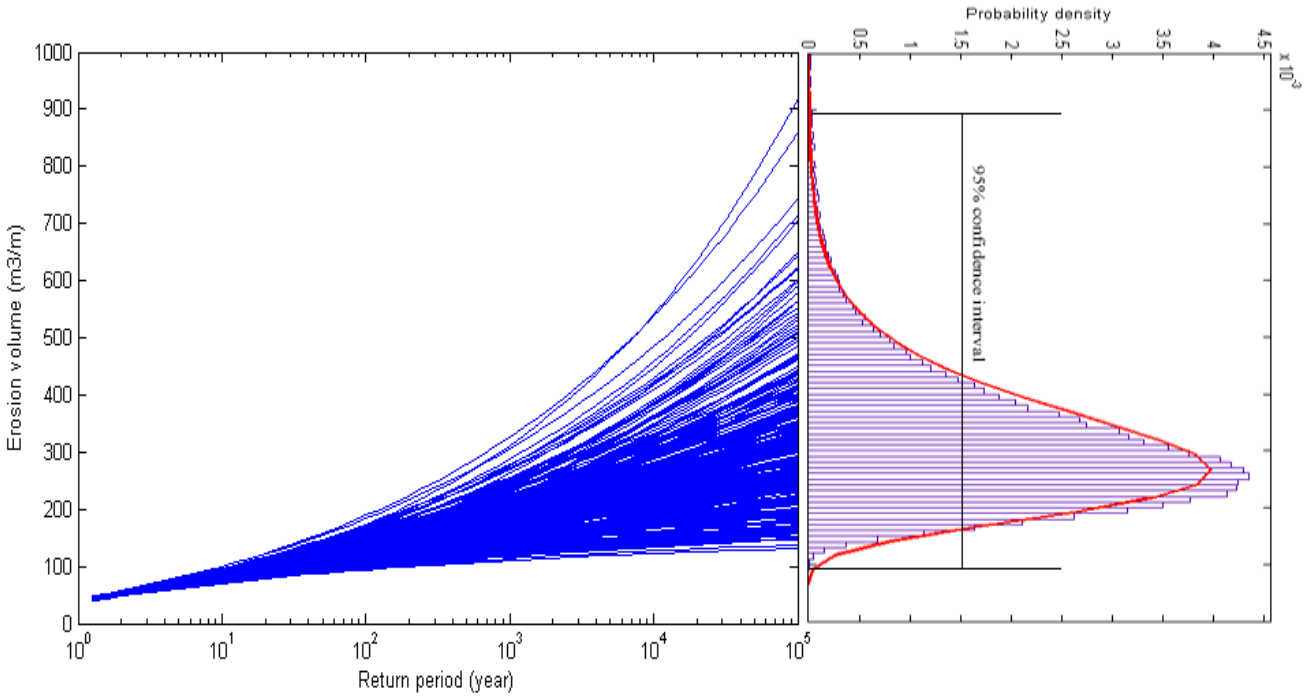

Figure 5.3 Ensemble of simulations (left) and the empirical and fitted lognormal probability density (right) for the quantile values (return period of 10^5 years with SLR=1.05m).

The Fig. 5.2 illustrates the cumulative distribution function of the *R*, while the Fig. 5.3 shows the return period. The return period (*T*) and the exceedance probability (*P*) can be related as follows:

$$(1-p)^{\frac{n}{t}} = \frac{1}{T}, \tag{5.1}$$

where *n* is the number of the events during the period *t*.

In summary, the probability distributions of the *R*, with three SLR scenarios were able to be obtained with the following steps:

1. generate one storm sequence ($H_{s,max}$, D, T_p, h, θ and F_s) for 2001~2100 using the Gaussian copula and the method mentioned in Chapter 3;
2. estimate the potential dune erosion volume of each storm event using the adjusted DUNERULE;
3. generate the inter-arrival time between two independent storms and compute the dune erosion *R* considering the dune recovery process (Fig. 4.5);
4. fit the computed *R* with a GP distribution and compute the quantiles of each concerned return period;
5. repeat the above steps for 10^4 times;
6. for each concerned return period, fit a lognormal distribution and compute the 95% confidence interval and the distribution mode.

The probabilistic estimate of the *R* (orange solid curves) with 95% confidence interval (red dash curves) for different SLR scenarios was shown in Fig. 5.4. For comparison, the erosion volume computed by the observed storm data was extrapolated with GP distribution and indicated with a black solid curves in Fig. 5.4. When SLR=0, the computed distribution mode is almost the same with that derived from the observed storm data, which is expected. When considering the rising sea level over the 21th century, the orange curves shift a little as expected.

The return period in Fig. 5.4 is different from the conventional meaning of the return period, which means for any year an event will be exceeded at a probability of 1/return period. For example, a 100-year R has a 1/100, or 1%, chance of being exceeded in any one year in the conventional sense. While considering the rising sea level over time, this chance is increasing over time in fact. Consequently, the return period in Fig. 5.4 should be interpreted like this, considering the 100 year as a whole, the return period is the inverse of the probability that the event will be exceeded in 100 years (or more accurately the inverse of the expected number of occurrences in 100 year). Thus, the 100-year R will be exceeded once in 100 years, rather than having a 1% chance of being exceeded in any one year.

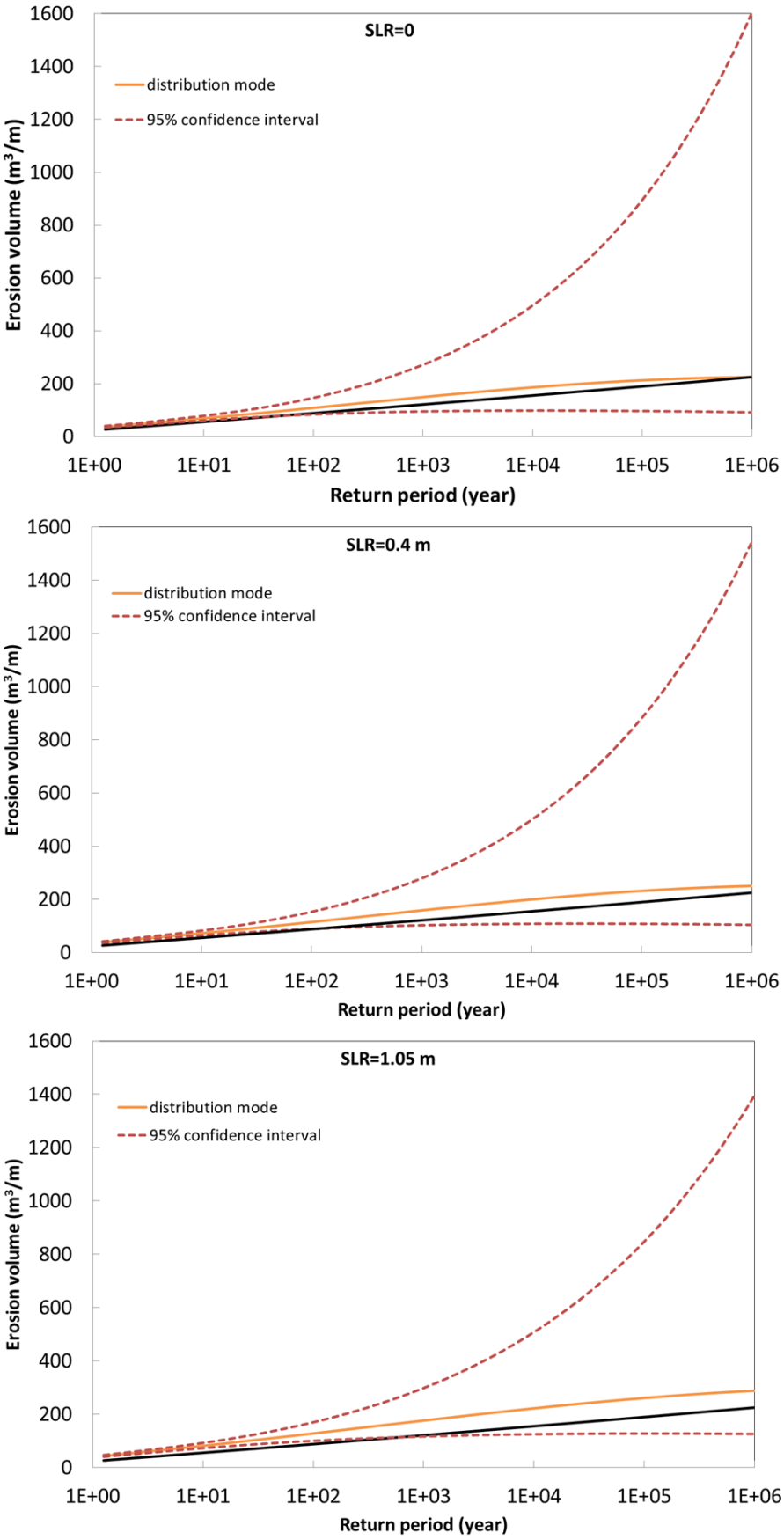

Figure 5.4 Return level plots for dune erosion volume with different SLR scenarios, the black solid curve is the erosion volume computed with the observed storm data and fitted to GP distribution.

5.4 Constrained uncertainties

The probabilistic model purely considers the statistical uncertainties without combining the limitation of the North Sea wave climate situation, i.e. the physical constraints of ($H_{s,max}$, D, h, T_p). Theoretically, the storm parameters of very low probabilities can become limitlessly high, thus the model will generate impractical samples which are impractical in reality. Moreover, the simulated samples with very long return period were not as many as the samples with shorter return period and led to large deviation, consequently the confidence interval at the long return period became dramatically huge. In Fig. 5.4, the confidence interval becomes smaller when SLR increases, the main reason is that the higher the SLR is the more the extreme value samples are, and thus the deviation is smaller which makes the confidence interval narrower. In this section, three methods were proposed to reduce the uncertainties and narrow the confidence interval.

5.4.1 Estimate maximum storm event

The concept of fully developed sea (FDS) was introduced for estimating the possible maximum R responding to the possible most extreme wave climate for the study site. The FDS condition is the maximum ocean waves or sea state that can be produced by a given wind force blowing over sufficient fetch and duration. (Le Roux, 2008) proposed the equations to calculate the wave height and wave period with insufficient fetch and duration:

$$H_s = 863.042(\rho_a/\rho_w)(2U^2/9g)(F_f/F_{f\_FDS})^{1/2}(T_D/T_{D\_FDS})^{3/4}, \tag{5.2}$$

$$T_p = (18\pi^2 H_s)^{1/2}, \tag{5.3}$$

where, ρ_a is the air density (kg/m^3), ρ_w is the sea water density (kg/m^3), U is the wind speed (m/s), F_f is the fetch (m) and F_{f_FDS} is the necessary fetch for a FDS state (m), T_D is the duration of the wind (s), and the T_{D_FDS} is the necessary duration for a FDS state (s).

The fully developed offshore significant wave height and wave period as a function of wind speed were given by (Le Roux, 2008):

$$T_{p\_FDS} = 2\pi U/g, \tag{5.4}$$

$$H_{s\_FDS} = gT_{p\_FDS}^2/18\pi^2. \tag{5.5}$$

For FDS conditions, given a wind speed, the necessary fetch (F_{f_FDS}) and duration (T_{D_FDS}) can be obtained with the fully developed wave height H_{s_FDS}:

$$F_{f\_FDS} = \frac{gH_{s\_FDS}^2}{1.70569\times10^{-3}U_*^2}, \tag{5.6}$$

$$T_{D\_FDS} = (\frac{gF_{f\_FDS}}{5.23\times10^{-3}U_*^2})^{2/3}(U_*/g), \tag{5.7}$$

where, the wind friction velocity U_* is given by:

$$U_* = \sqrt{0.001(1.1U + 0.035U^2)}. \tag{5.8}$$

Most of the winds along the Holland coast come from the North Sea, a marginal sea of the Atlantic Ocean. From 1971, about a total of 500 years wind observation data are available in 20 stations in the Netherlands. The prevailing wind direction is southwest (23%), similar as the prevailing wave direction, followed by west (16%), east (13%) and northwest (12%) (Stolk, 1989). The storm winds causing the largest wind set-up along the coast are coming from northwest (van Rijn et al., 2002), where the sea will suffer the longest fetch to the Dutch coast. The highest measured wind speed is 28.1 m/s at Leeuwarden in 13 November, 1972 with a direction of 310° to the map north, and the strongest wind only lasted less than one hour. Based on the geomorphic and the climatic feature of the North Sea, some extreme values for the wave climate parameters were designed for calculating the possible maximum *R*.

The upper limit of the wind speed was assumed to be 50 m/s (Holthuijsen et al., 1994), this is a crude estimation. According to the statistical analysis of the observations for all the Dutch stations (Smits, 2001), the wind speed of 10^4 years return period is about 40 m/s, then, it is reasonable to use 50 m/s as the upper limit. The wind fetch and duration were set as 500 km and 20 hours respectively. According to the extreme wind speed measurement at all stations, the 50 highest wind speed event occurs within the direction ranging from 210° to 310°, and within this wind direction range, the longest fetch is about 500 km. The wind duration was set as 20 hours, while in reality, it is impossible to last such a long time for an extremely strong wind event. The maximum significant wave height (11.29m) and wave period (14.30s) were then obtained by Eq. (5.2-5.8).

For computing the extreme *R*, 10^6 years return period *h* and *D* were computed from their GP distributions, which are 4.4 m and 145 hours. Ignoring the impact of wave direction (which actually will decrease the *R*), the maximum *R* obtained by DUNERULE for the return period of 10^6 years is 811 m^3/m, 924 m^3/m and 1088 m^3/m with different SLR scenarios, *i.e.* at this return period, the upper confidence interval is constrained by the maximum possible *R*. In Fig. 5.5, the original confidence interval was constrained by the blue lines connecting the computed maximum *R* and the upper limit of 10^4 years confidence interval. The simulations results actually are the theoretical physical upper limit, but on the safe side, the upper confidence levels were set as the maximum values.

5.4.2 Constant SLR

In section 5.3, SLR was assumed to increase gradually over the 100 years. Therefore, the extreme storms tend to occur when close to the year of 2100 and consequently large variance was caused by the less extreme storms. That means, the more the extreme values are, the smaller the variance is and thus the narrower the confidence interval is. In Fig. 5.4, the confidence interval for the worst case SLR projection is the narrowest, which is contrary

to the common sense. This phenomenon was induced by having more extreme values under the worst case SLR projection scenarios.

To reduce the variance thereby reduce the confidence interval, the worst case SLR scenario (1.05m) was added to every year, that is to say, SLR=1.05 (m) is constant from 2001 to 2100. Then in this case, the probabilistic distribution and the 95% confidence interval of the *R* was computed. The computed distribution mode is larger than the result in Fig 5.4 apparently, but the confidence interval becomes narrower. In fact, the original confidence interval should not wider compare to the hypothetical scenario. Thus, for the purpose of reducing the uncertainties, the upper limit of the confidence interval in Fig. 5.4 was replaced. The result was shown in Fig. 5.5 with blue dot dash curves.

5.4.3 A pragmatic method

A pragmatic method can also be proposed to represent a more realistic estimation of the erosion. In this study, the uncertainty was simply constrained by keeping the lognormal distribution standard deviation parameter constant for the return period higher than 10^4, which was chosen pragmatically based on the research of Roscoe and Diermanse (2011). That is, the difference between constrained confidence interval and the distribution mode is constant from 10^4 year return period. In Fig. 5.5, the dot lines illustrate the constrained confidence intervals.

This method should be used with great caution. Although, the uncertainties can be reduced very simply, this method does not supported by any theoretical basis, it is pragmatic and empirical. Thus, this method should be applied coupled with expert advices and the specific situations on the ground.

Table 5.1 lists all the computed critical erosion volume and the upper limits of confidence intervals obtained from different methods.

Table 5.1 Estimation of dune erosion volume (m^3/m) probability and the constrained confidence interval (CI, m^3/m), the values in column constrained upper CI are the computed result using the method in section 5.4.1, 5.4.2 and 5.4.3 respectively.

Return period (year)	Observation fitting	SLR = 0			SLR= 0.4 m			SLR = 1.05 m		
		Mode	CI	Constrained upper confidence limit	Mode	CI	Constrained upper confidence limit	Mode	CI	Constrained upper confidence limit
10^2	88	109	(84, 146)		115	(89, 153)		128	(100, 170)	
10^3	121	150	(95, 271)		159	(103, 279)		177	(117, 299)	
10^4	155	186	(98, 496)	496, 445, 496	200	(108, 500)	500, 445,500	222	(126, 508)	508, 445, 508
10^5	190	213	(97, 895)	654, 612, 522	230	(108, 882)	712, 612, 532	261	(128, 806)	798, 612, 543
10^6	225	225	(92, 1602)	811, 823, 534	251	(105, 1544)	924, 823, 550	289	(126, 1396)	1088, 823, 574

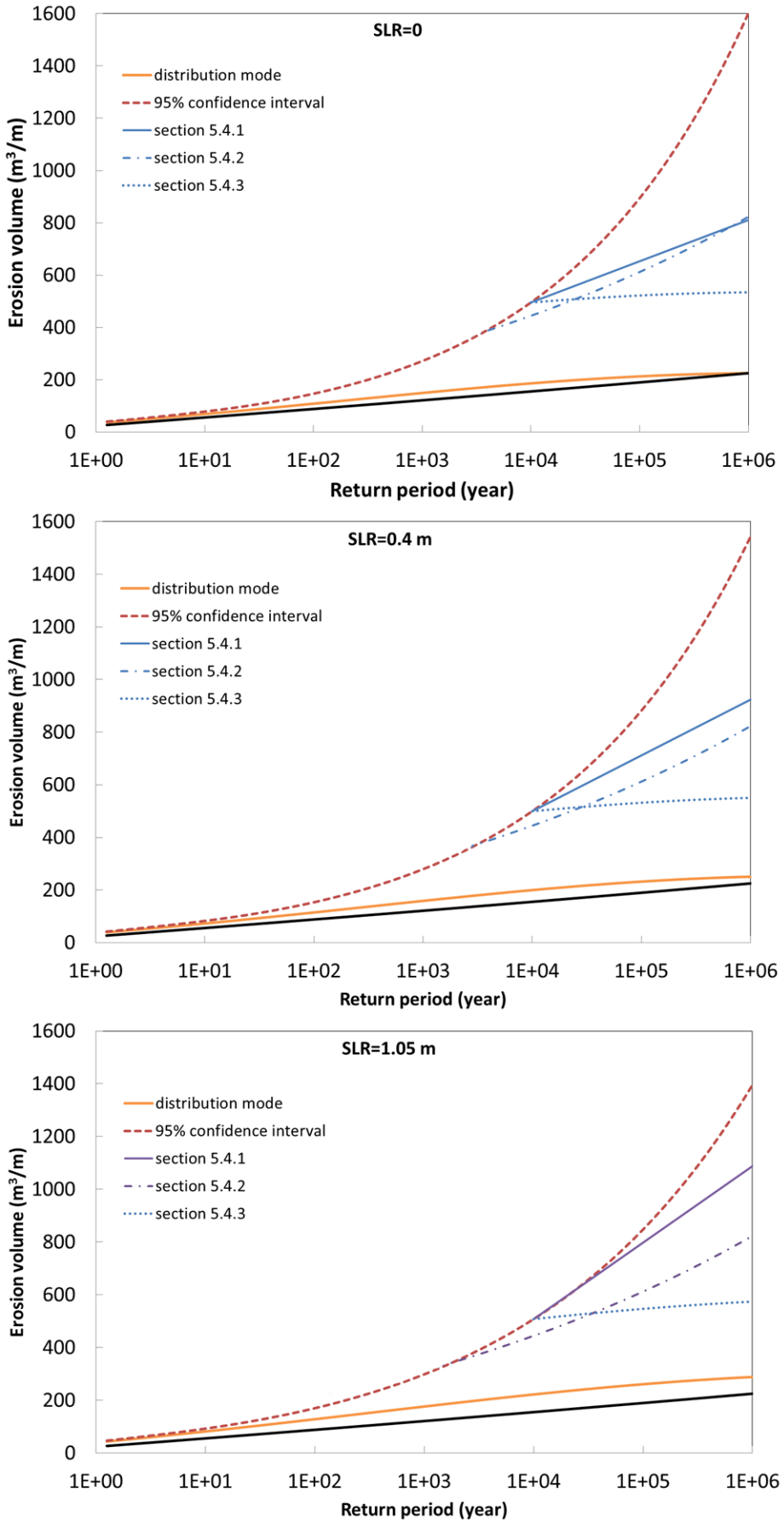

Figure 5.5 Constrained upper confidence intervals by using the methods in section 5.4.

5.5 Probability of dune retreat distance

5.5.1 Short term retreat distance

The *RD* which is induced by the episodic storms is defined as short term *RD*. It can be obtained by converting erosion volume to a retreat distance according to the correlation between *R* and *RD* in Fig. 5.1. The critical *RD* with different return periods were computed by interpolation and presented in Table 5.2.

Table 5.2 Critical *RD* (m) of distribution mode with reference to dune foot (+3.00m NAP).

Return period (year)	$RD_{SLR=0}$(m)	$RD_{SLR=0.4}$(m)	$RD_{SLR=1.05}$(m)
10^2	40	41	44
10^3	49	51	54
10^4	56	58	62
10^5	61	63	68
10^6	62	67	72

5.5.2 Long term retreat distance

Besides the short term dune erosion induced by episodic storms, the long term dune erosion is also worthy of attention. The long term retreat distance is the final retreat distance at the end of 2100. The long term *RD* shows the cumulative effect of *R*, and therefore it can be used as an indicator of beach profile evolution over a long period, for instance, 100 years in this study. Here, the alongshore sentiment transport was neglected, as the main objective of the research is to investigate the extreme dune erosion probabilities due to SLR, and on the other hand, the coastline in the study site is quite stable according to the field measurement (JARKUS dataset).

The first three computation steps are the same with that in section 5.3. At the end of step 3, a simulated net *R* value of 2100 will be obtained. Then repeat (1)-(3) for 10^3 times. After that, fit the simulated net *R* with an empirical distribution. The probabilistic estimation of net *R* at Noordwijk aan Zee coast is shown in Fig. 5.6. Then, according to the correlation between net *R* and *RD* (Fig. 5.1), the *RD* can be obtained by interpolation. When SLR=0, the retreat distance has a 1% probability of exceeding 35m, and a 10% probability of exceeding 21m. When SLR=1.05m, the critical value for 1% probability is 50m and 35m for 10% probability (Table 5.3). When dealing with the final dune retreat distance, the simulation stops at the end of winter season of 2100, when the dune had experienced a storm season before being recovered dramatically, as the worst case erosion consequence is the most significant for coastal safety.

Table 5.3 Exceedance probability of *RD* (m) and R (m^3/m) for different SLR scenarios.

Exceedance probability	$[RD, R]_{SLR=0}$	$[RD, R]_{SLR=0.4}$	$[RD, R]_{SLR=1.05}$
0.5	[8, 20]	[13, 29]	[21, 46]
0.1	[21, 48]	[27, 63]	[35, 91]
0.01	[35, 91]	[41, 114]	[50, 154]

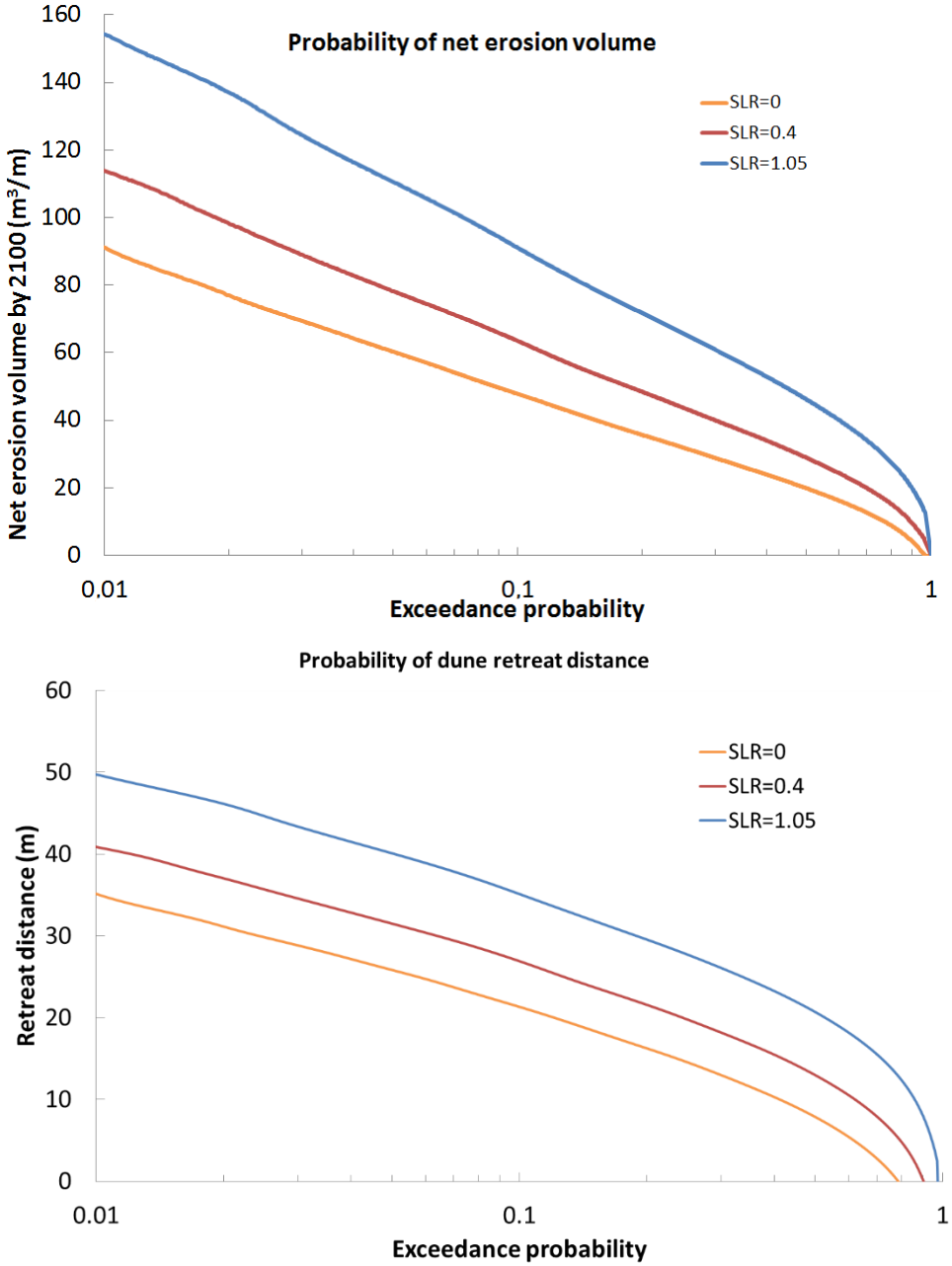

Figure 5.6 The exceedance probability of net erosion volume and retreat distance by 2100.

5.6 A comparison with Bruun Rule

The first and best known model relating coastal retreat to SLR is the Bruun Rule (Bruun, 1962). This simple model is based on the principle of two dimensional mass conservation to estimate the sand eroded from the beach and deposited to the offshore. The Bruun Rule is expressed as:

$$RD = L_c S / (B + DoC), \tag{5.9}$$

Where, *DoC* (m) is the depth of closure, the maximum depth of exchange of material between nearshore and offshore, at the point of closure, the water is presumed to be sufficiently deep that sediment transport by waves is negligible, L_c is the distance from closure depth to coastline (m), *S* is SLR (m), *B* is the dune crest height with respect to MSL (m), and *RD* is the dune retreat distance (m), Fig. 5.7.

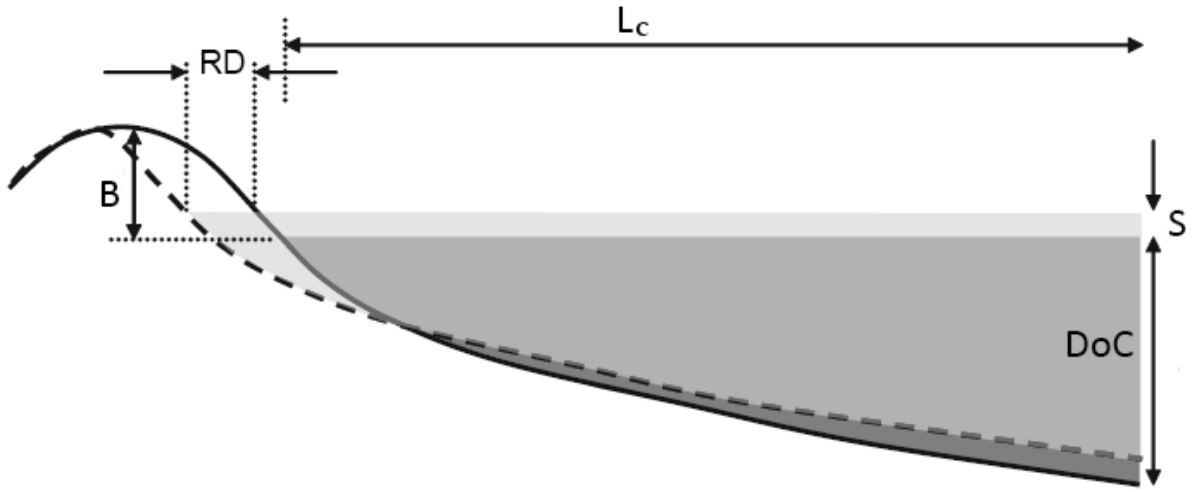

Figure 5.7 Bruun rule for coastal retreat due to SLR (after Ranasinghe et al. (2012)).

Bruun rule is a very simplistic analysis tool. Recent comprehensive and objective reviews of all attempts to verify the Bruun Rule to date have concluded that while it may be suitable for qualitative first-pass regional scale assessments, its relatively low quantitative accuracy and robustness renders the Bruun Rule unsuitable for local scale assessments in which reliable estimates are required (Ranasinghe and Stive, 2009; Stive et al., 2009). Because the position of *DoC* in the Bruun rule determines the value of L_c, the cross-shore distance to *DoC*, uncertainty in shoreline position predictions will vary systematically (FitzGerald et al., 2008). For example, overestimates of *DoC* will result in longer cross-shore profiles, L_c, and consequently produce larger values of shoreline recession (Komar et al., 1991). And the determination of the *DoC* is always associated with significant uncertainty. This uncertainty range in the active profile slope alone would produce Bruun rule recession estimates that could vary by about 500% at Sydney, Australia (Ranasinghe and Stive, 2009).

For comparison, the Bruun rule was applied to the study site. Before using the Eq. 1, the closure depth should be estimated, which is the main input for the Bruun rule. (Hallermeier, 1981); Hallermeier (1983) defined three profile zones, i.e. the littoral zone, shoal or buffer zone and offshore zone. This partition defined two closure depths, namely: (1)an "inner" (closer to shore) closure depth h_{in} at the seaward limit of the littoral zone, and (2) an "outer" or "lower" (further from shore) closure depth h_{out} at the seaward limit of the shoal/buffer zone.

From Hallermeier (1981):

$$DoC_{in} = 2.28H_e - 68.5(\frac{H_e^{\ 2}}{gT_e}), \tag{5.10}$$

where H_e is the effective significant wave height exceeded for 12 hours per year (that is, the significant wave height with a probability of exceedance of 0.137%), and T_e is similarly defined for wave period. Based on measured Dutch offshore wave data, H_e is about 5.0m and T_e is about 7.7s.

From Hallermeier (1983):

$$DoC_{out} = 0.018H_mT_m\sqrt{\frac{g}{D_d(S_g - 1)}}, \tag{5.11}$$

where H_m and T_m are the median wave heights and periods respectively, D_d is the median sediment diameter which is 0.2mm in the study site, and S_g is the specific gravity of sand (about 2.6). Based on measured Dutch offshore wave data, H_m is about 1.07m and T_m is about 4.3s.

Houston (1995) used properties of a Pierson-Moskowitz wave spectrum (Rijkswaterstaat, 1986) and a modified exponential distribution of significant wave height over time to express the *DoC* in terms of mean annual significant wave height $\overline{H}_s$ (about 1.25m for the study site):

$$DoC_{in} = 6.75\overline{H}_s. \tag{5.12}$$

Table 5.4 shows the calculated *DoC* and the corresponding coastal retreat distance obtained by Bruun rule.

For the moderate SLR scenario (0.4m), the Bruun rule estimates of coastal retreat distance lie between 25% and 5% probability of exceedance when compared to Fig. 5.6. While for the worst case SLR scenario (1.05m), exceedance probabilities of the Bruun estimates are smaller than 1%. The Bruun rule estimations appear to highly conservative for both the moderate and the worst case scenarios. In terms of retreat rate, regardless of SLR scenarios,

the coastal retreat rate is the same for the same *DoC*. This indicates that SLR and the *RD* have a linear relation (Eq. 5.9), which is the basic assumption of Bruun rule. It is due to the lack of taking into account the physical processes of coastal recession when applying the Bruun rule. Moreover, a set of discrete values of *RD*, which is lack of corresponding exceedance probability, obtained by using Bruun rule is quite insufficient for future risk analysis and management.

Table 5.4 Coastal retreat distance estimation by using Bruun rule.

Method	Depth of closure (m)	SLR (m)	Coastal retreat distance (m)	Coastal retreat rate (*RD/SLR*) (-)
Hallermeier (1981)	8,45	0.4	22	55
		1.05	58	55
Hallermeier (1983)	14,25	0.4	37	93
		1.05	98	93
Houston (1995)	8,44	0.4	22	55
		1.05	57	54

5.7 Discussion

While the probabilistic modelling framework presented here is generic, the definition of independent storm events and the parameters of the adjusted DUNERULE model are only valid for the study site. For application to the other locations, the model has to be adjusted according to the local situation. XBeach model simulation results were assumed to represent the actual erosion volume in the case study. This is a compromise necessitated by the lack of morphological change measurements before and after storms at the study site. The ideal situation is that the DUNERULE model can be adjusted based on the measured data if it exists, however this cannot be satisfied in most cases. If surveys of the coastal erosion volume change exists, not only should the erosion model be calibrated, but also the definition of a storm event should be carefully evaluated. In general, increasing the threshold wave height of storms will lead to a shorter storm duration, and decreasing the threshold will increase the storm duration. Therefore, the threshold for the storm definition needs to be carefully studied on the basis of the field measurements. Besides the XBeach and DUNERULE model, alternative erosion models that have been previously used within the same modelling framework include SBEACH (Larson et al., 1990), Kriebel & Dean model (Kriebel and Dean, 1993) and an analytical model, presented by Larson et al. (2004). Generally speaking, the best model is the model that has been calibrated and/or developed for a specific coastal stretch. When applying the Monte Carlo simulation technique, using the most complicated model might not be feasible due to the computational cost.

In the present application only the sea level trend is considered while the other climate change impacts such as variations in storm wave characteristics are ignored. This is partially justified by recent studies (De Winter et al., 2012) which conclude that not enough scientific

evidence is available to support scenarios with increased wave height or storminess in the North Sea. This combined with the fact that SLR is unlikely to affect deep water wave conditions (an increase of maximum 2% is projected during the most extreme events). De Winter et al. (2012) implies that it is not unreasonable to assume that the probabilistic distribution functions of deep water $H_{s,max}$ and the T_p will not change significantly.

For the method of reducing the confidence interval for the probability estimation, the method in section 5.4.2 is recommended. The other two optional methods are quite crude, which are very relied on the rough guess. For example, in the section 5.4.1, the upper limit of the wind speed and the fetch were estimated with large uncertainty, while the wind duration was over estimated a lot. Besides, in reality, the wind will vary irregularly over time. Therefore, the assumed wind speed and wind duration will make the estimation higher than the true value. On the other hand, the *D* and the *h* were obtained from their probability distributions with a return period of 10^6, but the concurrent probability is lower than 10^{-6} in the study period. Over all, this method will give a higher estimation without quantifiable uncertainties. If this method is selected to determine the upper limit of the maximum possible storm, those parameters should be estimated more accurately and carefully. The method in section 5.4.2 was computed under the assumption that SLR=1.05m is constant over time. Therefore, the confidence intervals of the other SLR scenarios were a little overestimated. The method in 5.4.3 should be employed before carefully investigating the study site.

Sensitivity analysis of the dune recovery rate indicates that, the dune recovery rate does not influence the high probability retreat distance, but that it does influences the high exceedance probability final net erosion volume magnitude. That is because that the recovered sand volume is much less than the erosion volume induced by extreme storm events and the recovery process is much slower.

Chapter 6 Model application to Narrabeen beach, Australia

In this chapter, the statistical framework of coastal erosion estimation is tested and validated by being employed to the Narrabeen beach, Australia. The case study indicates the effectiveness and universality of the model when compare to the field observations and the existing research results.

6.1 Review of the methods

Callaghan et al. (2008) used the joint probability to simulate the wave climate ($H_{s,max}$, D, TA, T_p) and used the non-homogenous Poisson distribution to simulate storm interarrival time. By using a time convolution shoreline response model developed by Kriebel and Dean (1993), the estimation of the coastal erosion probability for the Narrabeen beach, Australia was made. The Kriebel and Dean erosion model will be introduced in detail in Section 6.4.1 The proposed full simulation method mainly includes three steps: (i) the simulation of forcing variates from statistical models that include the joint probability between key variates; (ii) the simulation of the time between storms using a non-homogenous Poisson process; (iii) and the simulation of each event to determine the erosion amount. The main objective of this model is to develop a full temporal simulation method instead of the design event approach.

Ranasinghe et al. (2012) applied an analytical model (Larson et al., 2004) which provides a Probabilistic estimates of SLR driven Coastal Recession model (PCR model). The PCR model completely departs from the traditionally used Bruun rule and provides probabilistic estimates of coastal recession based on governing physical processes.

Instead of the dune erosion model mentioned above, Riesenkamp (2011) used XBeach to refine the calculated return periods and Callaghan et al. (2013) improved that method.

In this Chapter, the storm events were simulated by using the methods in Chapter 3, and the adjusted DUNERULE (Chapter 4) was applied and validated. In the end, the probabilistic estimation of dune erosion and coastal recession results (method in Chapter 5) were calculated and compared to the existing findings.

6.2 Study site description

The long on-going beach survey in Narrabeen beach makes it a favourite study site for the model validation. The Narrabeen beach is about 3.6km long which is bounded by Long Reef Point to the south and Narrabeen Headland to the north (Fig. 6.1). The beach experiences a microtidal (spring tidal range = 1.3m), semi-diurnal tidal regime and is composed of fine to medium (d_{50} = 300–400µm) quartz and carbonate sands. The deep water mean significant wave height is 1.6m and the mean deep water peak wave period is 10s (Short and Trenaman, 1992).

Narrabeen Beach is also subjected to beach rotations from the slowly varying imbalance between northerly and southerly directed longshore sediment transport and long-shore variations in cross-shore transport (Harley et al., 2011; Ranasinghe et al., 2004) resulting from wave climate oscillations. Short and Trembanis (2004) quantified the magnitude and this arrangement of the beach rotation from field measurements and concluded that profile 4 (at the centre of the embayment, Fig. 6.1b) is the beach rotation fulcrum. Consequently, a focus was put on profile 4 and the other profiles were excluded that being impacted (to some extent) by longshore processes. During a particular short period of several days during stormy conditions, it is reasonable to assume that the cross-shore processes will dominate long-shore processes (Roshanka et al., 2013).

The offshore wave measurements were obtained from Botany Bay (Lawson and Abernethy, 1975; Trindade et al., 1993; Youll, 1981) and Long Reef (Kulmar et al., 2005), both located near Sydney (Fig. 6.1b). The non-directional Botany Bay wave buoy is located at approximately E338770 m; N6231900 m (ICSM, 2002) and the measurements used in this thesis extend from 8 April 1971 to 22 May 2006. The Long Reef wave buoy has been located at 13 positions that are within 2km of E353492 m; N6261660 m. Long Reef measurements for directional wave statistics cover the period extending from March 1992 through to

March 2006, a sample length of 14 years with 83% of this period captured (Kulmar et al., 2005). Both buoys are located in approximately 80m water depth. The tidal level measurements, that exclude wave set-up and run-up, were measured at Fort Denison (Anonymous, 1995) and extend from June 1914 through to December 2005. Fig. 6.2 shows the cross-section of the coastal zone.

Figure 6.1 Locality map for field measurements. a. Location of Sydney within Australia; b. The Botany Bay and Long Reef wave buoy locations and the Fort Denison tidal recording station; and c. The location of long term beach profile surveys at Narrabeen Beach (profile 4)(after Callaghan et al. (2008)).

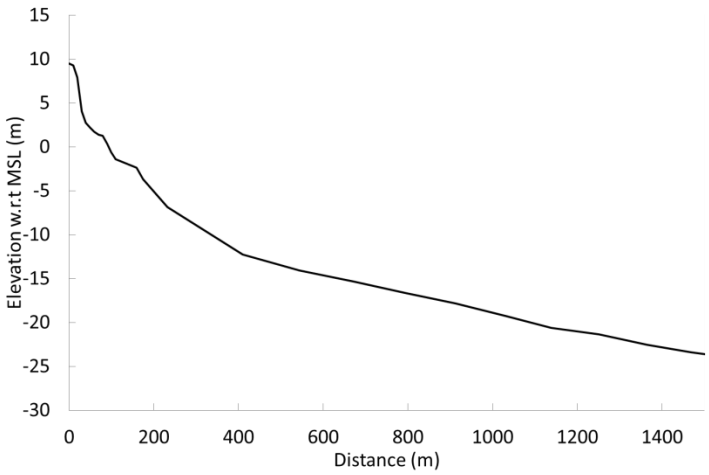

Figure 6.2 Coastal dune profile of Narrabeen beach

6.3 Storm simulation

6.3.1 Storm event definition

Storm events were identified as periods where significant offshore wave height (H_s) exceeded 3m (Kulmar et al., 2005; Lord and Kulmar, 2001). These periods were then manually assessed (accepted with or without adjustment or rejected) to ensure that each

wave event represents one meteorological system (Callaghan et al., 2008). Fig. 6.3 shows the definition used for storm duration and $H_{s,max}$.

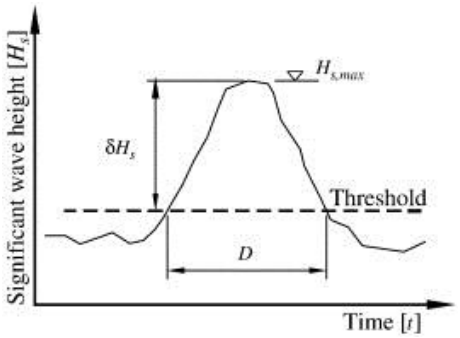

Figure 6.3 Definition sketch for storm duration (Callaghan et al., 2008).

6.3.2 Fit marginal GP distributions to the univariables ($H_{s,max}$, D, T_p and TA)

According to the statistical characteristics of the wave climate parameters, they were fitted to the GP distributions. Different from the Dutch case, the tidal anomaly (*TA*) was employed for wave climate analysis and simulation instead of the surge level (*h*). The tide level in the study site is normally 3 to 5 times bigger than the *TA*. Therefore, it is not reasonable to add a large deterministic process with an stochastic process and then fitting to GP distribution. Callaghan et al. (2008) gave the fitting result for the $H_{s,max}$, D and TA, and for simplicity in this study, the T_p was also fitted to GP distribution (Table 6.1) and limited by Michell rule (Michell, 1893). A comparison between the observations and the simulations in terms of return period is presented in Fig. 6.4.

6.3.3 Fit the empirical distribution to θ and F_s

The wave direction (θ) was assumed to be independent of the other wave climate parameters, as Callaghan et al. (2008) did (Fig. 6.5). While the storm frequency was simply simulated by the fitted empirical distributions of each month(Fig. 6.6).

Table 6.1 GP distribution parameters, 95% confidence limits are in the brackets.

Variate	u	ξ	σ
$H_{s,max}$(m)	4.5	0.03 (-0.11, 0.24)	0.86 (0.68, 1.08)
D(h)	40	-0.03 (-0.17, 0.11)	24 (19, 30)
T_p(s)	10.8	-0.09 (-0.27, 0.08)	0.97 (0.72, 1.21)
TA(m)	0.175	0.11 (-0.04, 0.32)	0.06 (0.04, 0.07)

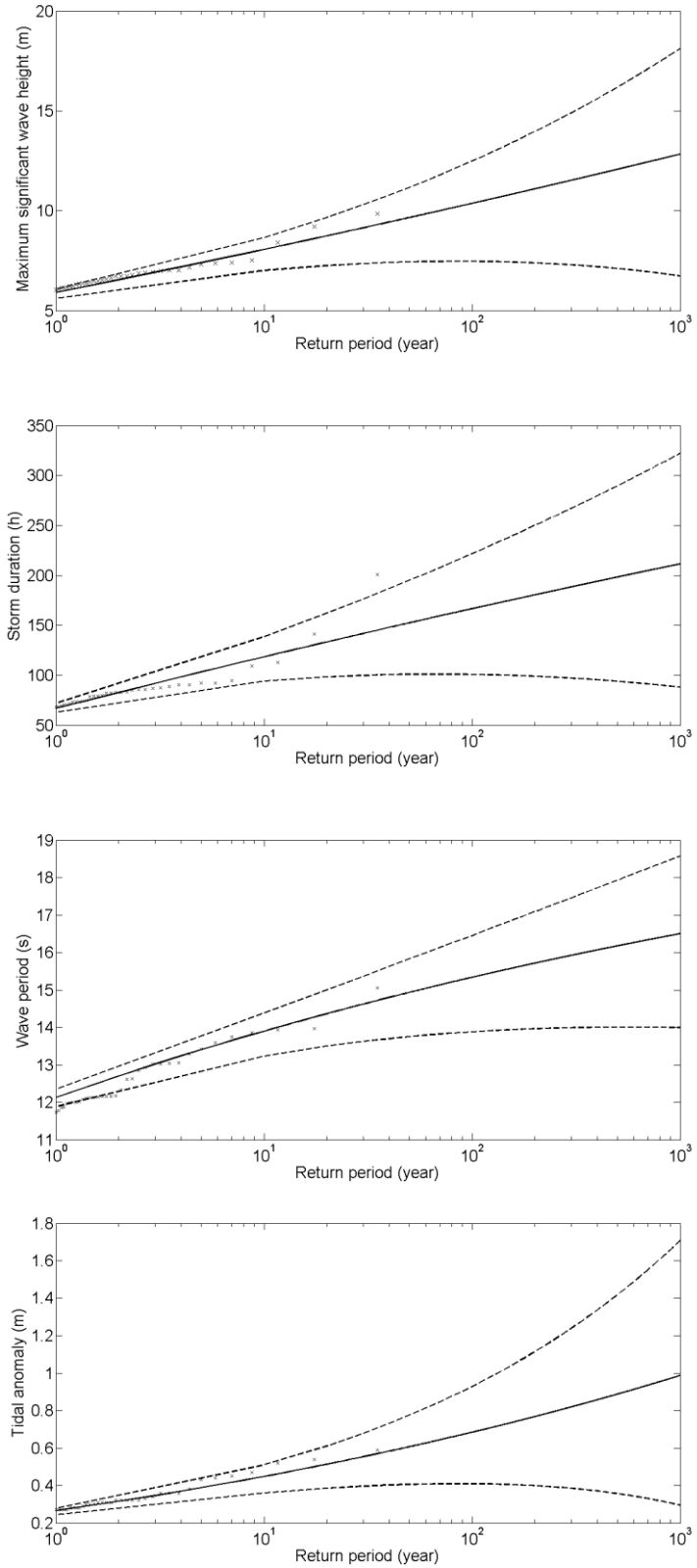

Figure 6.4 The return level plot for $H_{s,max}$ (m), D (h), T_p (s) and TA (m), × are the empirical estimations, the black solid lines are the fitted models and the dash lines are the 95% confidence limits.

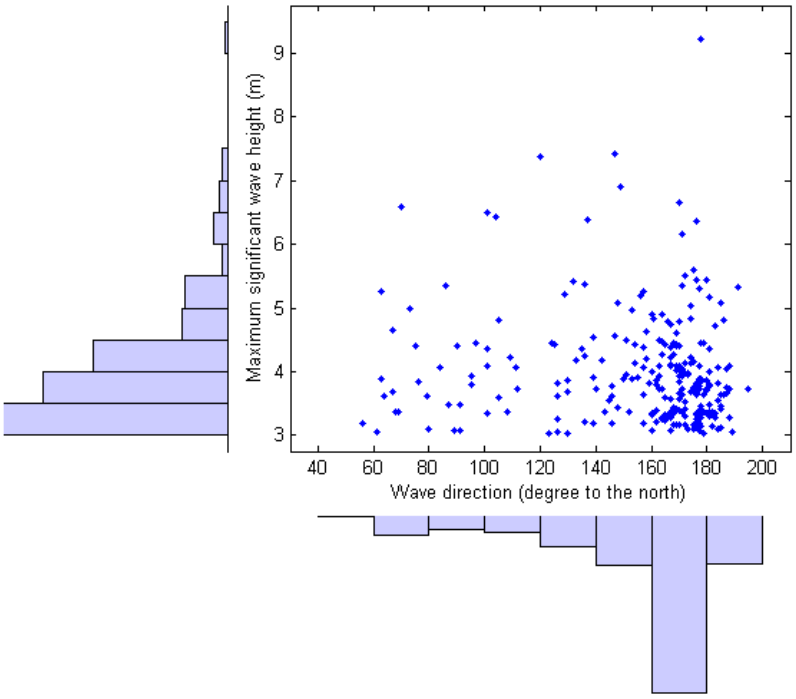

Figure 6.5 Measured θ and $H_{s,max}$, the histograms are the corresponding empirical PDFs.

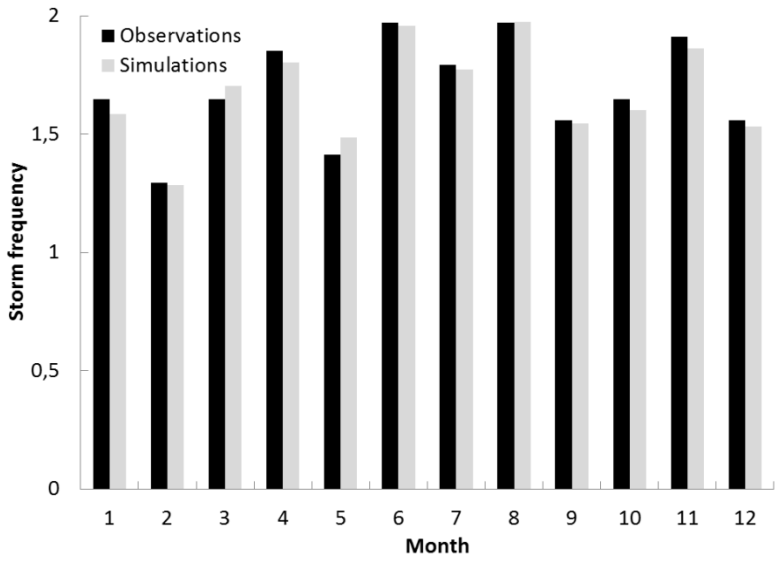

Figure 6.6 Average monthly storm frequencies of simulations and observations.

6.3.4 Dependency structures

Three methods were employed to construct the dependency structures that mentioned in Chapter 3, excluding the physics-combined Gaussian copula method. Analysis indicates that the wave steepness and the maximum significant wave height have a very strong dependency (the correlation coefficient is about 0.6, where in the Dutch case, the correlation coefficient is about 0.08), which does not meet the basic assumption that used in

the physics-combined Gaussian copula method. Therefore, the rest three methods were tested in this case study. When using the Archimedean copula, the ($H_{s,max}$, D) was fitted to Clayton copula, the ($H_{s,max}$, TA) and ($H_{s,max}$, T_p) were fitted to Frank copula respectively according to their statistical characters. Fig. 6.7-6.9 show the simulation results. Again, the Chi-square test was used to test the fitting quality (Table 6.1).

Table 6.1 Chi-square test for univariate and joint simulation.

	Archimedean copula		Gaussian copula		Logistics model	
	$C_{0.95,f}$ ($C_{0.99,f}$)	χ^2	$C_{0.95,f}$ ($C_{0.99,f}$)	χ^2	$C_{0.95,f}$ ($C_{0.99,f}$)	χ^2
$H_{s,max}$	21.03	5.86	22.36	10.89	28.87	8.52
D	25.00	20.17	23,68	12.83	37.65	35.69
TA	27.59	10.97	16,92	9.70	28.87	12.27
T_p	25.00	21.19	15,51	11.94	28.87	25.66
Multivariate ($H_{s,max}$, D, TA, T_p)	381(401)	263	329(347)	280	409(430)	532

The Chi-square test indicates that the Archimedean copula and the Gaussian copula methods are acceptable for the wave climate simulation, while the Logistics model does not pass the goodness-of-fit test. Therefore, currently speaking, both the Gaussian and the Archimedean copula were considered as a reasonable method for the wave climate simulation.

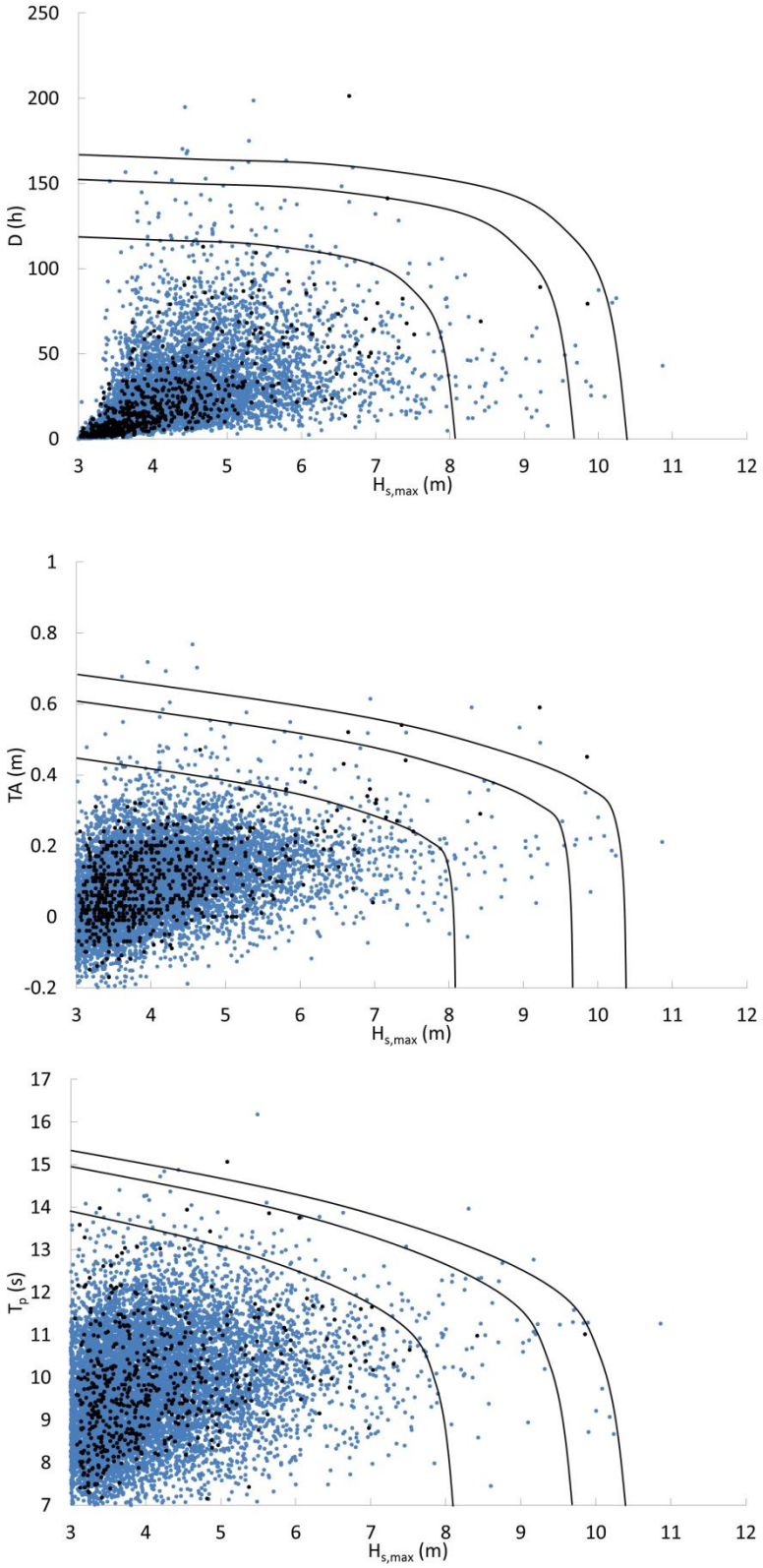

Figure 6.7 Simulated 10^4 storms (blue dots) and observed wave climate (black dots), ($H_{s,max}$, D), ($H_{s,max}$, h) , and ($H_{s,max}$, T_p) (from top to bottom) by using Archimedean copula, the solid black curves are the return period contours (10, 50 and 100 years respectively).

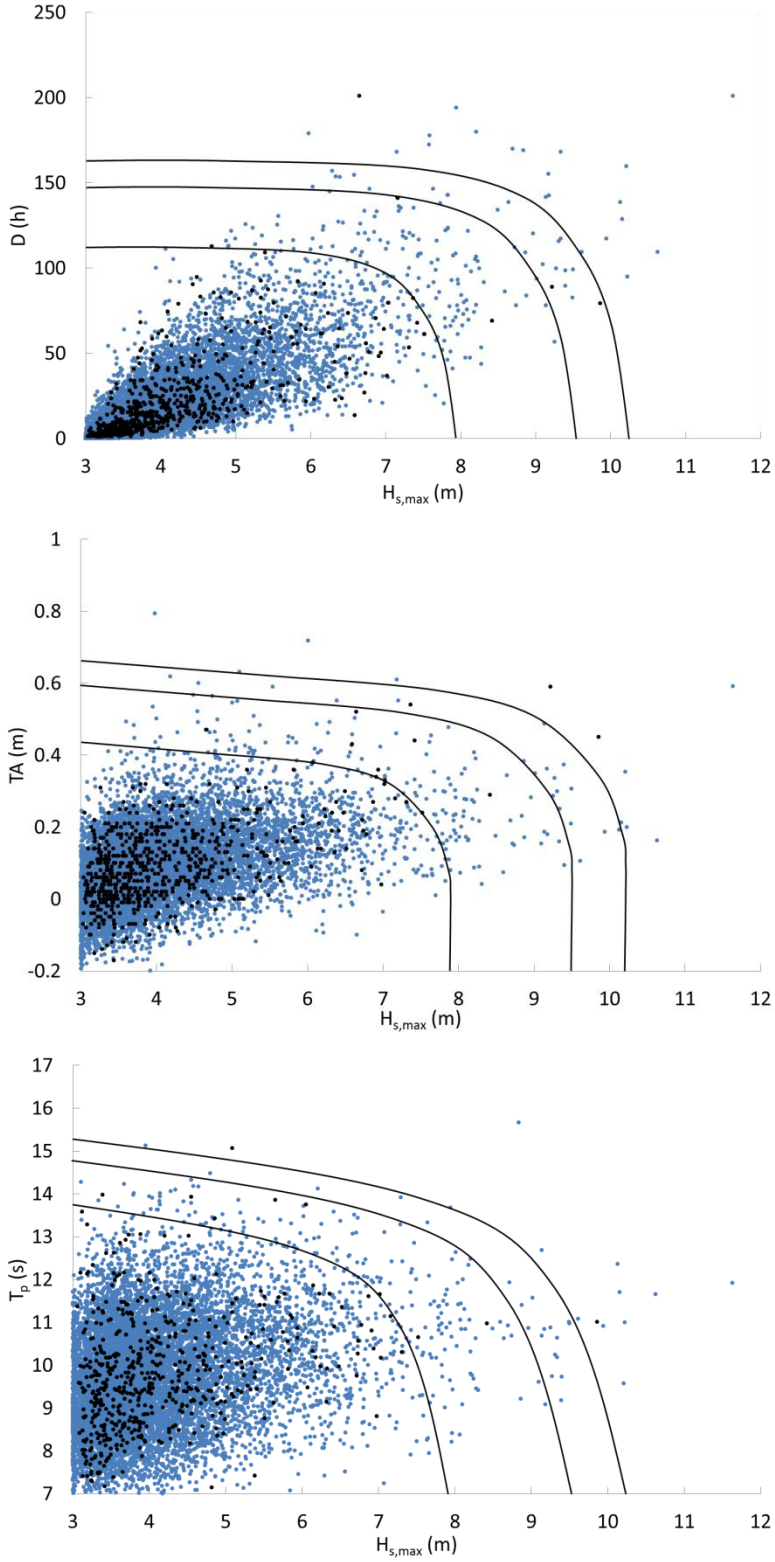

Figure 6.8 Simulated 10^4 storms (blue dots) and observed wave climate (black dots), ($H_{s,max}$, D), ($H_{s,max}$, h) , and ($H_{s,max}$, T_p) (from top to bottom) by using Gaussian copula, the solid black curves are the return period contours (10, 50 and 100 years respectively).

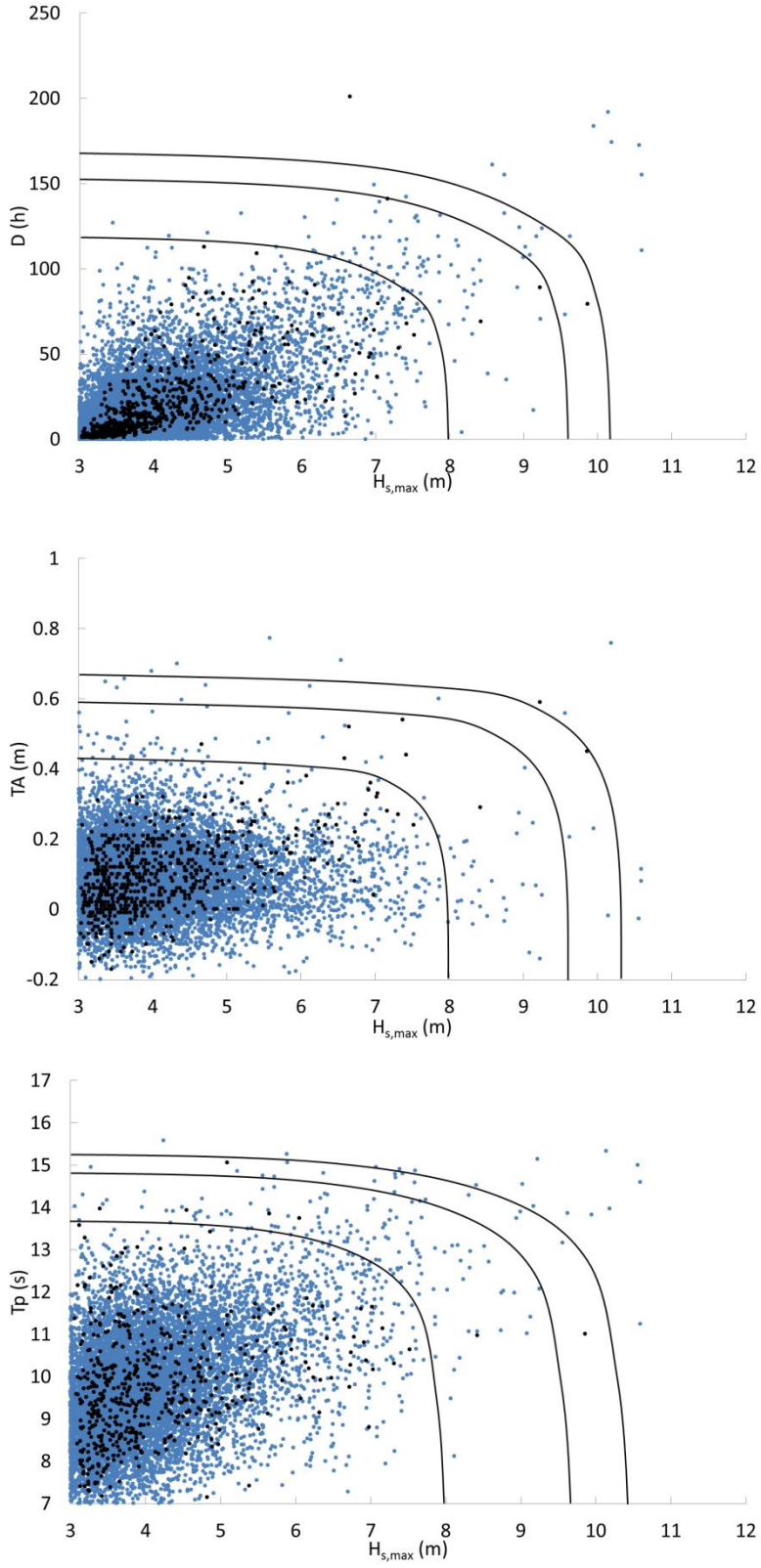

Figure 6.9 Simulated 10^4 storms (blue dots) and observed wave climate (black dots), ($H_{s,max}$, D), ($H_{s,max}$, h) , and ($H_{s,max}$, T_p) (from top to bottom) by using Logistics model, the solid black curves are the return period contours (10, 50 and 100 years respectively).

6.4 Dune erosion model

6.4.1 Kriebel and Dean's dune erosion model

This time convolution model is based on the equilibrium profile concept and was applied by Callaghan et al. (2008). The ideal equilibrium profile (Fig. 6.10) is given by Eq. 6.1.

$$h_d = \begin{cases} -Bx & \le -\dfrac{B}{m} \\ mx & -\dfrac{B}{m} \le x \le \dfrac{4A^3}{9m^3} \\ A(x-x_0)^{\frac{2}{3}} & x \ge \dfrac{4A^3}{9m^3} \end{cases}, \tag{6.1}$$

where, h_d (m) is the water depth, x is the cross-shore seaward coordinate, B (m) is the dune height above the MSL, m is the beach slope, A is an empirical coefficient, $A = 2.25(\frac{w_s}{g})^{\frac{1}{3}}$, w_s (m/s) is the sediment fall velocity (Kriebel and Dean, 1993) and $x_0 = \dfrac{4A^3}{27m^3}$. Based on the concept of equilibrium profile, the maximum potential RD is

$$RD_\infty = \frac{S[x_0 + (\frac{h_b}{A})^{\frac{3}{2}} - \frac{h_b}{m}]}{B + h_b - 0.5S}, \tag{6.3}$$

where, S is the vertical shift of the sea level if the MSL were to change permanently, h_b (m) is the water depth where the wave breaking occurs.

The maximum potential erosion volume when exposure to an increased sea level is

$$R_\infty = \begin{cases} RD_\infty B & \text{z>S-}\dfrac{4A^3}{9m^2} \\ RD_\infty B + \dfrac{h_t^2 - 2Sh_t^2 + S^2 - z^2}{2m} + \dfrac{8A^3(15Sm^2 - 4A^3)}{405m^5} - \dfrac{\sqrt{S-z}(2S^2 + Sz - 3z^2)}{5A^{\frac{3}{2}}} & \text{z} \le \text{S-}\dfrac{4A^3}{9m^2} \end{cases}, \tag{6.2}$$

where, R_∞ (m^3/m) is the maximum potential dune erosion volume, h_t (m) is the depth where the beach slope changes from constant to slope which is given by Eq. 6.1, z is the elevation of the seaward boundary contour (shown in Fig. 6.11), in this study, z = 2m.

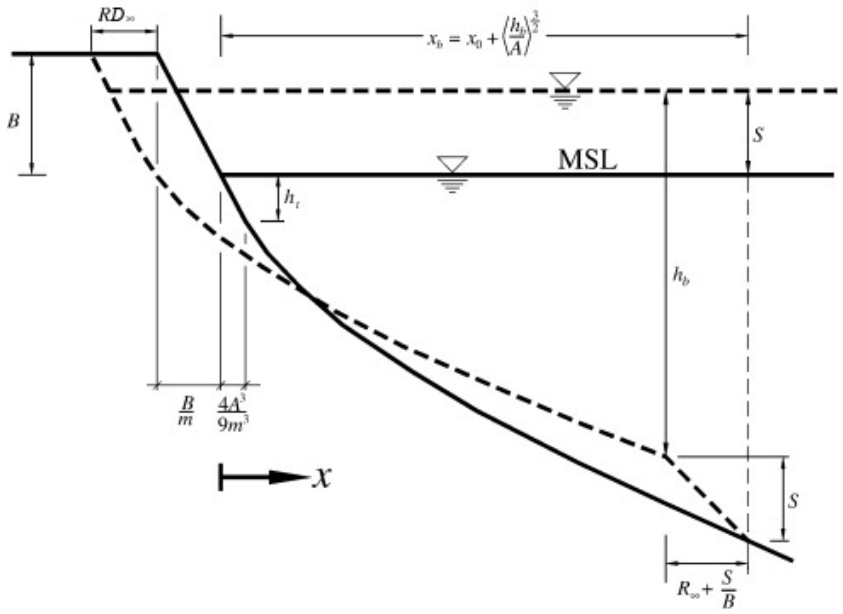

Figure 6.10 Maximum potential coastal dune retreat distance, (RD_∞), of equilibrium profile to the surge level (S) (Callaghan et al., 2008).

According to the Kriebel and Dean model, when a storm occurs, the erosion volume is approaching to the R_∞ over time. And the temporal behaviour is

$$R(t)=\begin{cases} R_{initial}e^{-\frac{t}{T_{s,a}}} & 0\le t\le t_s \\ \dfrac{R_\infty}{T_{s,e}}\displaystyle\int_0^t f(\tau)e^{-\frac{t-\tau}{T_{s,e}}}d\tau & t_s\le t\le t_m, \\ V(t=t_m)e^{-\frac{t-t_m}{T_{s,a}}} & t>t_m \end{cases} \tag{6.3}$$

where, t (h) is the time measured from the start of a storm, $R_{initial}$ (m^3/m) is the initial erosion volume, $T_{s,e}=320\dfrac{H_b^{3/2}}{\sqrt{g}A^3}(1+\dfrac{h_b}{B}+\dfrac{mx_b}{h_b})$ (the subscript b means the position of wave breaking) and $T_{s,a}$ (h) are the characteristic time scales of the exponential response under erosive (see Kriebel and Dean (1993)) and accretive (taken as $T_{s,a}$ = 400h, conservatively estimated using the measurements from (Ranasinghe et al., 2004)) conditions respectively, t_s (h) is the time when storm erosion is greater than the initial erosion, and t_m (m) is the time when the maximum erosion occurs during the storm and $f(t)=\dfrac{\sin^2\pi t}{D}$ is the storm shape function. The Kriebel and Dean (1993) profile model parameters are A = 0.14 $m^{1/3}$, obtained from the measured medium sand grain diameter and using Dean and Dalrymple (2002), the beach face slope, m = 0.07 and dune height above mean sea level, B = 10m was obtained from profile surveys (Callaghan et al., 2008).

The block averaging and consecutive volumes methods (Callaghan et al., 2008) were used to convert beach profile measurements to estimate the erosion volume statistics. The block averaging method estimate average beach volume in 1.5 month bins and then determines the maximum change within 12 months. The consecutive volumes method estimates the beach erosion volume from successive profile measurements and corrected by the effective number of storms. The erosion volume return periods estimations with these two methods and the comparison between the Kriebel and Dean model estimation and the field measurement are shown in Fig. 6.12.

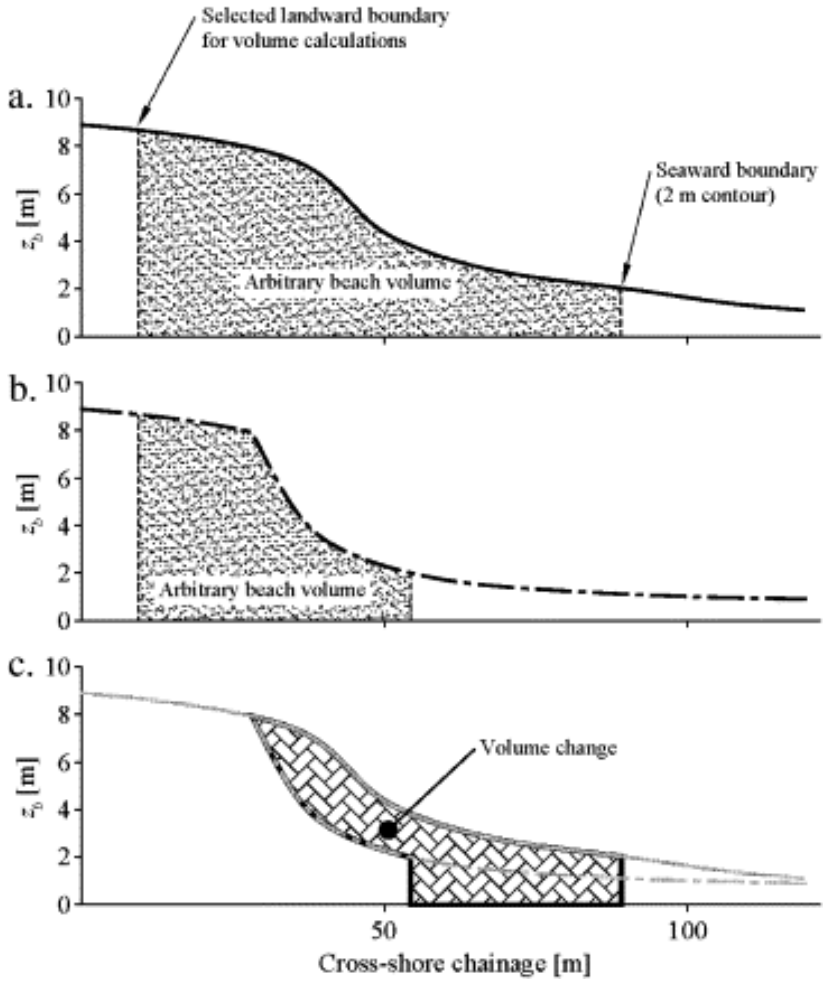

Figure 6.11 Beach volume change definition sketch for (a) pre-storm, (b) post-storm and (c) beach volume change (Callaghan et al., 2008).

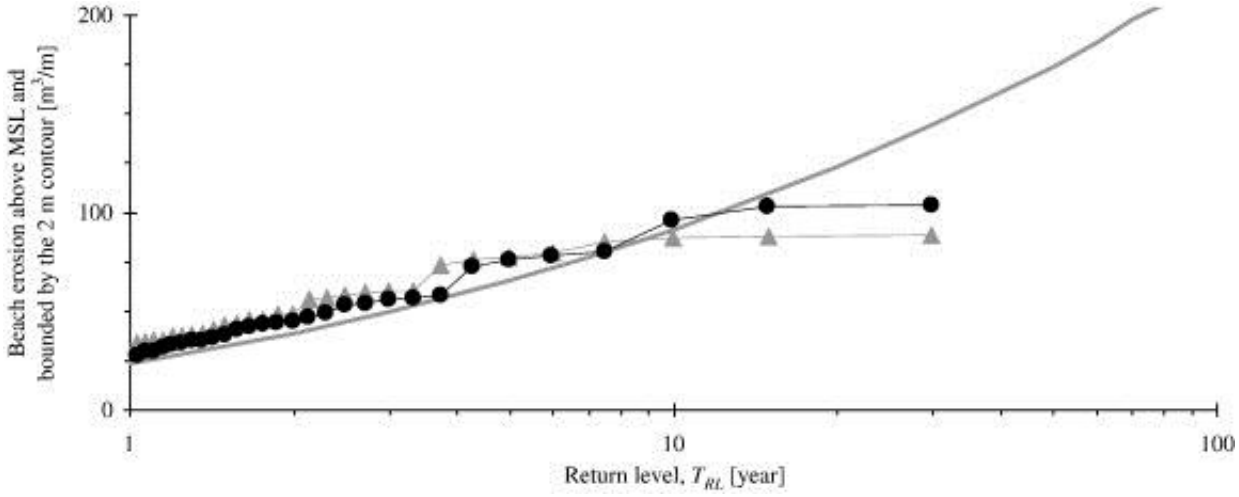

Figure 6.12 The eroded sand volume above MSL at Narrabeen Beach from; profile measurements (the grey triangles represent the block averaging procedure and the black circles represent the continuous volumes method) (Callaghan et al., 2008).

6.4.2 Analytical model

Ranasinghe et al. (2012) tried to use an analytical dune erosion model (Larson et al., 2004) as the structural function to estimate the dune recession beyond the Bruun rule. The model assumes that there is a linear relationship between the wave impact, F_W (N) and the weight of the sand eroded from the dune, ΔW (kg):

$$\Delta W = \Delta R(1-p)\rho_s = C_E F_W , \tag{6.4}$$

where, R is the erosion volume (m^3/m) p is the porosity, ρ_s is the density of sediment (kg/m^3), C_E is an empirical coefficient and F_W is given by:

$$F_W = \frac{1}{2}\rho_w \frac{{u_0}^4}{g{C_u}^2}\frac{\Delta t}{T} , \tag{6.5}$$

where, ρ_w is the water density (kg/m^3), u_0 is the bore velocity, C_u is an empirical coefficient, t is the time (s), T is the wave period (s). After some mathematical manipulations and under some simplifying assumptions, the average rate of dune erosion is

$$\frac{\Delta R}{\Delta t} = -4C_s \frac{(Z_R - z_0)^2}{T} , \tag{6.6}$$

$$C_s = \frac{1}{2}\frac{C_E}{C_u^2}\frac{\rho_w}{\rho_s}\frac{1}{(1-p)} , \tag{6.7}$$

where, Z_R is the run-up height (m), z_0 is the elevation difference between dune toe and the beginning of the swash zone (m), C_s is a function of H_{rms}/d_{50} (Larson et al., 2004). The definition sketch is shown in Fig. 6.13.

The dune retreat distance return period estimated by (Ranasinghe et al., 2012) is shown in Fig. 6.14.

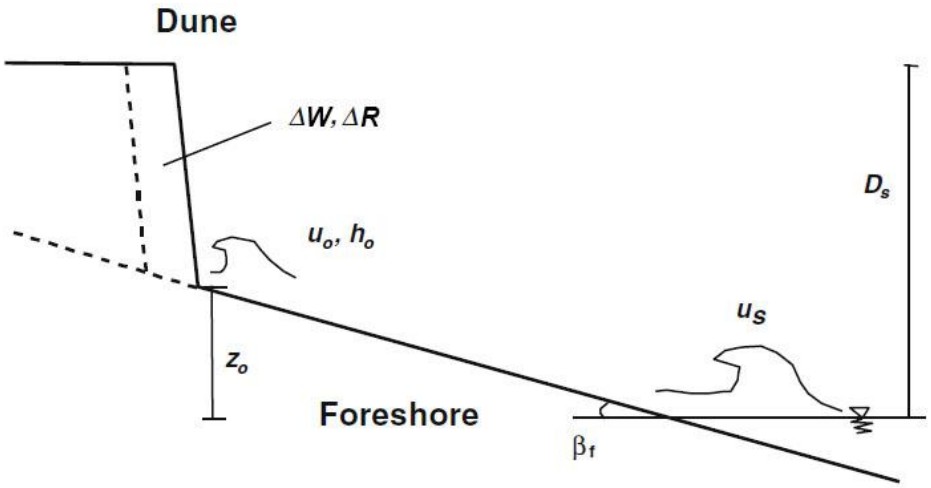

Figure 6.13 Definition sketch for modelling dune erosion due to the impact of run-up waves (Larson et al., 2004).

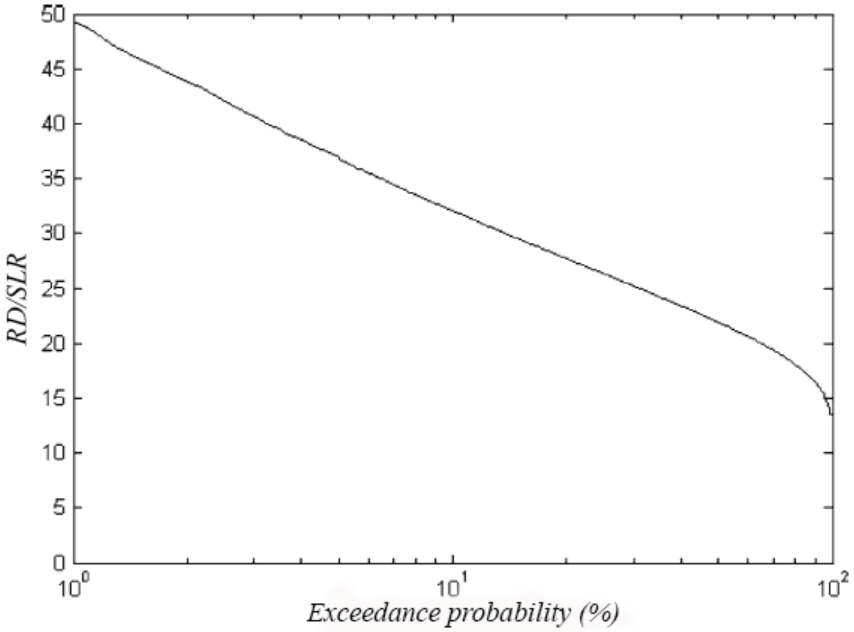

Figure 6.14 Model predicted probabilistic estimate of coastal recession rate (RD/SLR) at Narrabeen beach, Sydney, Australia by the year 2100 compared to 1990 (Ranasinghe et al., 2012).

6.4.3 XBeach

The XBeach was generally described in Chapter 4.2.2. Riesenkamp (2011) calibrated the model with one storm event in 1997 and the long term beach erosion measurement. The computationally expensive character was mitigated by implementing a high density input matrix instead of random input parameters. For each combination of wave climate parameters, the erosion volume was obtained by running the XBeach. With the erosion volume, a transfer matrix was obtained. The transfer matrix is a $6 \times n$ matrix, where n is the total simulated storm events. Erosion volume caused by storms which are not transfer matrix are determined using linear inter- or extrapolation. The estimation result is shown in Fig. 6.15.

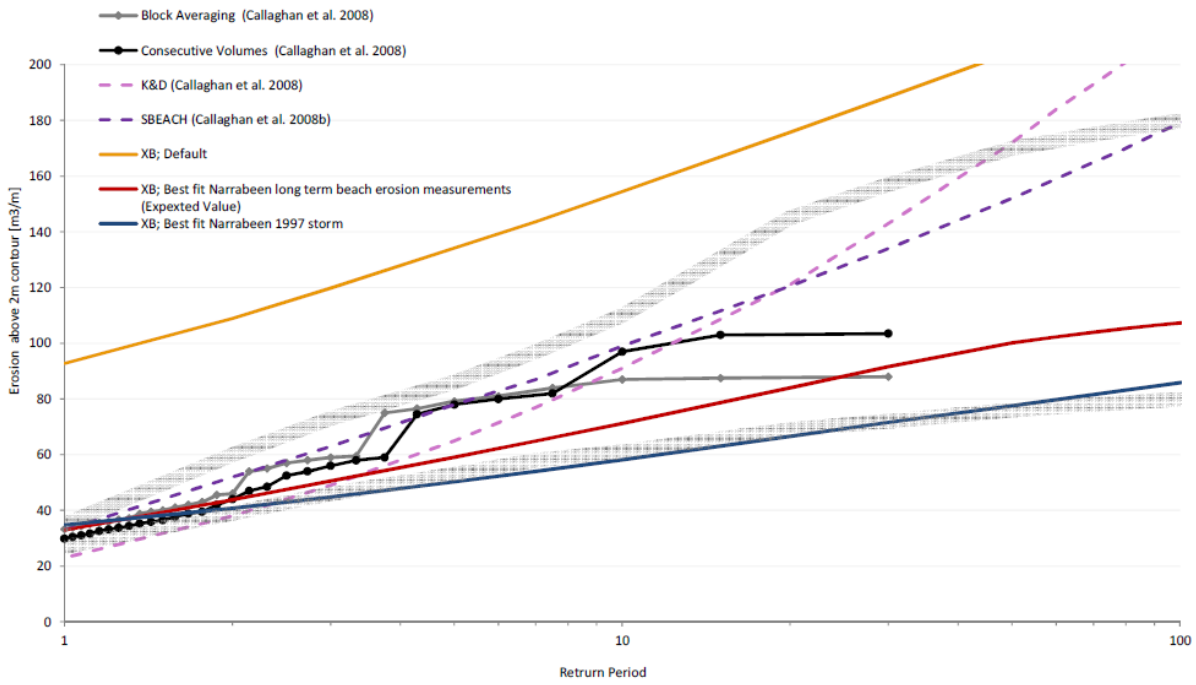

Figure 6.15 Erosion volume return period for Narrabeen beach. The grey and black lines represent the calculated Return Periods based on measurements. The red line resembles the best approximation to these measurements from the 20 simulations. The blue line is the approximation using the setup giving the best result on the single 1997 Narrabeen storm. The thick grey lines are the 95% confidence intervals of the data (Riesenkamp, 2011).

Callaghan et al. (2013) analysed and find the lowest tabulation density (i.e. number of XBeach simulations required to fill the table) that is able to reproduce similar results to the full tabulation. The XBeach predictions is shown in Fig. 6.16.

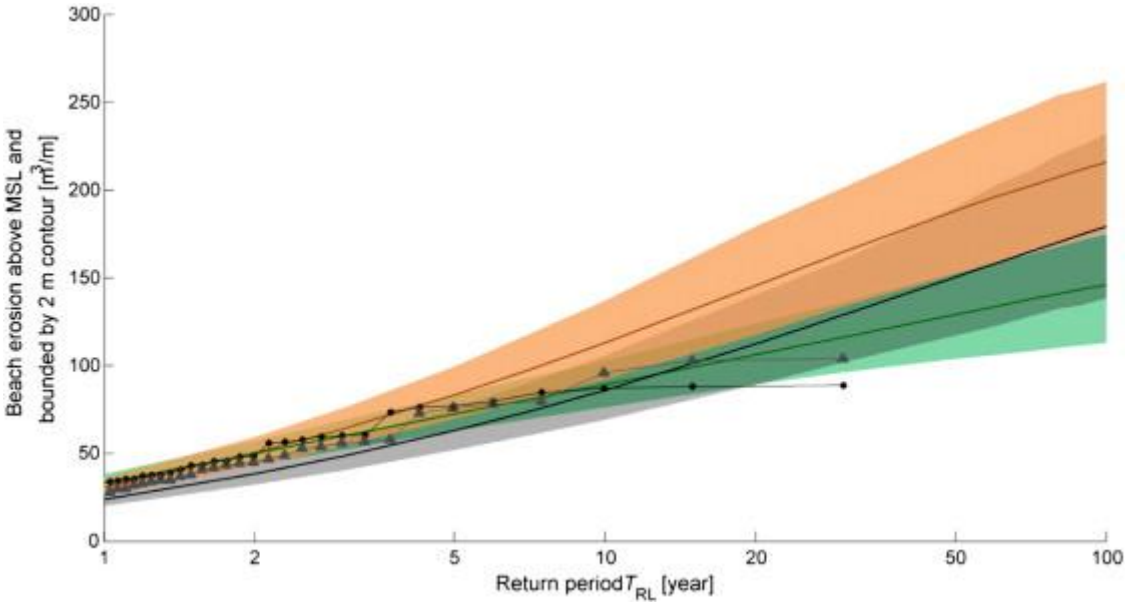

Figure 6.16 The eroded sand volume above MSL at Narrabeen Beach from profile measurements (empirical estimates by block averaging and consecutive volumes); and beach erosion predictions for Kriebel and Dean model (Kriebel and Dean , 1993, continuous black line), SBeach (Larson, 1988, continuous green line) and XBeach (Roelvink et al., 2009, continuous orange line). Shaded areas are estimated 95% confidence intervals calculated by bootstrapping techniques(Callaghan et al., 2013).

6.4.4 DUNERULE

The DUNERULE should be calibrated according to the local specific circumstance before being employed. In Chapter 4, the DUNERULE was calibrated on the basis of XBeach due to the lack of sufficient beach profile measurements. While in the Narrabeen Beach, the coastal profile measurement from 27 April 1976 to 2 March 2006 was used to adjust the parameters of the DUNERULE. By inputting the observed wave climate data, the DUNERULE is able to predict the dune erosion volume probabilities, hence the model parameters were determined by comparing the extreme dune erosion volume probabilities obtained by the DUNERULE and the field measurements. The missing wave period data was simulated by the joint distribution of ($H_{s,max}$, T_p), while the missing wave direction data was randomly generated according to its empirical distribution.

While seeking for the best model parameters, the dune recovery process (Fig. 4.6) was also included. Long term survey indicates that the average dune foot is located at about 2m above the MSL, and the dune recovery rate which can maintain this position is selected. Thus the dune recovery rate is assumed as 0.1m^3/m/day calculated based on observations at Narrabeen beach, Sydney, and Gold Coast, Queensland, Australia (Ranasinghe et al., 2012). The DUNERULE was fitted to the dune erosion probabilities obtained by the consecutive volumes (Callaghan et al., 2008) which is corrected by the effect of storm numbers. Fig 6.17 shows the comparison between the adjusted DUNERULE and the measurements.

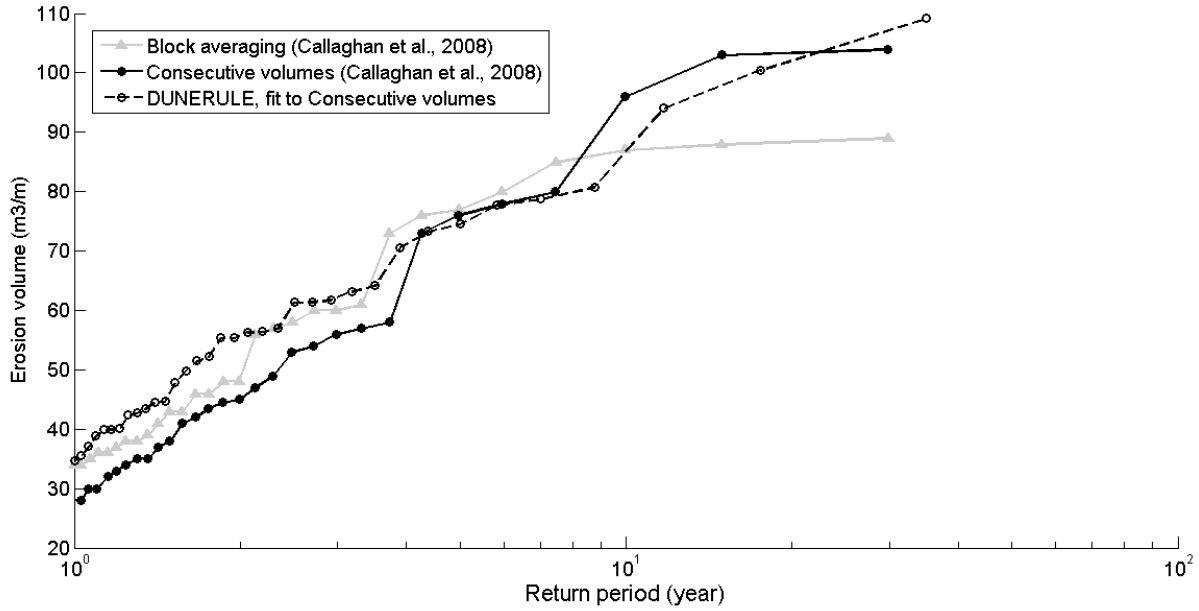

Figure 6.17 Adjusted DUNERULE and the field measurement.

The dune erosion calculated by the DUNERULE fitted to the block averaging data is more conservative than that fitted to the consecutive volumes. On the safety side, hereafter, the dune erosion probabilities were estimated by using the DUNERULE fitted to the consecutive volumes.

And the parameters adjusting result of the DUNERULE for the Narrabeen beach is:

$$R = 128A_d\left(\frac{h}{5}\right)^{\alpha_1}\left(\frac{H_{s,\max}}{7.6}\right)^{\alpha_2}\left(\frac{D}{5}\right)^{\alpha_3}\left(\frac{T_p}{12}\right)^{\alpha_4}, \tag{6.8}$$

where,

$$\begin{cases} \alpha_1 = 2.2 \\ \alpha_2 = 1.9 \text{ for } H_{s,\max} \le 7.6 \text{ and } \alpha_2 = 0.5 \text{ for } H_{s,\max} > 7.6 \\ \alpha_3 = 0.6 \\ \alpha_4 = 0.5 \end{cases}$$ for fitting to the consecutive volumes,

and *a* is the wave direction impact coefficient, given by:

$$A_d = \begin{cases} \left(1+\frac{\theta_0}{100}\right)^{0.5} & \theta_0 \le 30 \\ 1.3^{0.5}\left[1-\left(\frac{\theta_0-30}{60}\right)\right]^{0.5} & 90 \ge \theta_0 > 30 \end{cases}, \tag{6.9}$$

where, θ_0 is the incidence angle. The impacts of the coastal slope (0.07) and the d_{50} (300μm) were included in the equation as constant.

The measurements of the profile only cover approximately 30 years and with large temporal interval between each profile measurement, hence the estimation return periods (30 years in this case) will be less accurate, due to the short period of the profile measurement the higher return period tends to have large bias (30 years in this case).

6.5 Erosion probability estimation

In this section, the coastal dune response to the sea states was estimated. The simulated sea states include the sea storms and the increasing sea level. As in Chapter 5, the dune erosion probabilities and the net dune erosion volume by the end of this century were predicted based on a Monte-Carlo simulation framework for the Australian case. In this case study, the sea level was assumed to rise 0.92m by 2100 compare to 1990 (McInnes et al., 2007). And SLR curve was approximated using a fourth order polynomial function (Ranasinghe et al., 2012).

6.5.1 Probability of dune erosion volume

The Archimedean copula and Gaussian copula were employed to simulate the wave climate data, and the adjusted DUNERULE which was fitted to the consecutive volumes (Fig. 6.12) was employed to estimate the dune erosion volume due to the storms. The dune erosion probabilities estimation results were shown in Fig. 6.18 and 6.19. The calculation approach was illustrated in Section 5.3.

The analysis result indicates that the estimation of dune erosion probability was underestimated by inputting the Archimedean copula simulations compare to inputting the Gaussian copula simulations (Fig 6.18, 6.19). This is expected when look back at the Archimedean simulations (Fig. 6.7). The joint simulated ($H_{s,max}$, D) then to approach the coordinate axis rather than the top right corner, while the Gaussian simulation tend to be more concentrated to the diagonal.

Compare to the existing calculated results and the erosion probabilities estimated on basis of the field measurement, the erosion probability curves obtained by employing the Archimedean and Gaussian copulas and DUNERULE are lower, but higher than the result obtained by Riesenkamp (2011) in Fig. 6.15 by using XBeach. When SLR is taken as 0.92m by the end of 2100, the orange curve in Fig. 6.18 and 6.19 shifts upward significantly. The critical erosion volumes with corresponding return periods are shown in Table 6.2.

Table 6.2 Probabilistic estimation mode of dune erosion volume (m^3/m) and the 95% confidence interval (CI, m^3/m).

		SLR = 0		SLR = 0.92m	
	Return period (year)	Mode	CI	Mode	CI
Gaussian simulator	10	75	(64, 89)	111	(96, 130)
	50	122	(93, 167)	188	(143, 257)
	100	145	(104, 216)	224	(160, 340)
	200	169	(113, 278)	262	(173, 445)
Archimedean simulator	10	58	(56, 60)	90	(81, 101)
	50	80	(76, 86)	128	(106, 158)
	100	91	(84, 98)	143	(114, 187)
	200	100	(92, 110)	176	(127, 265)

6.5.2 Probability of dune retreat distance

According to the correlation between *R* and *RD* obtained in the Eq. 6.2, the coastal recession distance in different SLR scenarios by the end of 2100 was estimated. The simulation starts at the beginning of 1990 and stops at the end of 2100. In order to ensure the convergence of the estimation, the simulation process of 111 years dune erosion was repeated for 10^4 times. In order to make a comparison with the existing research results, coastal retreat rate curves (dash lines) were plotted in Fig. 6.20 and 6.21. The coastal retreat distance exceedance probability of 10% and 1%, obtained by using Archimedean copula simulator, are 15m (RD/SLR = 16) and 24m (RD/SLR =26). The estimation result in Fig. 6.21, which is closer to the calculation result of Ranasinghe et al. (2012), indicates that when SLR is 0.92m, a 10% probability of coastal retreat distance exceeding 25m (RD/SLR = 27), and a 1% probability of exceeding 43m (RD/SLR = 46). In Fig. 6.20, the exceedance probabilities of 10% and 1% are about 15m (RD/SLR = 16) and 30m (RD/SLR = 33).

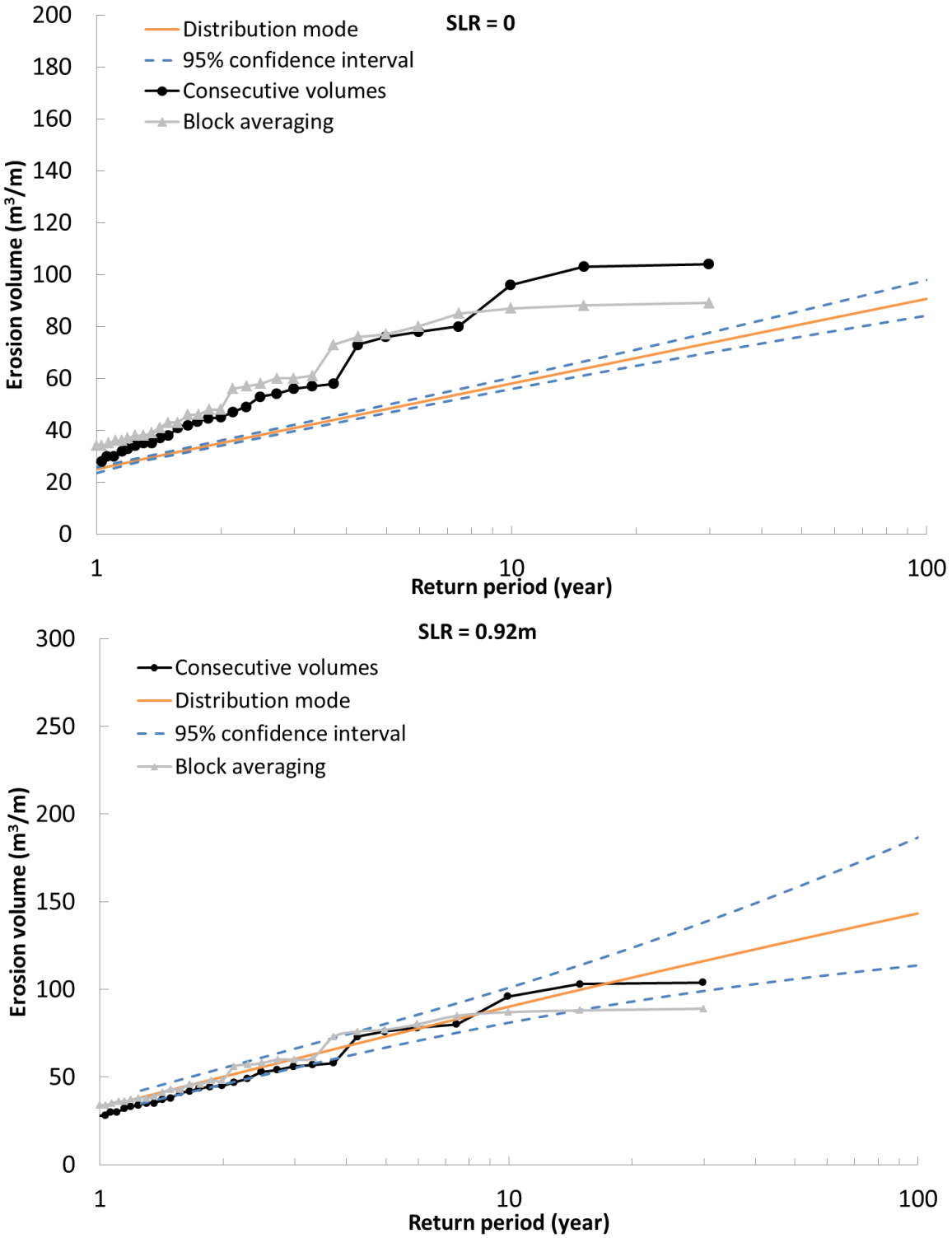

Figure 6.18 Return level plots for dune erosion volume with different SLR scenarios obtained by using Archimedean copula simulator, the dash curves indicate the 95% confidence interval.

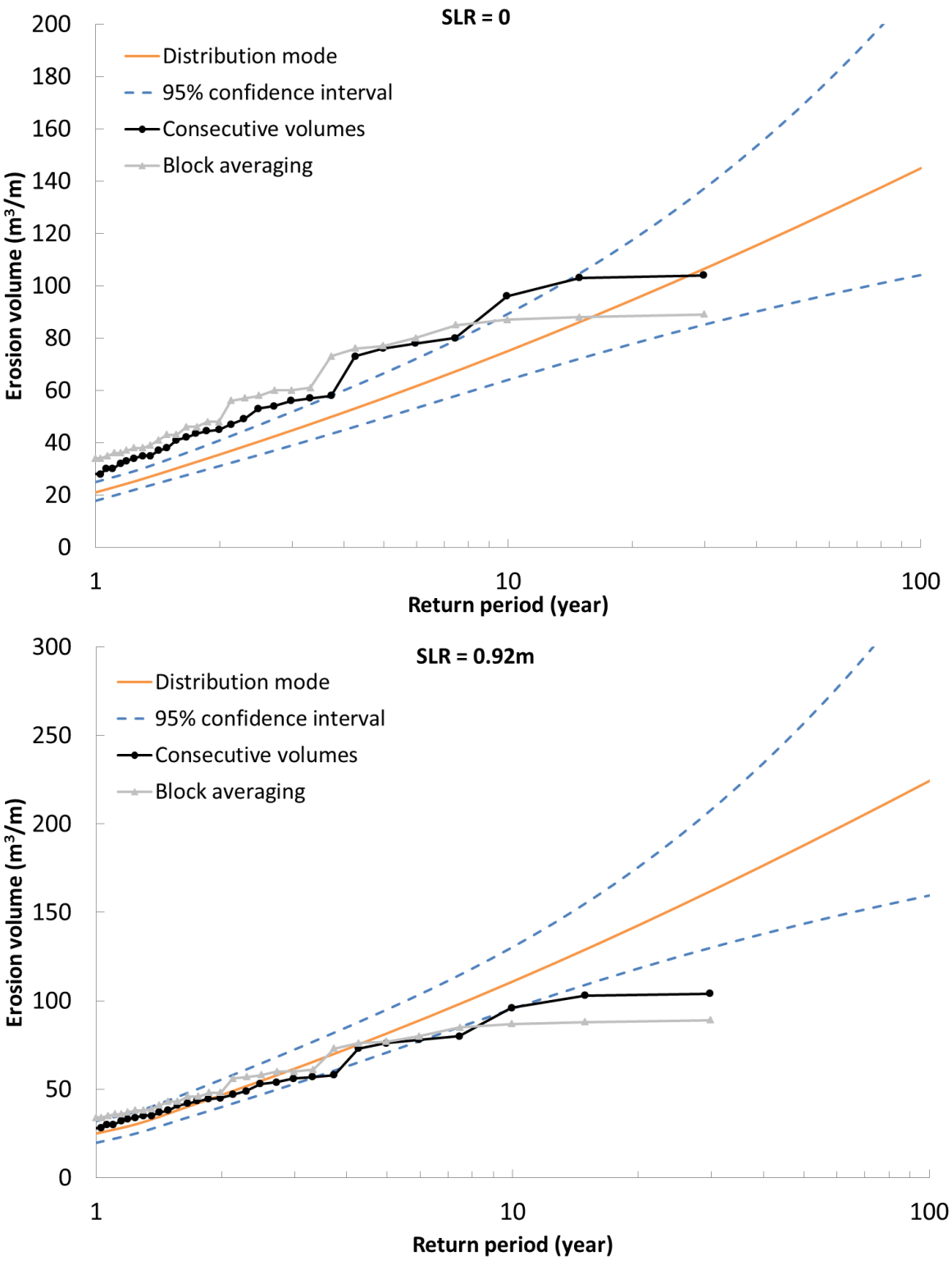

Figure 6.19 Return level plots for dune erosion volume with different SLR scenarios obtained by using Gaussian copula simulator, the dash curves indicate the 95% confidence interval.

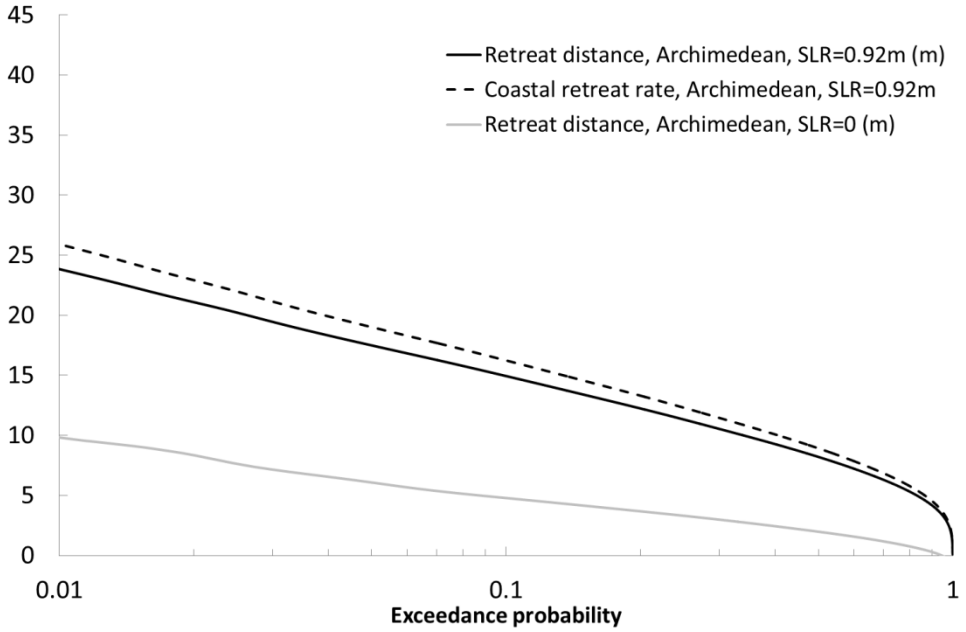

Figure 6.20 The exceedance probability of coastal dune retreat distance by 2100 using Archimedean copula simulator.

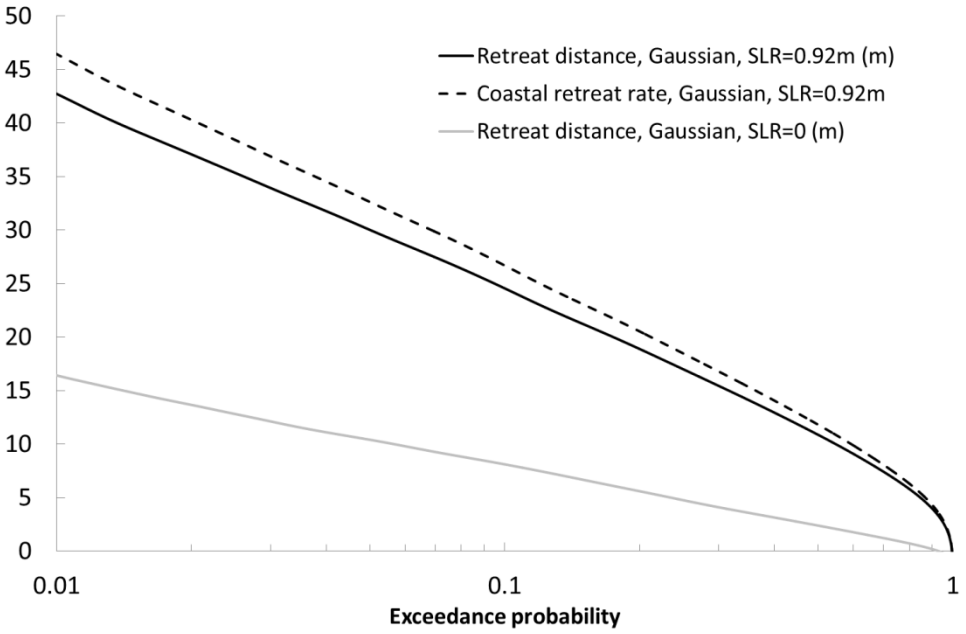

Figure 6.21 The exceedance probability of coastal dune retreat distance by 2100 using Gaussian copula simulator.

6.6 Discussion

Different from the Netherlands, the Australian coastal safety standard is much lower. Hence, the maximum return period considered in the estimation is 100 years. And at this return period level, the uncertainty that represents by the 95% confidence interval is not beyond

the physical limits. So, the uncertainty reduction method discussed in Section 5.4 are not suitable for the Narrabeen Beach case.

The storminess was simulated with twelve empirical distributions of storm numbers in each month. Compare to the Joint Probability Method model (JPM) developed by Callaghan et al. (2008), the advantage of this method is simple, while the disadvantage is that it is weak when simulating the monthly extreme storminess. Based on the measured wave event occurrences, the seasonality is less obvious than the Dutch case, hence the seasonal characteristics of wave climate was ignored, and the wave climate was not simulated separately for the winter and summer seasons.

Compare to the existing findings (Callaghan et al., 2008; Callaghan et al., 2013; Ranasinghe et al., 2012), the proposed statistical estimation of coastal dune erosion and recession obtained by using Gaussian copula simulator is comparable, while the estimation result obtained from the Archimedean copula simulator is smaller for long return periods. This is caused by the dependency structure. Although the copula methods will give a better results according to the Chi-square test, it cannot conclude that the copula methods are better than the Logistics model, because the goodness-of-fit test for multivariable is still developing, and the Chi-square test is weak when test the fitting quality for the extreme values. Therefore, the dependency structures for multiple variables should be better studied and acknowledged, for example, introducing more inner physical relationships among the variables and finding a more effective goodness-of-fit test for multivariable.

In this chapter, three dependency structures were employed to simulate the wave climate, and the Archimedean copula and Gaussian copula method were chosen, which is different from the JPM model (Callaghan et al., 2008). Compare to the Logistics model in JPM model, the Archimedean copula method is more flexible to choose an appropriate joint distribution for the two dimensional data, moreover the Gibbs sampling method decreases the complication of applying the Archimedean copula to higher dimensions by avoiding solving the complicated integral operations. The Gaussian copula method is much easier to understand and to extend to higher dimension. According to the Chi-square test, the copula simulations also show better consistency with observations. The probabilistic estimation of dune erosion volume obtained by applying the copula method is less conservative than the return levels calculated by the field measurements. This consequence maybe caused by two main reasons: the accuracy of the structural function, that is the DUNERULE in this case, especially when the storms are extremely heavy, and the other one is the statistical modelling bias.

In Fig. 6.4, all the fitted distribution curves are below the maximum observations, and the largest discrepancy occurs when fitting to the storm duration (D). This indicates that on average each of the wave climate component corresponding to a return period simulated by the fitted distributions will be smaller than the observation. This is confirmed by Fig. 6.7, 6.8

and 6.9, some of the observation points of 30-year are beyond the 50-year return period contour, or even beyond the 100-year contour. Therefore, the dune erosion volumes calculated by inputting these simulated wave climate data (simulated by Archimedean copula and Gaussian copula) will tend to be systematically lower. In order to improve the probabilistic dune erosion estimations, longer observations data are required to reduce the sampling errors, or introducing some historical extreme storm events to improve the distribution fitting quality and credibility.

Due to the large temporal interval between each profile survey, the erosion volumes corresponding to their return periods will have bias, and the bias will influence the accuracy of dune erosion model which was adjusted by the consecutive volumes procedure. The ideal situation is that the structural function can be calibrated by sufficient and consecutive profile measurements before and after storms. Besides, the missing observations also bring bias to the procedure of model calibration.

Chapter 7 Land-use strategies for coastal erosion zone

Dune erosion during severe storms may lead to dramatic coastal recession that threatens property located within the eroded strip. Yet the development of coastal zone also brings profits. Hence a prudent land-use strategy is required to balance the potentially huge economic profits with the high erosion risks. In this chapter, a guideline which is based on a trade-off analysis and the time-dependent probability of coastal recession distance is developed to maximize the total profit function. The probabilistic economic model will provide an optimal land-use planning tool for sandy coastal zones, which can assist decision makers in efficiently exploiting coastal resources.

7.1 Introduction

It is known that the world's coastal regions are generally more heavily populated than the continental interior (Small et al., 2000). Many metropolises are located in coastal regions and attracting more and more people to inhabit and invest in. Moreover, many coasts with sunny beach and warm water are popular tourist resorts, where have lots of hotels, restaurants, shops and houses near the sea. Unfortunately, any investors who intend to gain benefit in the coastal zone will not only face the market risk but also the natural hazards from the changeable sea than other investors. Coast erosion is one of the risk resources.

While protecting the coast, dunes along the coast will be eroded due to the severe storms and SLR. Therefore, in the coastal context a land-use strategy is expected to propose a compromising solution between the huge commercial potential and the high erosion risk.

Based on the dune erosion probabilistic estimation method mentioned above, a probabilistic estimation of dune recession distance can be obtained, that is, an erosion contours paralleling to the coastline is available. Building on the previous work by Vrijling et al. (2002) and Jongejan et al. (2010), two alternative strategies are studied in this paper: i.e. set a buffer zone to keep far from the high probability of being eroded and extend the coast width to move the iso-risk contours seaward.

The main purpose of this study is to provide a method to optimize the property configuration in coastal zone according to the time dependent erosion probability. More specifically, the study aims to achieve the following objectives: (i) to develop a coastal land-use planning framework considering the changing trend of coastal erosion probabilities; (ii) to determine the economical optimal setback line position (i.e. buffer zone width) or beach nourishment width.

7.2 Coastal zone risk assessment

The definition of risk contains three components: outcomes that have an impact on what humans value, the possibility of occurrence (uncertainty) of an event and a formula to combine both elements (Renn, 1998). In the case of coast zone, risk can be defined as the damage (economic, social, ecological and environmental) induced by a storm event times the occurrence probability of the event. If the occurrence probability is expressed by return period, the risk equals to the expected annual cost for storm hazards. In this chapter, “risk” refers to the expected annual cost due to the erosion, it is important to note that the probability of erosion itself does not represent risk. It is a component factor of risk.

Generally, there are three aspects concerning the risk assessment, and corresponding to them, there are three types of criteria for evaluating the coastal erosion risk, they are the individual criteria, societal criteria and economic criteria (Woodroffe et al., 2012).

The individual risk criteria, concerning the individual who decides to undertake an activity weighing the risks against the direct and indirect personal benefits. The societal criteria considers if an activity is acceptable in terms of the risk-benefit trade-off for the total population (Vrijling et al., 1998). In the view of economic criteria, the economically optimal protection levels (without considering the life safety) are expected, which can be obtained from cost-benefit analyses. This optimisation procedure, that has been used in the Netherlands since the 1950s, is shown schematically in Fig. 7.1 (Van Dantzig, 1956).In this chapter, only the economic criteria is analysed and discussed.

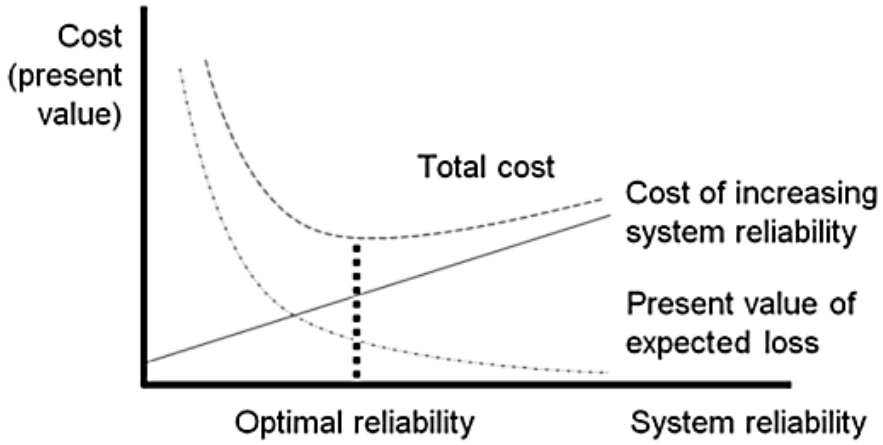

Figure 7.1 The optimization of a system reliability (Woodroffe et al., 2012).

7.2.1 Damage probabilities due to erosion

Dune erosion is usually the result of a combination of reasons, both episodic erosion and long term shoreline retreat trend with different time scales. Short term dune erosion is that, once the storm impacts on the sandy beach, sediments from the mainland and upper parts of the beach are eroded and settled at deeper water, while the long term dune erosion is caused by climate change, alongshore sediment transport and anthropogenic impacts et al..

In Table 5.2, the probabilistic estimation of coastal retreat distance were provided, meanwhile, the figures also illustrate the connection between the erosion probabilities and the distance from the coastal line. Vrijling et al. (2002) made a simple approximation to the probability of exceedance of retreat distance with exponential distribution:

$$P(X > x) = p(x) = b \cdot e^{-cx}, \tag{7.1}$$

where, $P(X > x)$ is the exceedance erosion probability per year and the *x* (m) is the distance from the dune foot and the *b* and *c* are the constant coefficients, the minus means that the probability decreases landward. Fig. 7.2 shows the exponential approximation for SLR=0 scenario in the Noordwijk aan Zee beach, where *b* is 1355.6 and *c* is 0.303. The dots are the computed result from Chapter 5.

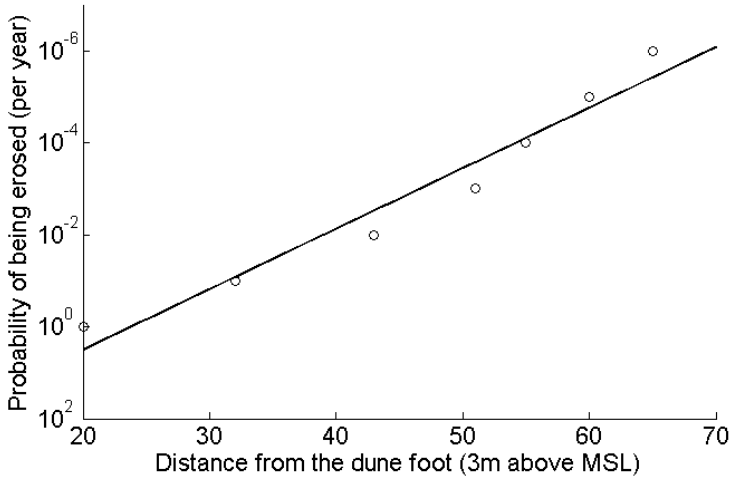

Figure 7.2 Erosion probability as a function of distance from dune foot.

The erosion probability contours are a set of parallel lines, on each of which the erosion probability is the same, as shown in Fig. 7.3. The contours are predicted to shift landward gradually due to the projected SLR, consequently the exceedance erosion probability at certain point in the erosion prone zone will increase over time. Jongejan et al. (2010) simulated the increasing probability trend by the way of establishing an exponential formula, that is, increasing rate is assumed to be exponential:

$$P(X > x,t) = p(x,0)e^{at} = be^{-cx+at} \quad \text{and } at \le -\ln p(x,0), \tag{7.2}$$

where *t* is the time (year), *a* is probability rising rate, which represents the climate change, that is SLR in this thesis. Fig. 7.4 shows the probability of erosion volume for different SLR scenarios. The solid black line is the erosion probability when SLR=0, meantime, it also means the erosion probability in the year 1990, i.e. the beginning time of the rising mean sea level. The dot line is the erosion probability in 2100 and SLR is 0.4m, while the dash line is obtained when SLR is 1.05m. Note that, these lines are different from the Fig 5.5, which show the erosion volume of various return periods from 1990 to 2100. In other words, the lines in Fig. 7.3 are the probability within one year (2100), while the lines in Fig. 5.5 are the probability within 111 years.

The probability rising rate, *a*, in Eq. 7.2 can be calculated on the basis of erosion volume probability calculated in Chapter 5, and the relationship between erosion volume and retreat distance. The calculation result is that when SLR = 0.4m, $a \approx 0.01$, and $a \approx 0.02$ for SLR = 1.05m.

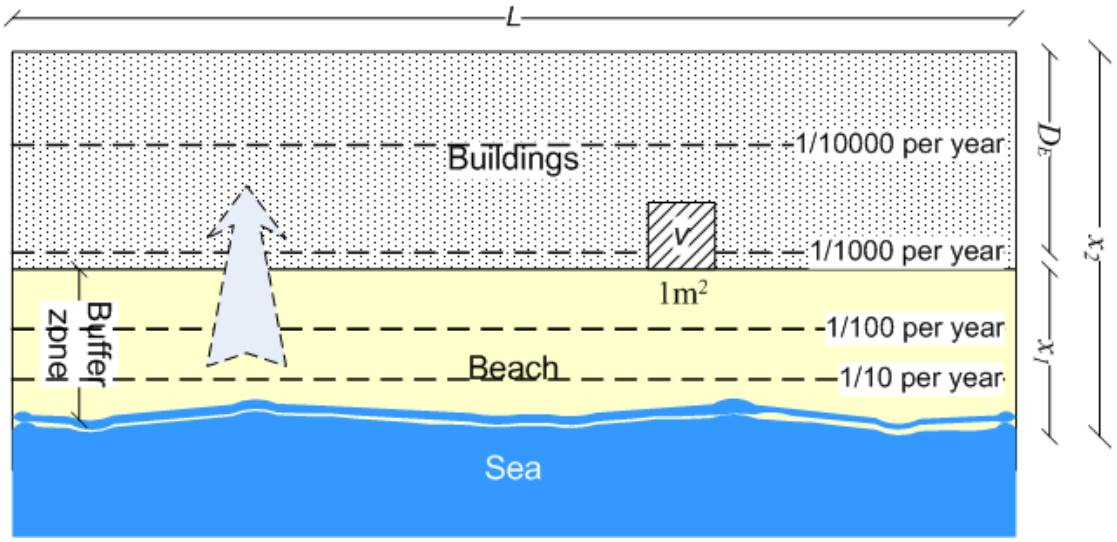

Figure 7.3 Sketch of the coastal zone and the erosion probability contours (Li et al., 2011).

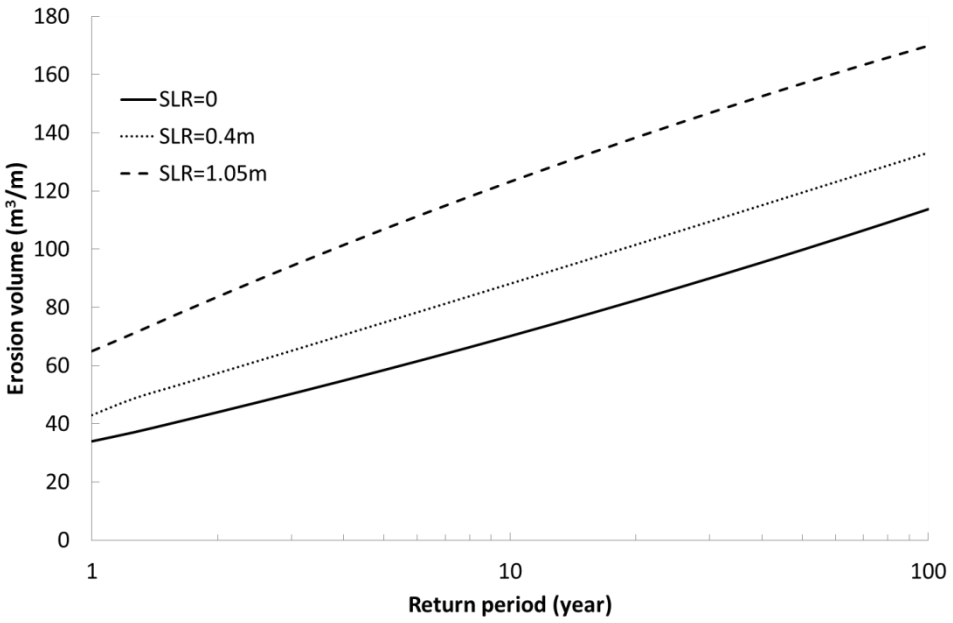

Figure 7.4 The erosion volume probability for different SLR scenarios.

7.2.2 Economic value in the coastal zone

Many coast regions can be characterized as high density land-use areas, where have booming economy and population. For instance, in a seaside resort, a large number of buildings are constructed for tourist trade, such as hotel, restaurant and waterfront promenade. The distribution of the economic value in the coast zone is parameterized as a function of the distance from the shoreline by the economic value density function *v(x)* (euro/m^2) (Vrijling et al., 2002), if *L* (m) is length of the coastal block, x_1 (m) and x_2 (m) are

distance from shoreline as indicated in Fig.3, the line corresponding to the x_1 is the setback line, then the total value of the properties *V* (euro) from x_1 to x_2 is:

$$V = L \cdot \int_{x_1}^{x_2} v(x)dx \tag{7.3}$$

For the quantification of property loss, several assumptions and simplifications are made here:

a. Only the property damage due to the erosion is considered. This paper aims to suggest a most reasonable coastal land-use planning in the view of economy, but it does not mean that other damage is less important or can even be neglected. On the contrary, environmental factors usually should come first;

b. The structures will be totally destroyed if being eroded, and will be rebuilt immediately after the erosion. That is, assuming that the reoccurrence of a small probability storm within a relative short period is not going to happen. This is reasonable when compare the build time to the return period.

c. We assume that the properties locate further than D_E (m, Fig. 7.5) from shoreline will have neither additional risk nor additional benefits from the sea. For the purpose of explaining the way of finding optimal position, the return rate on investment is simply assumed as:

$$\begin{cases} R_E(x) = A_E - B_E \cdot x & \text{for } (0<x<D_E) \\ R_E(x) = R_m & \text{for } (x \geq D_E) \end{cases}, \tag{7.4}$$

where, A_E, B_E and D_E are constant coefficients, and R_m is the mean return rate where properties locate inland.

d. *v(x)* , as shown in Fig.3, is assumed as a constant, and Eq. (7.3) becomes:

$$v = \frac{V}{(x_2 - x_1) \cdot L}. \tag{7.5}$$

And the uncertainty of the value at risk is ignored at present.

e. Damage is only caused by coastal erosion. The effect of e.g. wave impacts beyond the erosion contour is ignored.

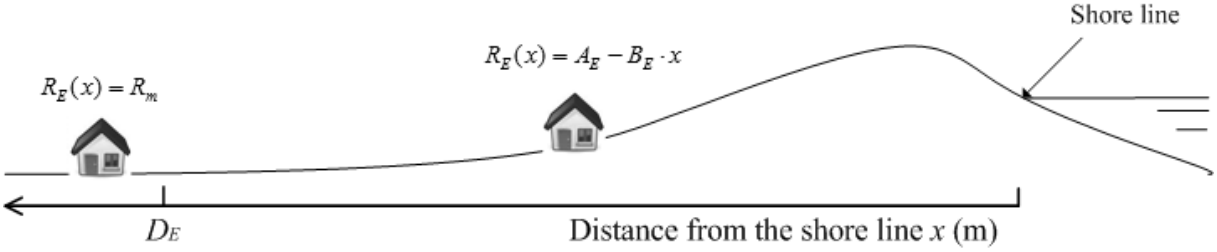

Figure 7.5 Sketch of the return rate on investment near the sea.

These approximations are made for easily explaining how this risk informed approach work. The limitations can be relaxed in reality by employing the expressions closer to practical circumstance.

7.3 Economic optimization of land-use strategy in coastal zone

7.3.1 Buffer zone

Buffer zone is the transition region between shoreline and the constructions development area. It is a natural land area where has intense interaction with ocean. And establishing a buffer zone is a land-use policy to keep properties away from unexpected storm hazards, as well as mitigate the anthropophagic intervenes to coastal zone. In the view of economy, buffer zone is an area with larger economic loss due to natural hazard than benefit from the investment. In this chapter, the buffer zone land-use policy means to move the properties landward to create a buffer area for the conflict between damage and profit.

To analyse the trade-off between benefit and loss, the Net Present Value (NPV) per unite length of shoreline (i.e. total NPV divided by shoreline length *L*) is calculated by considering the time value of money. Hereafter, the NPV represents the total NPV_{total}/L (euro/m). In this context, the optimal width of the buffer zone is where the properties on the coast can gain its maximum NPV. And the NPV can be expressed as the sum of present value of annual return minus investment and the sum of present value of annual payment for erosion.

Jongejan et al. (2010) gave a general equation, which proposes an optimal position for a single property during its limitless economic lifetime (T_E, year), the total Net Present Value for a single property is:

$$\mathrm{NPV}_{total\_s} = \int_0^{T_E} R_E(x)\cdot I_E(x)\cdot e^{-\gamma t}\cdot dt - I_E(x) - \int_0^{T_E} P(x,t)\cdot I_E(x)\cdot e^{-\gamma t}\cdot dt\,. \tag{7.6}$$

Where the $I_E(x)$ (euro) is the initial investment per m^2 at distance *x, r* is the interest rate. The first term is the benefit from the investment and the last term is the annual cost due to the storm erosion, i.e. the erosion risk.

In the proposed case study (Fig. 7.3), the artificial coastal zone, considering the limit economical lifetime of the properties and the changing damage probabilities, the equation becomes:

$$\mathrm{NPV} = v\cdot\int_{x_1}^{x_2} R_E(x)dx\cdot\beta - v\cdot(x_2-x_1) - v\cdot\sum_{t=1}^{T_E}[\int_{x_1}^{x_2} p(x,t)dx\cdot\frac{1}{(1+r)^t}], \tag{7.7}$$

$$\beta = \sum_{t=1}^{T_E} \frac{1}{(1+r)^t} \approx \frac{(1+r)^{T_E} - 1}{r \cdot (1+r)^{T_E}}, \tag{7.8}$$

Where, $\mathrm{NPV} = \mathrm{NPV}_{total} / L$ (Euro/m), $v = V / L$ (Euro/m^2) and β is the transfer coefficient of net present value and the ordinary annuity.

To find the optimal value of x_1 which makes NPV maximal, Eq.(7) is differentiated with respect to x_1:

$$\frac{d\mathrm{NPV}}{dx_1} = v[R_E(x_2) - R_E(x_1) + \sum_{t=1}^{T_E} \frac{p(x_1, t)}{(1+r)^t}] = 0. \tag{7.9}$$

Generally, x_2 will be long enough and make $R_E(x_2) = R_m$ and makes $p(x_2, t) = 0$.

Rearranging Eq. (7.9):

$$\beta \cdot [R(x_1) - R_m] = p(x_1, 0) \cdot \sum_{t=1}^{T_E} \frac{e^{a \cdot t}}{(1+r)^t} \tag{7.10}$$

Hence, the solution of Eq. (7.10) is the optimal width of the buffer zone, x_{opt}. When *a* = 0, that is to say, the coast is under a stationary morphological condition, the erosion probability contours do not shift landward over time. Then Eq. (10) becomes:

$$R(x_1) - R_m = p(x_1, 0) \tag{7.11}$$

This result is the same with the research of Jongejan et al. (2010). x_{opt} should be where the erosion probability equals to the difference between the return rate at x_1 and the inland mean return rate. This is also indicates that the higher return rate at the coastal zone is offset by the additional erosion risk compare to the inland conditions.

From the Eq.7.10 and 7.11, we can find that the optimal buffer zone width is independent of the economic value of the properties on the beach. In order to understand the impact of some key parameters to the optimal buffer zone width, several comparisons were made in Fig.7.6-7.8 (assuming *r* = 0.025, A_E = 0.1, B_E = 0.0003, D_E = 200m and R_m = 0.04 here). In Eq. 7.7, the *v* is relatively constant, so the ratio between NPV and *v* (NPV/*v*) can be used to compare the economic profits obtained from different situations. Hereafter the *NPV/v* was used to make the comparison in this chapter for the reason of simplicity.

When the economic lifetime of the properties is assumed as 50 years, Fig. 7.6 illustrates the effect of probability rising rate *a* on the NPV and x_{opt}. The vertical coordinate is NPV/*v*. As expected, the buffer zone will be wider according to the higher *a*, meanwhile the NPV/*v*

decreases. The shape of the curves is related to $R_E(x)$. The NPV/*v* increases rapidly at first as the erosion probability falls down more significantly than return rate, and after reaching the peak value, the NPV/*v* decrease gradually with the slop according to the return rate coefficient *B* in Eq. 7.4. In Fig. 7.6, when *a* = 0.01, SLR is 0.4m from 1990 to 2100, and when *a* = 0.02, SLR is 1.05m for the same period, so, *a* = 0.05 is quite large. It can be concluded from the figure that the effect of the probability rising rate on the optimal setback line and the maximum NPV/*v* is not great.

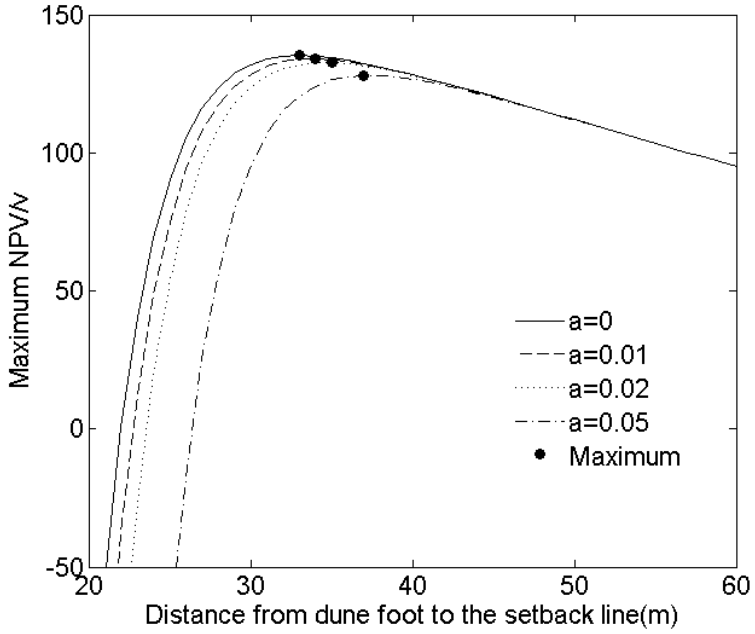

Figure 7.6 The effect of probability rising rate, *a*, on optimal x_1 and the black dots are the maximum NPV/*v* according to optimal x_1.

Fig. 7.7 and 7.8 show the NPV/*v* and the optimal x_1 as a function of the economic lifetime of the properties with different probability rising rate. The greater the erosion probability rising rate (*a*) the larger optimal buffer zone width (x_1), but the NPV/*v* does not decrease dramatically. As illustrated by these two figures, the rate of the long-term trend, *a*, does not impact the maximum NPV/*v* significantly, but the optimal x_1. One reason for less impact on the NPV/*v* is that, within the large coastal block, only the forward part of the block, where the damage probability is very high, will be strongly influenced by erosion hazard, for the rest part of the block, NPV/*v* does not change a lot. As long as the NPV/*v* is positive, an investment is worthwhile, therefore, according to the Fig. 7.7, it is not advisable to construct a property with a shorter economic lifetime. And the critical lifetime has a close relationship

with the interest rate, *r*. The optimal buffer zone width for different erosion probability rising rate were listed in Table 7.1.

Table 7.1 The optimal buffer zone width under different SLR scenarios.

	Buffer zone			
	a=0	a=0.01	a=0.02	a=0.05
Buffer zone width (m)	33	34	35	37
Maximum NPV/v (-)	135	134	132	128

7.3.2 Beach nourishment

An alternative land-use strategy for coastal zone is extending the dune width by beach nourishment. Beach nourishment is the supply of sand to the shore to increase the recreational value and/or to secure the beach against coastal erosion by feeding sand on the beach (Mangor, 2004). The beach nourishment can be carried out through three ways: once at the beginning, periodical beach nourishment and the over-threshold beach nourishment. The main aim of the section is to find the optimal beach nourishment for each way and compare them.

In this section, the average economic lifetime of the coastal properties is assumed as 50 years. A planning timeframe of 50 years is considered suitable, considering that the present lifetime cycles of building projects are approximately the same (Winckel et al., 2008). However this assumption can be adjusted according to the local situations.

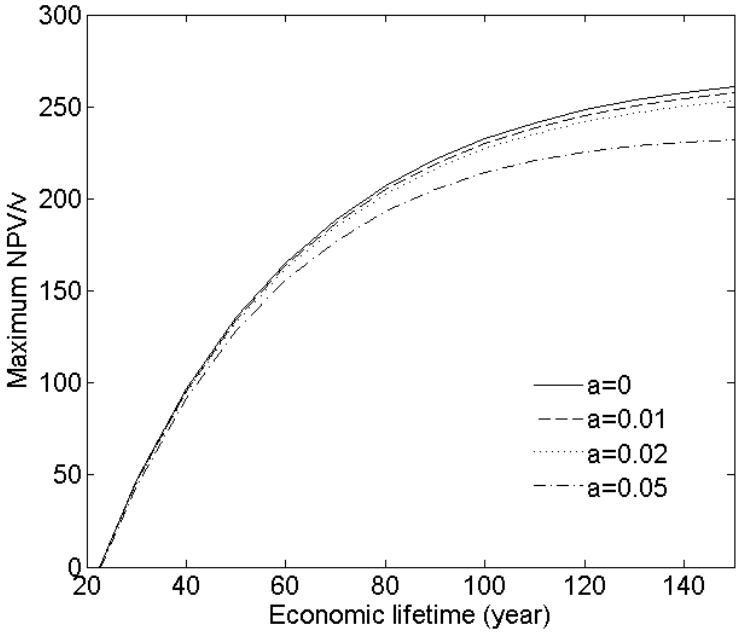

Figure 7.7 The effective of economic lifetime on maximum *NPV*/*v*.

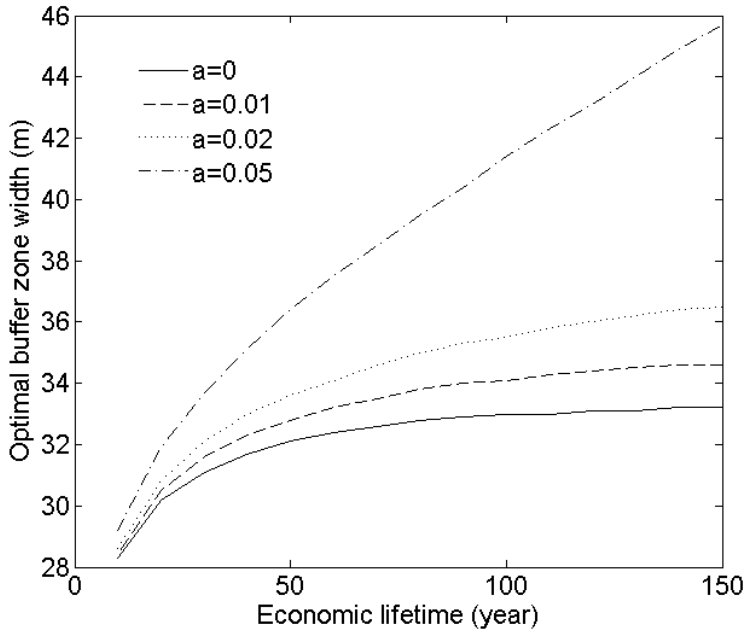

Figure 7.8 The effective of economic lifetime on optimal x_1.

7.3.2.1 One-time beach nourishment

One-time beach nourishment means, the beach nourishment is carried out at the *t* = 1 in Eq. 7.6. For each nourishment, the volume of sand is a function of the sand nourishment width *w* (m) in the following way (Van Noortwijk and Peerbolte, 2000):

$$M(w)/L_N = h_N \cdot w + \frac{\sin(\alpha_0)}{2}[\cos(\alpha_0) + \frac{\sin(\alpha_0)}{\tan(\varphi_0 - \alpha_0)}] \cdot w^2, \qquad (7.12)$$

where, *M* (m^3) is the nourishment sand volume, L_N (m) is the nourishment length, α_0 and φ_0 are the angles (degree) of the sea floor and beach profile slope (Fig. 7.9). For the reason of simplicity, it is assumed that the beach nourishment length is the same as the beach zone length, that is $L_N = L$ in Fig. 7.3.

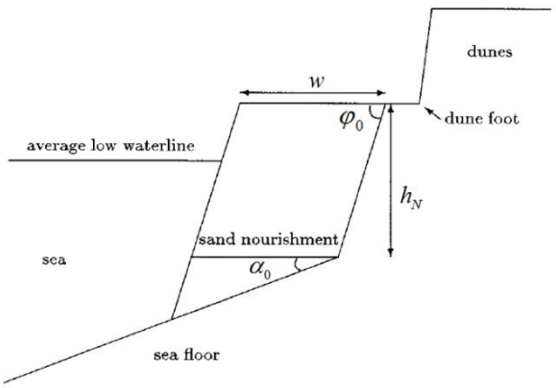

Figure 7.9 Sketch of sand nourishment volume, modified after Van Noortwijk and Peerbolte (2000) .

In the proposed coastal area, the total NPV is:

$$\mathrm{NPV} = v \cdot \int_{x_1}^{x_2} R_E(x+w)dx \cdot \beta - v \cdot (x_2 - x_1) - v \cdot \sum_{t=1}^{T_E} [\int_{x_1}^{x_2} p(x+w,t)dx \cdot \frac{1}{(1+r)^t}] - N(w), \quad (7.12)$$

where, $N(w)$ is the cost of the sand nourishment of w (m) in width. In order to make comparisons, it is assumed that the ratio between the cost of per m^3/m sand nourishment and the value density v is1/4, that is $1/4 \cdot v \cdot M(w) = N(w)$. Hence, Eq.7.12 becomes

$$\mathrm{NPV}/v = \int_{x_1}^{x_2} R_E(x+w)dx \cdot \beta - (x_2 - x_1) - \sum_{t=1}^{T_E} [\int_{x_1}^{x_2} p(x+w,t)dx \cdot \frac{1}{(1+r)^t}] - \frac{1}{4} \cdot M(w). \quad (7.13)$$

According to the analysis result of the optimal buffer zone width (Fig. 7.6), the NPV/v falls down below 0 when the buffer zone width is about 20m, in this situation, a beach nourishment is required. Therefore, the initial buffer zone width (x) in Eq.7.13 is fixed as 20m. The other assumptions are the same as in Section 7.3.1. Fig. 7.10 shows the NPV/v as a function of various nourishment volumes. As expected, the beach nourishment will increase the NPV/v by reducing the cost of damage at first. With the increasing nourishment volume, the cost of nourishment will impact the total NPV/v more and more significantly and make the strategy uneconomical. On the basis of the assumptions made above, the Fig. 7.10 gives an optimal one time beach nourishment volume of 14m for a=0.05 and 12m for a=0.01.

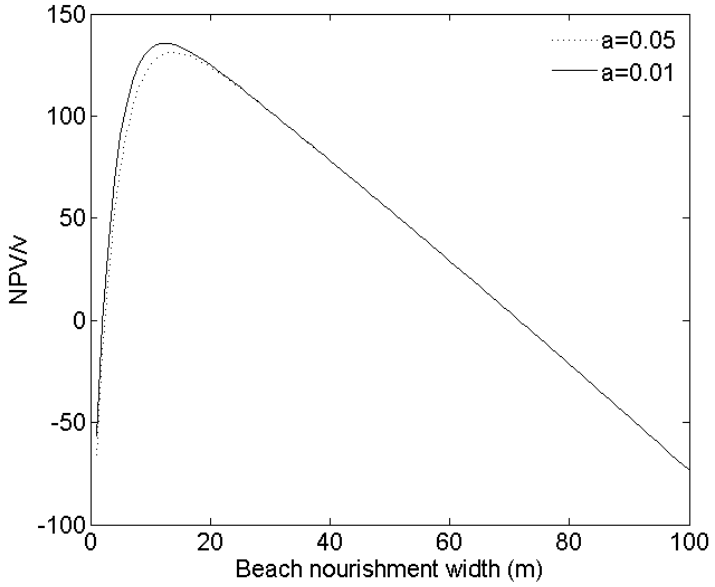

Figure 7.10 NPV/v as a function of beach nourishment width by applying the one-time beach nourishment method.

7.3.2.2 Periodical beach nourishment

Another way of sand nourishment is to carry out periodically instead of once at *t*=1. Assuming that the nourishment was going to carry out *j* times within the next 50 years, so the time interval is *i*=50/*j*, for each time interval between the nourishment, the *j*th NPV/*v* for the study site is:

$$\begin{aligned} \mathrm{NPV}_j / v = & \int_{x_1}^{x_2} R_E(x + w_j)dx \cdot \beta_j - (x_2 - x_1) \\ & - \sum_{t=i\cdot j-i+1}^{i\cdot j} [\int_{x_1}^{x_2} p(x + w_j, t)dx \cdot \frac{1}{(1+r)^t}] - \frac{1}{4} \cdot M(w_j) \cdot \beta_j^*, \end{aligned} \tag{7.14}$$

where, w_j is the nourishment width at *j*th period, and

$$\begin{aligned} \beta_j &= \sum_{t=i\cdot j-i+1}^{i\cdot j} \frac{1}{(1+r)^t}; \\ \beta_j^* &= \frac{1}{(1+r)^{i\cdot j-i+1}}. \end{aligned} \tag{7.15}$$

And the total *NPV/v* is:

$$NPV / v = \sum NPV_j / v\,. \tag{7.16}$$

For simplicity, six time interval were chosen to make comparison, they are 1, 2, 5, 10, 25 years respectively, corresponding to 50, 25, 10, 5 and 2 times of sand nourishment. Fig. 7.11 shows the NPV/*v* under different beach nourishment frequencies and different probability rising rates. No matter what the probability rising rate is, the most favourite nourishment frequency is twice within 50 years, while the optimal nourishment amount differs. As expected, the larger the *a* is, the more sand is required to protect the beach and gain the maximum profit. When *a*=0.01, the optimal nourishment width is 21m, for a=0.05, the optimal nourishment width is 24m.

7.3.2.3 Over-threshold beach nourishment

The last method, over-threshold beach nourishment, selects a threshold of storm erosion level. And if a worst case storm erosion event occurs, which is higher than the designed level, the sand nourishment should be carried out. For instance, if the threshold level is P_{th}, when

an erosion event with a smaller exceedance probability than P_{th} occurs, a beach nourishment is expected.

The selected threshold can be exceeded every year. Within the 50-year economical lifetime of the properties, it is supposed that the threshold was exceeded twice at k th year and ($k+n$)th year (*k* and *n* are the positive integer, and $k+n \le 50$). Then the whole period was then divided into three parts, so was the NPV/*v* (indicated by NPV_1/v, NPV_2/v and NPV_3/v). The NPV_1/v before the *k*th year can be computed by using Eq.7.7, and the T_E equals to *k*.

$$\mathrm{NPV}_1 / v = v \cdot \int_{x_1}^{x_2} R_E(x)dx \cdot \sum_{t=1}^{k}[\frac{1}{(1+r)^t}] - v \cdot (x_2 - x_1) - v \cdot \sum_{t=1}^{k}[\int_{x_1}^{x_2} p(x,t)dx \cdot \frac{1}{(1+r)^t}] \tag{7.17}$$

The NPV_2/v which is the value between the *k*th and (*k+n*)th year, and NPV_3/v which is the value between the (*k+n*)th year and the T_E become:

$$\begin{aligned}\mathrm{NPV}_2 / v = &\int_{x_1}^{x_2} R_E(x+w)dx \cdot \sum_{t=k+1}^{k+n}[\frac{1}{(1+r)^t}] - (x_2 - x_1) - \\ &\sum_{t=k+1}^{k+n}[\int_{x_1}^{x_2} p(x+w,t)dx \cdot \frac{1}{(1+r)^t}] - \frac{1}{4} \cdot \frac{1}{(1+r)^k} M(w)\end{aligned} \tag{7.18}$$

$$\begin{aligned}\mathrm{NPV}_3 / v = &\int_{x_1}^{x_2} R_E(x+w)dx \cdot \sum_{t=k+n+1}^{T_E}[\frac{1}{(1+r)^t}] - (x_2 - x_1) - \\ &\sum_{t=k+n+1}^{T_E}[\int_{x_1}^{x_2} p(x+w,t)dx \cdot \frac{1}{(1+r)^t}] - \frac{1}{4} \cdot \frac{1}{(1+r)^{k+n}} M(w).\end{aligned} \tag{7.19}$$

When the threshold is not very low (P_{th} <4%), it will be exceeded more than twice on average, the entire period will be divided into more parts. Due to the uncertainty of the occurrence time and frequency of the over-threshold storm erosion event, the value of NPV/*v* will also has uncertainty which is different from the other two methods. So, instead of comparing the deterministic values, the mathematical expectation of the NPV/*v* for the whole economic lifetime was computed and compared (Fig. 7.12). The Monte-Carlo technique is used to simulate the expected value of NPV/*v* for different combinations of the threshold and the nourishment width.

For example, a 50-year storm erosion process is firstly generated by using the methods in Chapter 3 and 4. Once an over-threshold event occurs, the NPV_1/v is computed according to Eq.7.17. When the second over-threshold event occurs, the NPV_2/v is calculated by using Eq. 7.18, and continue this till the end of time. After this, the NPV/*v* of one simulation is computed. Repeat this process for 10^4 times, the mathematical expectation of the NPV/*v* is obtained.

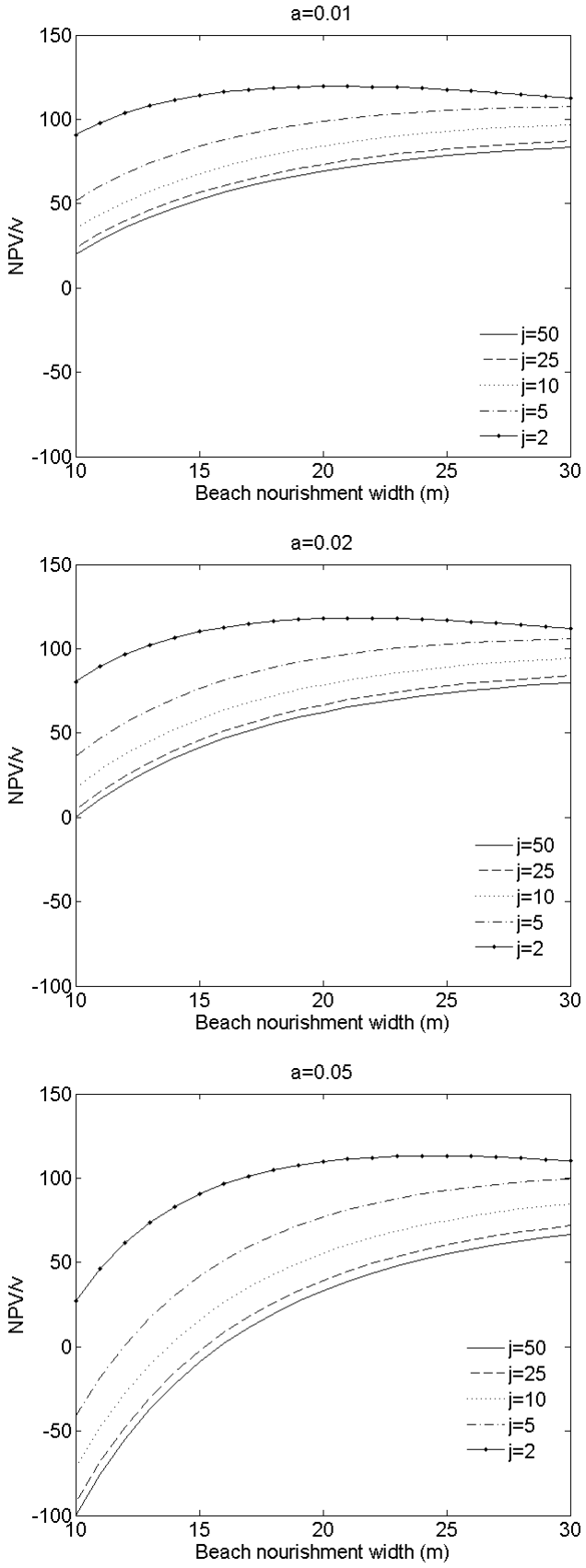

Figure 7.11 *NPV/v* as a function of beach nourishment width by applying the periodical beach nourishment method, *j* is the number of times.

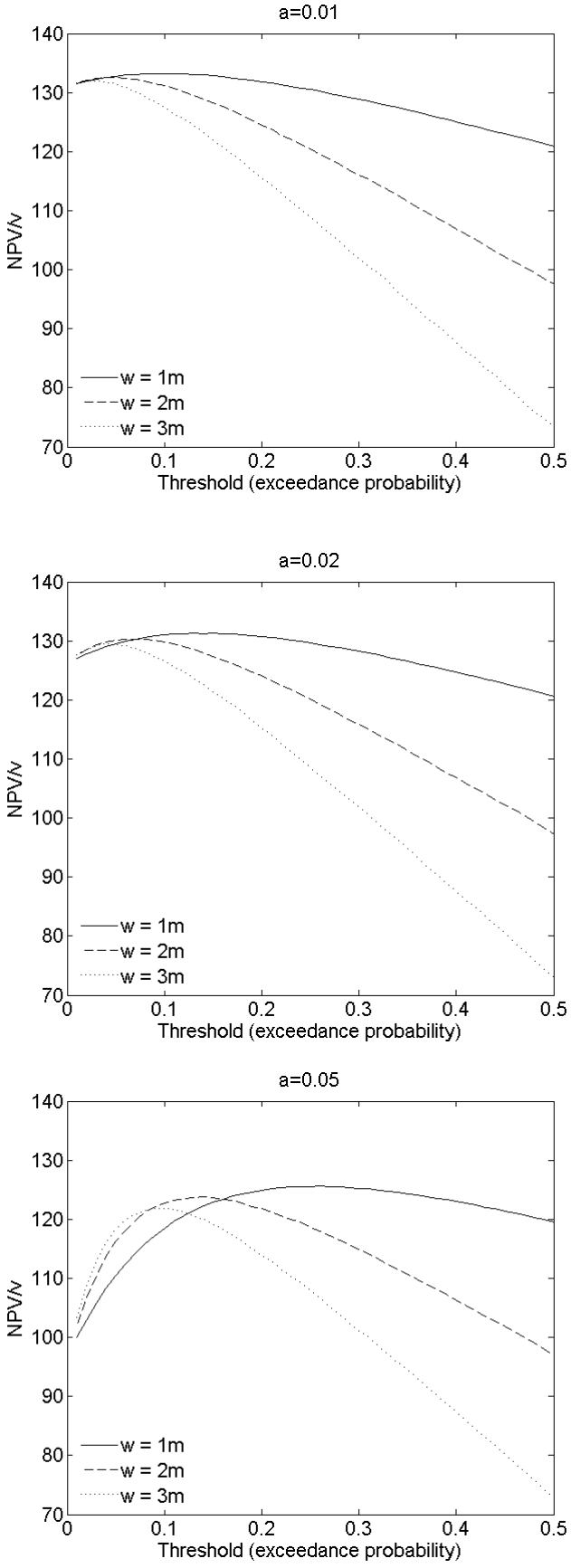

Figure 7.12 NPV/*v* as a function of the threshold by applying the over-threshold beach nourishment

In Fig. 7.12, when the threshold is relative small, the difference between the different between the curves are small, and the differences become larger and larger the threshold increasing. For the higher threshold, the 1m nourishment width is always preferred for different probability rising rate. When probability rising rate is high and the threshold is small, the nourishment width is expected to increase to get the maximum NPV/*v*.

7.4 Discussion

The most economical solutions on the basis of buffer zone strategy and the sand nourishment strategy are given in Table 7.1 and 7.2. In the study site with the assumptions, in this specific situation, the best land-use strategy is beach nourishment, which should be carried out once at the beginning, as its NPV/*v* is the largest. However there are a lot of hypothesis and the approximations in the computation process, it is meaningless to discuss and compare the absolute magnitude of the values.

Table 7.2 The optimal beach nourishment length using different methods under three SLR scenarios.

	one-time			periodical			threshold**		
	a=0.01	a=0.02	a=0.05	a=0.01	a=0.02	a=0.05	a=0.01	a=0.02	a=0.05
Nourishment width* in total (m)	12	13	14	21	21	24	5	6.5	13
Nourishment frequency (times/50 years)	1	1	1	2	2	2	5	6.5	13
Threshold, *P(X>x)*							0.1	0.13	0.26
Maximum NPV/*v*	136	135	131	120	118	113	133	131	126

*The nourishment width is the total width in this table;

**The values calculated by using over-threshold method are the expected values.

The assumed value density in the coastal zone was crude. It is reasonable when the coastal zone length is long enough, and with a large amount of properties the uncertainties will be cancelled a lot. And so as the return rate. Instead of considering the entire dynamic coastal business zone as a whole, one property can be solely analysed to find an optimal setback position. In this case, the property value and return rate can be estimated more precisely.

The alongshore sediment transport was ignored in this Chapter, therefore, the total sand volume in the interactive zone of ocean and land before the beach nourishment is invariable. And the long-term erosion was assumed to be caused by SLR only. If the coastal zone suffers

long-term permanent erosion induced by loss of sand from the system, more sand should be added to compensate this influence on the basis of alongshore sediment transport investigation.

In general, the cost of beach nourishment can be divided into two parts (Van Noortwijk and Peerbolte, 2000), the fixed cost (cost of mobilization) and the variable cost (cost of per cubic meter sand). The fixed cost was ignored in this Chapter, for the reason of little influence in the way of calculation and the large uncertainty in estimation. By considering the fixed cost, the curves in the Fig.7.10-7.12 should be lower. And in the reality, the fixed cost should be considered carefully, especially for the approach including more than one construction stage.

In this case study, the one-time sand nourishment guideline was recommended, but it is should be noted that, this is a very specific case, therefore, one cannot conclude that the one-time beach nourishment is the best decision. The selection of the strategies and also the detailed operation method are closely related to the local situation. Such as the coastal erosion contour density, local discount rate, local property density, et al.. These will alter the final calculation result significantly and influence the final decision.

Other types of coastal zone protection method are not discussed in the present studies, such as dike reinforcement or breakwaters. Besides the aspect of economic, the technical and environmental factors are also required to be taken into account.

Chapter 8 Conclusions and recommendations

8.1 General reflection

One critical question will arise when look back at the statistics jumping out of a specific case: is it reliable to predict the event that has not happened ever on the basis of probability statistics? In other words, is the variable really obey the law given by the fitting probabilistic distribution? Because the whole thesis is based on the answer of "yes".

In order to answer it, an important philosophical concept should be introduced first, the determinism. This thesis is mainly based on the opinion of the world view supported by the determinists, among them, Albert Einstein revealed his devout belief and stated in the letter sent to the physicist Max Born:

'You believe in a God who plays dice, and I in complete law and order in a world which objectively exists, and which I in a wildly speculative way, am trying to capture. I firmly believe, but I hope that someone will discover a more realistic way, or rather a more tangible basis than it has been my lot to find. Even the great initial success of the

quantum theory does not make me believe in the fundamental dice game, although I am well aware that some of our younger colleagues interpret this as a consequence of senility.'(Adams, 1995).

Determinism is often contrasted with free will. The argument between them has puzzled philosophers for thousands of years (even the issue that whether the principles of the statistics belong to determinism or non-determinism is still under dispute). And it will not stop in the near future. The determinism and the free will belong to the category of world view, while the statistics belongs to the category of methodology which is developed from the summary of long term human experiences. The statistics cannot explain the world completely, but it will help us to understand the world. At present, it is one of the best ways to know the world. The meaning of the statistics is to tell the human beings that the universe is so complicated and huge, we should never stop exploring. Therefore, with one of the best ever known methodologies, we have reasonable ground to believe the validity of the statistics in practice.

8.2 Conclusions

Storm forecasting is great of important to the coastal defence and management, in this thesis we have shown the incorporation of multivariable simulation in the coastal storm estimation has the capability to predict the coastal erosion due to the storm for a coastal safety system. The Monte-Carlo method was applied to overcome the disadvantage of design event method, and the copulas were introduced to simulate the multivariate and the dependency structures. The research was carried out by using the Noordwijk aan Zee coast, the Netherlands as a study site and the method was tested in the Narrabeen Coast, Australia. In the end, a guideline of coastal zone development and utilization is proposed in the view of economic criteria, make a simple artificial coast zone as a case.

8.2.1 Wave climate simulation

In summary, the storm simulation includes three steps: fit each observed storm variables with marginal distributions; construct the dependency structure; simulate the wave climate from the obtained joint probability.

In the Dutch case, the Gaussian copula method is the most appealing approach among others because of its best fitting quality and simplicity. While for the Australian case, both the Archimedean copula and Gaussian copula method provide plausible consistency with the measurement according to the Chi-square test. When using the simulated storms obtained by Archimedean copula, the erosion quantile value of each return period trends to be much smaller than that obtained from the measurements. Therefore, the Gaussian copula method was also recommended for the Narrabeen Beach.

The copula method for multivariate is constructed and tested in this thesis, which is an extension and simplification of the existing researches.

8.2.2 Dune erosion model

The simple empirical dune erosion model, DUNERULE is feasible to act as a structural function to estimate the dune erosion volume. The DUNERULE should be adjusted by XBeach model before application. It should be adjusted with the field measurements, like what has been done in Chapter 6. When the sufficient measurements are not variable, it can be adjusted by comparing to a sophisticated erosion model, such as XBeach in Chapter 4.

The widely used erosion model DUROS in the Netherlands is appropriate for the design beach erosion assessment method. It is developed based on the concept of profile equilibrium. The input for this model is the design events, in which the parameters are not time dependent. While the adjust DUNERULE takes the storm duration and time varying wave climate parameters into account, hence it can give the profile response during a storm before it reaches the equilibrium state. Because of that, the adjusted DUNERULE can be implemented in the Monte Carlo method.

The method of simplifying a highly complex model (XBeach model) by calibrating a simple model (DUNERULE model) is valid for the probabilistic estimation of coastal dune erosion. The DUNERULE model which coupled with Monte-Carlo technique can produce robust erosion estimates within an acceptable computation time.

8.2.3 Erosion probability estimation

The dune erosion probabilities were presented in the form of return period. For the Netherlands, a low-lying country, the damage of an unexpected storm will lead to massive loss. Moreover, the land resources are of great significant for a small area

country. Therefore, the safety level for the Dutch is much higher than the other countries, like the Australia in Chapter 6.

The dune erosion volume and retreat distance corresponding to the critical return periods were calculated by employing the Monte-Carlo technique. And the confidence limits were also obtained from the Monte-Carlo simulation processes. Considering one of the most concerned consequences of global warming, SLR, its impact on the future dune erosion probability was also analysed. The results indicate that SLR does not increase the incidental storm intensity significantly but increase the long term dune net erosion a lot by the end of 2100.

Due to the lack of being constrained by the physical limitation, three methods were used to constrain the 95% confidence interval derived from the pure statistical estimation. These methods can reduce the uncertainties a lot, one can select one of them according to specific local situations.

Comparing to the Bruun rule, which only provide one rough definite estimation, the advantage of the probabilistic model is it can give a more accurate description of the coastal retreat distance in terms of probability.

8.2.4 Coastal zone land-use strategy

In the view of economic criteria, two types of land-use strategies were proposed and analysed to fully develop the land resources in the coastal zone. They are the buffer zone and beach nourishment strategies. A computing method of searching the optimal buffer zone width was given in Eq.7.10 and 7.11. And the impact of the landward moving erosion probability contours was analysed. The projected SLR (0.4m or 1.05m from 1990 to 2100) increases the buffer zone width, and the increasing extent has a close relationship with the interest rate.

Three approaches of beach nourishment were discussed. Under the given assumptions and the calculated erosion probability, the one-time beach nourishment is the most economical approach, however this is not what the Dutch government did for decades. Actually, this study is trying to find a computing method rather than a decision making. The assumptions in this thesis will vary from place to place according to the reality, therefore, the analysis in the Section 7.3.2 only proposes some nourishment approaches and provides the method of comparing and calculating the optimal nourishment width for each approach.

The corresponding chapter extends the method of Vrijling et al. (2002) and Jongejan et al. (2010) by considering the beach nourishment as an optional land-use strategy.

8.3 Recommendations

Some parts of this thesis can be improved for the future work, and on the basis of this thesis several recommendations are made below:

- In order to include more physical constraints in the purely statistical model, the storm driving forces and the local climatic system are recommended to be investigated. And the accuracy of the dependency structures will benefit from the introduction of more inner physical relationship among the wave climate variables.
- Longer time series wave climate data and the coastal profile measurements are recommended, this will improve the distribution fitting quality. The investigation of the historical extreme values will help for the statistic modelling of extreme values.
- Non-stationary statistics model can be used to improve the wave climate simulation under the changing climatic conditions. Time dependent probability distribution parameters can be used to simulate the time dependent wave climate.
- A more effective multivariate distribution goodness-of-fit technique is recommended to test the simulation quality.
- Besides SLR, other factors induced by the global climate change are recommended to be taken into account, such as the storm frequency, wave height, etc..
- A more sophisticated dune recovery model is recommended. That needs more bathymetry and profile survey after a storm. It will improve the model accuracy of dune erosion and recovery process.
- It is recommended to take the alongshore sediment transport into account in the future work. It will enable the current framework to be applied for the coast where the alongshore sediment transport cannot be ignored.
- The probabilistic economic model only provides a risk-informed tool within the context of economics, more aspects are recommended for the development of integrated coastal zone management policy.

Coastal dune erosion has an intricate mechanism. A lot of knowledge gaps still remain. I hope this thesis will assist in improving the coastal erosion simulation and developing the coastal zone management.

References

Adams, J., 1995. Risk. University College London Press, 228 pp.

Andrews, D. and McIntyre, M., 1978. An exact theory of nonlinear waves on a lagrangian-mean flow. Journal of Fluid Mechanics, 89(04): 609-646.

Anonymous, 1995. New south wales ocean tide levels annual summary 1994/95, Manly Vale, NSW.

Borgman, L.E., 1973. Probabilities for highest wave in hurricane. Journal of the Waterways, Harbors and Coastal Engineering Division, 99(2): 185-207.

Bortot, P., Coles, S. and Tawn, J., 2000. The multivariate gaussian tail model: An application to oceanographic data. Journal of the Royal Statistical Society: Series C (Applied Statistics), 49(1): 31-049.

Callaghan, D.P., Nielsen, P., Short, A. and Ranasinghe, R., 2008. Statistical simulation of wave climate and extreme beach erosion. Coastal Engineering, 55(5): 375-390.

Callaghan, D.P., Ranasinghe, R. and Roelvink, D., 2013. Probabilistic estimation of storm erosion using analytical, semi-empirical, and process based storm erosion models. Coastal Engineering, 82: 64-75.

Coles, S., 2001. An introduction to statistical modeling of extreme values. Springer Verlag.

Coles, S.G. and Tawn, J.A., 1991. Modelling extreme multivariate events. Journal of the Royal Statistical Society. Series B (Methodological): 377-392.

Corbella, S. and Stretch, D.D., 2012. Multivariate return periods of sea storms for coastal erosion risk assessment. Natural Hazards and Earth System Science, 12(8): 2699-2708.

Corbella, S. and Stretch, D.D., 2013. Simulating a multivariate sea storm using archimedean copulas. Coastal Engineering, 76: 68-78.

De Michele, C., Salvadori, G., Passoni, G. and Vezzoli, R., 2007. A multivariate model of sea storms using copulas. Coastal Engineering, 54(10): 734-751.

De Ronde, J., Mulder, J. and Spanhoff, R., 2003. Morphological developments and coastal zone management in the netherlands. International Conference on Estuaries and Coasts November, p.^pp. 9-11.

De Waal, D. and van Gelder, P., 2005. Modelling of extreme wave heights and periods through copulas. Extremes, 8(4): 345-356.

De Winter, R.C., Sterl, A., de Vries, J.W., Weber, S.L. and Ruessink, G., 2012. The effect of climate change on extreme waves in front of the dutch coast. Ocean Dynamics, 62(8): 1139-1152.

Dean, R. and Dalrymple, R.A., 2002. Coastal processes with engineering applications, xi. Cambridge University Press, Cambridge.

Ferreira, J. and Guedes Soares, C., 2000. Modelling distributions of significant wave height. Coastal Engineering, 40(4): 361-374.

FitzGerald, D.M., Fenster, M.S., Argow, B.A. and Buynevich, I.V., 2008. Coastal impacts due to sea-level rise. Annual Review of Earth and Planetary Sciences, 36(1): 601-647.

Forristall, G., 1978. On the statistical distribution of wave heights in a storm. Journal of Geophysical Research: Oceans (1978–2012), 83(C5): 2353-2358.

Galappatti, R., 1983. A depth integrated model for suspended transport.

Geman, S. and Geman, D., 1984. Stochastic relaxation, gibbs distributions, and the bayesian restoration of images. Pattern Analysis and Machine Intelligence, IEEE Transactions on(6): 721-741.

Hallermeier, R.J., 1981. A profile zonation for seasonal sand beaches from wave climate. Coastal engineering, 4: 253-277.

Hallermeier, R.J., 1983. Sand transport limits in coastal structure design, Coastal Structures ' 83. American Society of Civil Engineers, pp. 703-716.

Harley, M., Turner, I., Short, A. and Ranasinghe, R., 2011. A reevaluation of coastal embayment rotation: The dominance of cross-shore versus alongshore sediment transport processes, collaroy-narrabeen beach, southeast australia. Journal of Geophysical Research: Earth Surface (2003–2012), 116(F4).

Havelock, T., 1918. Periodic irrotational waves of finite height. Proceedings of the Royal Society of London. Series A, 95(665): 38-51.

Hawkes, P.J., Gouldby, B.P., Tawn, J.A. and Owen, M.W., 2002. The joint probability of waves and water levels in coastal engineering design. Journal of Hydraulic Research, 40(3): 241-251.

Hillen, R., 1991. De basiskustlijn: Een technisch/morfologische uitwerking. Directoraat-Generaal Rijkswaterstaat, Dienst Getijdewateren.

Holthuijsen, L., De Ronde, J., Eldeberky, Y., Tolman, H., Booij, N., Bouws, E., Ferier, P. and Gal, J.A., 1994. The maximum significant wave height in the southern north sea. Coastal Engineering Proceedings, 1(24).

Houston, J., 1995. Beach-fill volume required to produce specific dry beach width. Coastal Engineering Technical Note CETN II-32, US Army Corps of Engineers, Waterways Experiment Station, Vicksburg, Mississippi.

Hydraulics, W.D., 1983. Valsnelheid van zand in zeewater van 5°c (settling velocity of sand in sea water of 5°c), WL|Delft Hydraulics.

ICSM, 2002. Geocentric datum of australia. Technical manual, version 2.2, Canberra.

Jongejan, R.B., Ranasinghe, R. and Vrijling, J.K., 2010. A risk-informed approach to coastal zone management, the 32nd International Conference on Coastal Engineering (ICCE 2010), Shanghai, pp. 1-12.

Katsman, C.A., Sterl, A., Beersma, J., Van den Brink, H., Church, J., Hazeleger, W., Kopp, R., Kroon, D., Kwadijk, J. and Lammersen, R., 2011. Exploring high-end scenarios for local sea level rise to develop flood protection strategies for a low-lying delta-the netherlands as an example. Climatic Change, 109(3-4): 617-645.

Komar, P., Lanfredi, N., Baba, M., Dean, R., Dyer, K., Healy, T., Ibe, A., Terwindt, J. and Thom, B., 1991. The response of beaches to sea-level changes: A review of predictive models. Journal of Coastal Research, 7(3): 895-921.

Kriebel, D.L. and Dean, R.G., 1993. Convolution method for time-dependent beach-profile response. Journal of Waterway, Port, Coastal, and Ocean Engineering, 119(2): 204-226.

Krogstad, H.E., 1985. Height and period distributions of extreme waves. Applied Ocean Research, 7(3): 158-165.

Kulmar, M., Lord, D. and Sanderson, B., 2005. Future directions for wave data collection in new south wales. the 17th Australasian Coastal and Ocean Engineering Conference and the 10th Australasian Port and Harbour Conference, p.^pp. 167-172.

Larson, M., Erikson, L. and Hanson, H., 2004. An analytical model to predict dune erosion due to wave impact. Coastal Engineering, 51(8-9): 675-696.

Larson, M., Kraus, N.C. and Byrnes, M.R., 1990. Sbeach: Numerical model for simulating storm-induced beach change. Report 2. Numerical formulation and model tests, US Army Engineer Waterways Experiment Station, Vicksburg, MS.

Lawson, N. and Abernethy, C., 1975. Long term wave statistics off botany bay. Proceedings of the 2nd Australian Australasian Coastal and Ocean Engineering Conference, p.^pp. 167-176.

Le Roux, J., 2008. An extension of the airy theory for linear waves into shallow water. Coastal Engineering, 55(4): 295-301.

Li, C. and Song, Y., 2006. Correlation of extreme waves and water levels using a third-generation wave model and a 3d flow model. Ocean Engineering, 33(5): 635-653.

Li, F., van Gelder, P.H.A.J.M., Callaghan, D.P., Jongejan, R.B., den Heijer, C. and Ranasinghe, R., 2013. Probabilistic modeling of wave climate and predicting dune erosion. Journal of Coastal Research, 1(Special Issue No. 65): 760-765.

Li, F., van Gelder, P.H.A.J.M., Jongejan, R.B., Ranasinghe, R. and Callaghan, D.P., 2011. Land-use strategies for coastal erosion zone based on a risk-informed approach. In: A.H.D.P.E. In H. Budelmann (Editor), 9th International Probabilistic Workshop. Technische Universitat Carolo-Wilhelmina, Braunschweig, Germany, pp. 331-341.

Li, F., van Gelder, P.H.A.J.M., Ranasinghe, R., Callaghan, D.P. and Jongejan, R.B., 2014. Probabilistic modelling of extreme storms along the dutch coast. Coastal Engineering, 86(0): 1-13.

Lord, D. and Kulmar, M., 2001. The 1974 storms revisited: 25 years experience in ocean wave measurement along the south east australian coast. Coastal Engineering Conference, p.^pp. 559-572.

Mangor, K., 2004. Shoreline management guidelines. DHI Water & Enviroment, Horsholm, Denmark, 294 pp.

Mathiesen, M., 1994. Estimation of wave height duration statistics. Coastal Engineering, 23(1): 167-181.

McInnes, K.L., Abbs, D.J., O'Farrell, S.P., Macadam, I., O'Grady, J. and Ranasinghe, R., 2007. Projected changes in climatological forcing for coastal erosion in nsw, NSW Department of Environment and Climate Change.

Michell, J., 1893. The highest waves in water. Philosophical Magazine and Journal of Science, 36(222): 430-437.

Mulder, J.P., Nederbragt, G., Steetzel, H.J., van Koningsveld, M. and Wang, Z.B., 2006. Different implementation scenarios for large scale coastal policy of the netherlands. Coastal Engineering Conference, p.^pp. 1705.

Myrhaug, D. and Hansen, E.H., 1997. Long-term distribution of seabed shear stresses beneath random waves. Coastal Engineering, 31(1): 327-337.

Nelsen, R.B., 2006. An introduction to copulas. Springer.

Nerzic, R. and Prevosto, M., 1998. A weibull-stokes model for the distribution of maximum wave and crest heights. International Journal of Offshore and Polar Engineering, 8(2).

Parry, M.L., Canziani, O.F., Palutikof, J.P., van der Linden, P.J. and Hansen, C.E., 2007. Climate change 2007: Impacts, adaptation and vulnerability: Working group i contribution to the fourth assessment report of the ipcc. 0521880106.

Pearson, K., 1900. X. On the criterion that a given system of deviations from the probable in the case of a correlated system of variables is such that it can be reasonably supposed to have arisen from random sampling. The London, Edinburgh, and Dublin Philosophical Magazine and Journal of Science, 50(302): 157-175.

Quartel, S., Ruessink, B.G. and Kroon, A., 2007. Daily to seasonal cross-shore behaviour of quasi-persistent intertidal beach morphology. Earth Surface Processes and Landforms, 32(9): 1293-1307.

Ranasinghe, R., Callaghan, D. and Stive, M.J.F., 2012. Estimating coastal recession due to sea level rise: Beyond the bruun rule. Climatic Change, 110(3-4): 561-574.

Ranasinghe, R. and Stive, M.J.F., 2009. Rising seas and retreating coastlines. Climatic Change, 97(3-4): 465-468.

Ranasinghe, R., Symonds, G., Black, K. and Holman, R., 2004. Morphodynamics of intermediate beaches: A video imaging and numerical modelling study. Coastal Engineering, 51(7): 629-655.

Renard, B. and Lang, M., 2007. Use of a gaussian copula for multivariate extreme value analysis: Some case studies in hydrology. Advances in Water Resources, 30(4): 897-912.

Renn, O., 1998. The role of risk perception for risk management. Reliability Engineering & System Safety, 59(1): 49-62.

Repko, A., Van Gelder, P., Voortman, H. and Vrijling, J., 2005. Bivariate description of offshore wave conditions with physics-based extreme value statistics. Applied Ocean Research, 26(3): 162-170.

Riesenkamp, M.J., 2011. Probabilistic modelling of extreme beach erosion using xbeach. Master Thesis, Delft University of Technology, Delft, the Netherlands, 73 pp.

Rijkswaterstaat, 1986. Manual on artificial beach nourishment. Delft Hydraulics Laboratory, the Netherlands.

Rijkswaterstaat, 2011. Kustlijnkaarten 2012, Ministry of Infrastructure and the environment, the Netherlands.

Roeland, H. and Piet, R., 1995. Dynamic preservation of the coastline in the netherlands. Journal of Coastal Conservation, 1(1): 17-28.

Roelse, P., 2002. Water en zand in balans: Evaluatie zandsuppleties na 1990; een morfologische beschouwing, Report RIKZ.

Roelse, P. and Mulder, J.P.M., 1995. Evaluation of nourishments in the netherlands, 8th Annual National Conference on beach preservation technology. Florida Shore and Beach Preservation Association, St. Petersburg Florida, pp. 118-132.

Roelvink, D., Reniers, A., van Dongeren, A., van Thiel de Vries, J., McCall, R. and Lescinski, J., 2009. Modelling storm impacts on beaches, dunes and barrier islands. Coastal Engineering, 56(11): 1133-1152.

Roelvink, J., 1993. Dissipation in random wave groups incident on a beach. Coastal Engineering, 19(1): 127-150.

Roscoe, K.L. and Diermanse, F., 2011. Effect of surge uncertainty on probabilistically computed dune erosion. Coastal Engineering, 58(11): 1023-1033.

Roshanka, R., Callaghan, D.P. and Roelvink, D., 2013. Does a more sophisticated storm erosion model improve probabilistic erosion estimates?, Coastal Dynamics 2013, Arcachon, France, pp. 1277-1286.

Salvadori, G., Michele, C.D. and Durante, F., 2011. On the return period and design in a multivariate framework. Hydrology and Earth System Sciences, 15(11): 3293-3305.

Scheffner, N.W. and Borgman, L.E., 1992. Stochastic time-series representation of wave data. Journal of Waterway, Port, Coastal, and Ocean engineering, 118(4): 337-351.

Schölzel, C. and Friederichs, P., 2008. Multivariate non-normally distributed random variables in climate research–introduction to the copula approach. Nonlin. Processes Geophys., 15(5): 761-772.

Schoonees, J. and Theron, A., 1995. Evaluation of 10 cross-shore sediment transport/morphological models. Coastal Engineering, 25(1): 1-41.

Short, A.D. and Trembanis, A.C., 2004. Decadal scale patterns in beach oscillation and rotation narrabeen beach, australia-time series, pca and wavelet analysis. Journal of Coastal Research: 523-532.

Short, A.D. and Trenaman, N., 1992. Wave climate of the sydney region, an energetic and highly variable ocean wave regime. Marine and Freshwater Research, 43(4): 765-791.

Sklar, M., 1959. Fonctions de répartition à n dimensions et leurs marges. Université Paris 8.

Small, C., Gornitz, V. and Cohen, J.E., 2000. Coastal hazards and the global distribution of human population. Environmental Geosciences, 7(1): 3-12.

Smits, A., 2001. Estimation of extreme return levels of wind speed: A modification of the rijkoort-weibull model. Royal Netherlands Meteorological Institute (KNMI), Climatological Services.

Solomon, S., 2007. Climate change 2007-the physical science basis: Working group i contribution to the fourth assessment report of the ipcc, 4. Cambridge University Press.

Soukissian, T.H. and Theochari, Z., 2001. Joint occurrence of sea states and associated durations. Proceeding of 11th International Offshore and Polar Engineering Conference, p.^pp. 33-39.

Stive, M.J., Ranasinghe, R. and Cowell, P., 2009. Sea level rise and coastal erosion. Handbook of coastal and ocean engineering. World Scientific: 1023-1038.

Stolk, A., 1989. Zansysteem kust – morfologische karakterisering. Kustverdediging na 1990, report geopro 1989-02.

Tawn, J.A., 1988. Bivariate extreme value theory: Models and estimation. Biometrika, 75(3): 397-415.

Trindade, J., Holthuijsen, L., Atkins, G. and Banks, L., 1993. Modelling wave penetration in botany bay. 11th Australasian Conference on Coastal and Ocean Engineering, p.^pp. 65-70.

V&W, 2000. Derde kustnota: Traditie, trends en toekomst, Ministry of Transport, Public Works & Water Management, The Hague, the Netherlands.

V&W, LNV, VROM and EZ, 2002. Towards an integrated coastal zone policy. Policy agenda for the coast., Ministry of Transport, Public Works and Water Management. The Hague, the Netherlands.

Van Dantzig, D., 1956. Economic decision problems for flood prevention. Econometrica: Journal of the Econometric Society: 276-287.

Van Dongeren, A., Bolle, A., Vousdoukas, M., Plomaritis, T., Eftimova, P., Williams, J., Armaroli, C., Idier, D., Van Geer, P. and De Vries, J.V.T., 2009. Micore: Dune erosion and overwash model validation with data from nine european field sites. Coastal dynamics 2009: Impacts of Human Activities on Dynamic Coastal Processes, Tokyo, Japan, p.^pp. 1-15.

van Gent, M.R.A., van Thiel de Vries, J.S.M., Coeveld, E.M., De Vroeg, J.H. and Van de Graaff, J., 2008. Large-scale dune erosion tests to study the influence of wave periods. Coastal Engineering, 55(12): 1041-1051.

Van Koningsveld, M. and Mulder, J.P.M., 2004. Sustainable coastal policy developments in the netherlands. A systematic approach revealed. Journal of Coastal Research: 375-385.

Van Noortwijk, J.M. and Peerbolte, E.B., 2000. Optimal sand nourishment decisions. Journal of Waterway, Port, Coastal and Ocean Engineering, 126(1): 30-38.

van Rijn, L., Ruessink, B.G. and Mulder, J., 2002. The behaviour of a straight sandy coast on the time scale of storms and seasons: Process knowledge and guidelines for coastal management: End document march 2002.

van Rijn, L.C., 2009. Prediction of dune erosion due to storms. Coastal Engineering, 56(4): 441-457.

Vellinga, P., 1982. Beach and dune erosion during storm surges. Coastal Engineering, 6(4): 361-387.

Vrijling, J., Van Hengel, W. and Houben, R., 1998. Acceptable risk as a basis for design. Reliability Engineering & System Safety, 59(1): 141-150.

Vrijling, J.K., Van Gelder, P.H.A.J.M. and Litjes van Loon, J., 2002. Coastal zone risk in the netherlands, Coastal Engineering 2002 28th International Conference, Cardiff, pp. 3508-3516.

Wahl, T., Mudersbach, C. and Jensen, J., 2012. Assessing the hydrodynamic boundary conditions for risk analyses in coastal areas: A multivariate statistical approach based on copula functions. Natural Hazards and Earth System Science, 12(2): 495-510.

Walstra, D., Roelvink, J. and Groeneweg, J., 2000. 3d calculation of wave-driven cross-shore currents. Proceedings 27th International Conference on Coastal Engineering, p.^pp. 16-21.

Winckel, P., Vrijling, J. and Van de Graaff, J., 2008. Developing a building policy for the erosion zone: Solutions to some key (dutch) questions. Coastal Engineering, 55(1): 79-92.

Woodroffe, C., Cowell, P., Callaghan, D., Ranasinghe, R., R, J., Wainwright, D., Barry, S., Rogers, K. and Dougherty, A., 2012. Approaches to risk assessment on australian coasts: A model framework for assessing risk and adaptation to climate change on australian coasts, National Climate Change Adaption Research Facility, Gold Coast.

Youll, P., 1981. Botany bay waverider system-10 years of records. Fifth Australian Conference on Coastal and Ocean Engineering, 1981: Offshore Structures, p.^pp. 245-251.

List of symbols

Symbol	Description	Unit
α	dependency parameter	-
$\alpha_1 \sim \alpha_7$	coefficients of the DUNERULE	-
$\tilde{\alpha}$	significance level	-
β	transfer coefficient of the net present value and the ordinary annuity	-
θ	wave direction	degree
θ_0	incidence angle	degree
κ	copula parameter	-
ξ	distribution shape parameter	-
ρ_a	air density	kg/m^3
ρ_s	sediment density	kg/m^3
ρ_w	water density	kg/m^3
σ	distribution scale parameter	-
σ_f	intrinsic wave frequency	-
$\varphi(x)$	generator function	-
Φ	standard normal distribution function	-
Φ_Σ	joint distribution function of the n-variate standard normal distribution function	-
a	probability rising rate	-
B	dune height	m
c	wave celerity	m/s
C	copula function	-
$C_{1-\tilde{\alpha},f}$	Chi-square distribution at the cumulative probability ($1-\tilde{\alpha}$)	-
C_d	depth averaged sediment concentration	kg/m^3
C_{eq}	equilibrium suspended sediment transport concentration	kg/m^3
d_{50}	0.5 grain size fractile of the sand	mm
D	storm duration	h

D_d	median sediment diameter	mm
D_h	horizontal diffusion factor	-
D_w	wave energy dissipation	w/kg
DoC	depth of closure	m
E_w	total wave energy	J
f	degrees of freedom	-
f_{mor}	morphological acceleration factor	-
f_{ref}	representative intrinsic frequency	-
f_{T_s}	sediment transport depth factor	-
F	Cumulative distribution function	-
F_W	wave impact	N
F_f	wind fetch	m
F_{f_FDS}	necessary wind fetch for a FDS state	m
F_s	storm frequency	-
g	gravity acceleration	m/s^2
h	sea water level	m
h_d	water depth	m
h_t	the depth where the beach slope changes	m
H_e	effective significant wave height exceeded for 12 hours per year	h
H_m	median wave heights	m
H_{rms}	root mean square wave height	m
H_s	significant wave height	m
$\bar{H}_s$	mean annual significant wave height	m
$H_{s,\max}$	maximum significant wave height	m
H_{s_FDS}	fully developed significant wave height	m
k	wave number	-
L	coastal length	m
L_c	distance from closure depth to coastline	m
L_0	wave length	m
L_N	sand nourishment length	m
m	beach slope	-

NPV	net present value per unit coastal length	Euro/m
NPV_{total}	total net present value in the coastal zone	Euro
p	porosity	-
P	event probability	-
r	interest rate	-
R	dune erosion volume per unite length	m^3/m
R	domain	-
R_m	mean return rate	-
$R_{initial}$	initial erosion volume	m^3/m
RD	dune retreat distance	m
s	relative density(ρ_s / ρ_w)	-
S	sea level rise	m
S_p	wave steepness	-
S_w	wave energy per directional bin	J
t_m	time when maximum erosion occurs	h
t_s	time when storm erosion is greater than the initial erosion	h
T	wave period	s
T_D	wind duration	h
T_{D_FDS}	necessary wind duration for a FDS state	h
T_e	effective wave period exceeded for 12 hours per year	s
T_E	economic lifetime of the buildings	year
T_m	median wave period	s
T_p	peak wave period	s
$T_{s,a}$	characteristic time scales of the exponential response under accretive conditions	h
$T_{s,e}$	characteristic time scales of the exponential response under erosive conditions	h
u^E	cross shore velocity	m/s
u_0	bore velocity	m/s
U	wind velocity	m/s
v	value density	$euro/m^2$
V	property value	euro
w	sand nourishment width	m

w_d	sediment fall velocity	m/s
W	weight of the sand eroded from the dune	kg
z	elevation of the seaward boundary contour	m
z_0	elevation difference between dune toe and the beginning of the swash zone	m
Z_R	run-up height	m

Acronyms

BCL	Basal Coastline
CDF	cumulative distribution function
FDS	fully developed sea
GLM	generalized Lagrangian Mean
GEV	Generalized Extreme Value
GP	Generalized Pareto
IPCC	Intergovernmental Panel on Climate Change
JARKUS	Yearly Dutch coastal bathymetry survey “JAaRlijkse KUStmeting (in Dutch)”
MCL	Momentary Coastline
MLE	maximum likelihood estimation
MLWL	Mean Low Water Level
MSL	mean sea level
NAP	Amsterdam Ordnance Datum (Normaal Amsterdams Peil in Dutch)
PDF	probability density function
RMSE	root mean square error

Acknowledgments

The China scholarship council (CSC) is acknowledged for its financial support during the research and the Lamminga fund is acknowledged for financing my visit to the University of Queensland, Australia. The results obtained in this thesis are mainly carried out at the section of Hydraulic Structure and Flood Risk, Delft University of Technology.

I would like to express my special thanks to my promoter Prof. J.K. Vrijling for giving me the golden opportunity to start my research career as a PhD candidate and giving me constructive advises to guide me during the whole study period. I still remember the day when you guided us forward in your boat. Captain, we really enjoyed the time with you.

I am grateful to my co-promoter Prof. Pieter H.A.J.M. van Gelder. Pieter, whenever I need your help, you will always be there and help me with great patience. You taught me to apply the statistical theory in the field of engineering, which now constitutes one of the most significant parts of this thesis.

Many thanks should also be addressed to the people who make this thesis possible. Advice given by Prof. Roshanka Ranasinghe and Dr. David Callaghan has been a great help in the basic principles of coastal engineering. Dr. R.B. Jongejan provided me with very valuable guidance in the aspect of economic model of the erosion risk. Dr. Kees den Heijer, thank you for helping me so much in running the XBeach. I want thank Prof. M.J.F. Stive for his approval of the Lamminga Fund.

I would like to thank the following institutions and organizations for their assistance with the data collection. The Dutch wave climate and the coastal bathymetry data were provided by the Ministry of Infrastructure and the Environment, and the Sydney tidal anomalies and waves were provided by Manly Hydraulic Laboratory on behalf of the NSW Department of Environment and Climate Change (Messrs M. Kulmer and P. Murphy). The Botany Bay offshore wave measurements were provided by Sydney Port (Mr G. Batman).

My special thanks are extended to Franca and Timmers in CICAT for their arrangement before and during my stay in the Netherlands. I am thankful to Mariette van Tilburg,

who gives me a lot of help during the PhD study. Assistance provided by our secretaries is greatly appreciated.

I wish to thank various people in the Netherlands I met, friends, colleges and strangers, who make my life colorful and challengeable.

Especially, I am very grateful to my wife, Dang Xiangxiang, for her company, support and encouragement during the tough period. Without you, my life will become completely boring. Finally, I would like to offer my great appreciation to my parents. Sorry for my wandering life, I cannot be with you whenever you need me. All you do is giving, all I do is thinking about myself.

Li Fan

November, 2013 in Delft

Curriculum Vitae

Fan Li was born in Yingkou, Liaoning, China, on July 25, 1982. He started studying Hydrology and Water Resources Engineering at Hohai University, Nanjing, China from 2001 to 2005. In 2005, he got a job in the Investigation and Design Institute of Water Resources and Hydropower of Liaoning Province. In 2007, he spent several months as an intern at the Ministry of Water Resources of China. After that, he started his MSc study at Hohai University and obtained the Master degree in Hydrology and Water Resources Engineering in 2009. In December 2009, he came to Delft University of Technology as a PhD student at the Section of Hydraulic Structure and Flood Risk, financially supported by the Chinese Scholarship Council (CSC). In 2012, Fan spent part of his PhD in the University of Queensland, Brisbane, Australia, supported by the Lamminga Fund.

Publications

Li, F., Xia, Z., Wang, Y., 2010. Influence of Gezhouba project on hydrological and hydraulic characteristics of Yichang river reach. Journal of Hohai University (Natural Sciences), 38(1), 38-40. (in Chinese, with English abstract)

Li, F., van Gelder, P.H.A.J.M., Jongejan, R.B., Ranasinghe, R., Callaghan, D.P., 2011. Land-use strategies for coastal erosion zone based on a risk-informed approach. In H. Budelmann, A. Holst & D. Proske (Eds.), International probabilistic workshop proceedings, pp. 331-341. Braunschweig: Technische Universitat Carolo-Wilhelmina.

Li, F., van Gelder, P.H.A.J.M., Ranasinghe, R., Callaghan, D.P., Jongejan, R.B., 2011. Probabilistic Modelling of Extreme Wave Climate along the Dutch Coast, LOICZ Open Science Conference, Yantai, China, Abstract pp153.

Li, F., van Gelder, P.H.A.J.M., Callaghan, D.P., Jongejan, R.B., den Heijer, C. and Ranasinghe, R., 2013. Probabilistic modeling of wave climate and predicting dune erosion. Journal of Coastal Research, 1(Special Issue No. 65): 760-765.

Li, F., van Gelder, P.H.A.J.M., Callaghan, D.P., Jongejan, R.B. and Ranasinghe, R., 2013. A comparison of extreme wave climate modelling methods: A case study for the Netherlands, Proceedings of 2013 IAHR world congress. Chengdu, China.

Li, F., van Gelder, P.H.A.J.M., Ranasinghe, R., Callaghan, D.P. and Jongejan, R.B., 2014. Probabilistic modelling of extreme storms along the Dutch coast. Coastal Engineering, 86(0): 1-13.

Li, F., van Gelder, P.H.A.J.M., J.K. Vrijling, Callaghan, D.P., Jongejan, R.B. and Ranasinghe, R., 2013. Probabilistic estimation of coastal dune erosion and recession by statistical simulation of storm events. Applied Ocean Research (accepted).

Huang, F., Xia, Z., Li, F., Guo, L. and Yang, F., 2012. Hydrological changes of the Irtysh river and the possible causes. Water resources management, 26(11): 3195-3208.

Huang, F., Xia, Z., Li, F. and Wu, T., 2013. Assessing sediment regime alteration of the upper Yangtze River. Environmental Earth Sciences: 1-9.


9 789065 623485